Università di Genova

DEPARTMENT OF EXPERIMENTAL MEDICINE

PhD COURSE IN EXPERIMENTAL MEDICINE

Curriculum of Biochemistry

DESIGN OF NEW MOLECULES AS A THERAPEUTIC STRATEGY FOR CYSTIC FIBROSIS

Candidate

Dr. Dario Lunaccio

Tutor

Prof. Enrico Millo

PhD Program Coordinator

Prof. Ernesto Fedele

Academic Year 2024-2025

XXXVIII Cycle

TABLE OF CONTENTS

Abstract

The approval of Cystic Fibrosis Transmembrane Conductance Regulator (CFTR) modulator therapy by global health agencies over the past few decades has fundamentally changed the course of patients affected by Cystic Fibrosis (CF). CFTR is a membrane protein that functions as a chloride channel in epithelial cells. Mutations in the CFTR gene lead to absent or impaired chloride transport across the apical membranes, primarily in the respiratory and glandular epithelia. This defect results in the extracellular accumulation of thick, sticky mucus, leading to chronic conditions such as sinusitis, bronchitis, pneumonia, and asthma, often refractory to standard therapy, as well as nasal polyposis, digital clubbing, and bronchiectasis.

CFTR modulators are categorized, based on their mechanism of action, as correctors, which enhance CFTR folding and trafficking to the cell surface, and potentiators, which improve ion transport through CFTR channels already present on the apical membrane. The four currently approved modulators are the potentiator Ivacaftor (VX770 or IVA) and the correctors Lumacaftor (VX809 or LUM), Tezacaftor (VX661 or TEX), and Elexacaftor (VX445 or ELX). Combinations of these modulators, such as the triple combination Ivacaftor/Tezacaftor/Elexacaftor (Kaftrio®), represent the best therapeutic option available for patients with sensitive CFTR mutations, including the most common one, the phenylalanine 508 deletion (F508del-CFTR). However, current therapies do not guarantee complete CFTR functional recovery, highlighting the need for developing new molecules to fill these therapeutic gaps.

This thesis reports on the development and study of novel molecules featuring an arylthiazole scaffold for their potential to restore CFTR functionality. The goal was to develop compounds that are more active than those already clinically approved, both when administered alone and in combination, aiming for a synergistic effect due to complementary mechanisms of action between them and already approved modulators.

Functional channel activity assays using the Yellow Fluorescent Protein (YFP) reporter in Fisher Rat Thyroid (FRT) and CFBE41o- cells stably expressing F508del-CFTR demonstrated a significant additive/synergistic effect when the novel VX809-hybrids **2a** and **3a** were combined with VX445.

Furthermore, eight other newly synthesized compounds (**4a**, **5a**, **1b**, **2b**, **3b**, **7b,** and **1c**), when tested individually, significantly increased F508del-CFTR activity compared to the vehicle treatment in CFBE bronchial epithelial cells. Notably, the combinations **2b** + **5a** and **7b** + **4a** resulted in

approximately 20% and 29% greater F508del-CFTR rescue, respectively, than the clinically used VX809 + VX445 combination.

To confirm this efficacy, a functional measurement of CFTR activity using the Fluorescence Microplate Polarimetry (FMP) assay was performed in Human Nasal Epithelial (HNE) primary cells from four CF patients homozygous for the F508del-CFTR mutation. The results confirmed that the novel corrector combinations (**2b** + **5a** and **7b** + **4a**) significantly increased FSK-activated and VX770-potentiated F508del-CFTR function compared to the rescue levels mediated by either the VX809 + VX445 or VX661 + VX445 combinations in HNE cells.

Finally, recognizing the emerging role of molecular chaperone modulators as a strategy to enhance F508del-CFTR rescue, combining them with already approved modulators, a small library of Hsc70/Hsp70 modulators was developed based on the scaffold of MKT-077, a known allosteric Hsp70 inhibitor. Among the new library, three MKT-077 analogues, i.e. **DL79**, **DL90**, and **AP161**, showed an inhibitory effect on human recombinant Hsp70 ATPase activity. Significantly, **DL79** demonstrated a higher ability than MKT-077 to enhance the corrective effect of VX809 on F508del-CFTR in CFBE41o- cells at a remarkably low concentration. The combination of **DL79** with other clinically approved correctors revealed a significant synergistic interaction with VX661 and with the VX661/VX445 combination, though no meaningful effect was observed in combination with VX445 alone.

Results reported in this thesis identified and characterized novel CFTR modulators and molecular chaperone enhancers that demonstrate superior efficacy, particularly in combination, compared to current standard-of-care therapies for F508del-CFTR.

In summary, these results provide strong preclinical evidence supporting the further development of these novel arylthiazole correctors and the Hsp70 modulators as potential next-generation therapeutic agents for CF patients with the F508del-CFTR mutation.

Abbreviations

AAT	Amino aryl thiazole
ACT	Airway Clearance Therapy
CA-RMSD	Carbon Atom Root Mean Square Deviation
CF	Cystic Fibrosis
CFF	Cystic Fibrosis Foundation
CFTR	Cystic Fibrosis Transmembrane Conductance Regulator
Cryo-EM	Cryogenic Electron Microscopy
DIPEA	Diisopropylethylamine
DMF	N, N-dimethylformamide
ELX	Elexacaftor
ER	Endoplasmic Reticulum
ERAD	Endoplasmic Reticulum Associated Degradation
ERQC	Endoplasmic Reticulum Quality Control
FDA	Food and Drug Administration
FMP	Fluorescence Microplate Polarimetry
FRT	Fisher Rat Thyroid
FSK	Forskolin
HEK	Human Embryonic Kidney
HNE	Human Nasal Epithelial
HPLC	High Performance Liquid Chromatography
hrHSP	Human Recombinant Heat Shock Protein
HSP	Heat Shock Protein
ICL	Intracellular Loop
IVA	Ivacaftor
LUM	Lumacaftor

MS	Mass Spectrometry
MSD	Membrane Spanning Domain
NBD	Nucleotide Binding Domain
NBS	Newborn Screening
NMR	Nuclear Magnetic Resonance
PDB	Protein Data Bank
PM	Plasma Membrane
ppFEV1	Forced Expiratory Volume in one second
pwCF	People with Cystic Fibrosis
QR	Quenching Rate
QSAR	Quantitative structure-activity relationship
R	Regulatory
SEM	Standard Error of the Mean
TEZ	Tezacaftor
TFA	Trifluoroacetic acid
THF	Tetrahydrofuran
TM	Transmembrane
TMS-OTf	Trimethylsilyl trifluoromethanesulfonate
TSA	Thermal Shift Analysis
WT	Wild Type
YFP	Yellow Fluorescent Protein

1. Introduction

1.1. Cystic Fibrosis disease: pathogenesis, epidemiology, clinical presentations, diagnosis

Cystic fibrosis (CF) is a multisystem hereditary disorder caused by genetic variants in the CFTR (Cystic Fibrosis Transmembrane Conductance Regulator) gene, located on chromosome 7q31.2. The CFTR gene encodes a membrane protein that functions as a chloride channel in epithelial cells. Defects in this protein lead to impaired or absent chloride transport across the apical membranes of the respiratory and glandular epithelium, resulting in the accumulation of thick and sticky mucus (Figure 1.1).

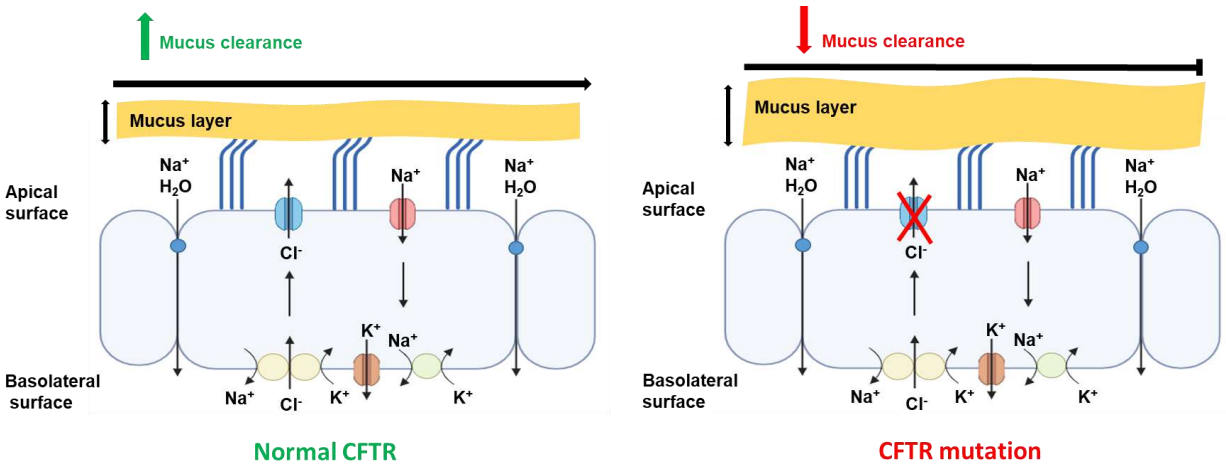

Figure 1.1. *CFTR protein defects in Cystic Fibrosis.* A mutation in the CFTR gene inhibits Cl^- efflux in the apical compartment, thus triggering unrestrained Na^+ absorption responsible for airway surface liquid dehydration and defective mucous clearance.

This impairs mucociliary clearance, promotes chronic respiratory infections, and leads to dysfunction in the pancreas, liver, and reproductive system [1]. CF also affects the sweat glands, leading to excessive salt loss in sweat, a phenomenon first described by Dr. Paul di Sant'Agnese during a 1948 New York heatwave, which paved the way for the development of the pilocarpine iontophoresis sweat test, now the gold standard for CF diagnosis [2].

CF is an autosomal recessive disease, meaning two pathogenic CFTR variants must be inherited for the condition to manifest. Several CFTR variants have been identified and classified into six groups based on their impact on CFTR protein synthesis, structure, and function [3, 4], though only a subset of those mutations is definitively linked to disease. The most common disease-causing variant is F508del, a Class II mutation in which the CFTR protein is produced but misfolded and fails to reach the cell membrane. Approximately 44.2% of individuals with CF are homozygous for

F508del, 40.5% are compound heterozygous (F508del plus another variant), and 15.3% carry two non-F508del variants [5]. The specific variants determine the amount of functional CFTR protein and are partially correlated with disease severity and organ involvement [6].

CF is one of the most common genetic disorders among Caucasians, with an incidence of 1:3,200 individuals [3]. The incidence does vary significantly by race/ethnicity, with an incidence of 1:13,500 in people of Hispanic background, 1:15,000 in people of African descent, and 1:35,000 in people of Asian descent [4]. It is estimated that one in every 35 Americans is a carrier of CF [7]. Based on statistics from the 2018 Annual Data Report published by the Cystic Fibrosis Foundation (CFF), there are an estimated 30,000 affected individuals in the United States living with CF [3]. Worldwide, there are an estimated 80,000 people, with the highest prevalence in North America, Europe, and Australia. Annually, approximately 1,000 new cases are diagnosed in the United States (although the rate of new cases may be declining related to pre-conception screening) [8], and the incidence is equal in males and females. Since 2010, all 50 states have screened neonates for CF [9], and as a result, 60% of new diagnoses occur via newborn screening [3].

Clinically, classic CF presents with a triad of recurrent respiratory infections, steatorrhea, and malnutrition, which in its most severe form may manifest as failure to thrive [1]. In the lungs, dehydrated mucus obstructs the airways, triggering inflammation, chronic infection, and the development of bronchiectasis, a permanent dilation of the bronchi that impairs clearance of secretions and increases infection risk [10]. Other affected organs include the pancreas, leading to exocrine pancreatic insufficiency and CF-related diabetes (CFRD), as well as the liver and gastrointestinal tract. In utero, ultrasound findings such as echogenic or dilated bowel may suggest intestinal obstruction, seen in over 50% of foetuses with CF [11]. Postnatally, delayed meconium passage or meconium ileus (present in 11.9% of CF infants) is a common early sign and may be associated with abdominal distension, bowel dilation, and complications such as intestinal perforation (in 30% of cases) [5]. Additional neonatal manifestations include rectal prolapse, prolonged jaundice, haemorrhagic disease due to vitamin K deficiency, and salt depletion syndrome with metabolic alkalosis and hypoalbuminemia from malabsorption [10, 12].

In adolescents and adults, CF may present later with chronic sinusitis, bronchitis, pneumonia, asthma unresponsive to standard therapy, nasal polyposis, digital clubbing, and bronchiectasis on imaging [10]. Gastrointestinal symptoms can include poor growth, malnutrition, intestinal obstruction, constipation, liver disease, or rectal prolapse [12]. Individuals with pancreatic-sufficient CF (more likely to be diagnosed later) may present with pancreatitis, although its pathophysiology is not fully understood [13].

More than 98% of men with CF are infertile due to congenital bilateral absence of the vas deferens, often discovered during infertility evaluations [14].

Although newborn screening (NBS) has decreased the rate of delayed diagnoses, false negatives still occur, particularly in specific populations. Introduced in the 1980s, NBS for CF relies on measuring immunoreactive trypsinogen (IRT) in dried blood spots. Elevated IRT triggers either repeat testing (IRT/IRT) or reflex genetic testing (IRT/DNA) to identify CFTR variants. A positive result, defined as persistent IRT elevation between days 7 and 14 of life or the presence of a CFTR mutation, requires prompt referral (within 72 hours) to a CFF-accredited centre for sweat chloride testing [15]. Early diagnosis in asymptomatic infants offers benefits, including preservation of lung function, early nutritional interventions, and psychosocial support for families [10]. However, NBS carries risks such as over-medicalization, caregiver anxiety [16], and higher false-positive rates in certain populations (e.g., African and American infants have higher IRT but lower CF prevalence) [17]. NBS may also miss some cases (false negatives), especially in neonates with meconium ileus or those with mutations not included in standard panels [18]. In some cases, infants may be classified with CRMS/CFSPID (Cystic Fibrosis Screen Positive, Inconclusive Diagnosis), where sweat chloride values are normal or intermediate and CFTR mutations of unclear significance are present [19].

According to the 2017 CFF consensus guidelines, a diagnosis of CF is established when there is a clinical presentation consistent with the disease (e.g., positive NBS, characteristic symptoms, or family history) plus evidence of CFTR dysfunction, such as a sweat chloride value ≥60 mmol/L [19, 20]. The quantitative pilocarpine iontophoresis sweat test, developed in 1959 by Gibson and Cooke, remains the diagnostic gold standard [21]. It can be performed as early as 48 hours after birth [22], but is ideally done after 10 days of life and before 4 weeks of age, provided the infant weighs at least 2 Kg or is corrected to 36 weeks of gestation [20]. Sweat testing should also be performed in any infant with meconium ileus or CF-related symptoms, regardless of NBS results. Abnormal results must be confirmed with repeat testing or genetic analysis. Sweat chloride values are interpreted as follows [19]:

- ≥60 mmol/L: diagnostic for CF (requires confirmatory testing or identification of 2 CF-causing variants)
- 30–59 mmol/L: intermediate, requires repeat testing and further evaluation at a CF centre
- <30 mmol/L: CF is unlikely, but if two CF-causing variants are found, a diagnosis can still be made.

Genetic testing complements sweat testing, especially for those with intermediate results. Identifying two known pathogenic variants on separate chromosomes confirms the diagnosis.

Most patients can be diagnosed using commercial CFTR panels that test for the most common mutations [23], but full gene sequencing may be needed in atypical presentations [10].

1.2. Cystic Fibrosis Transmembrane Conductance Regulator protein

The CFTR protein is a member of the ATP-binding cassette (ABC) transporter superfamily. Structurally, CFTR comprises two membrane-spanning domains (MSDs or TMDs), each containing six transmembrane (TM) helices (TM1–TM6 in MSD1 and TM7–TM12 in MSD2) and two intracellular loops per domain (ICL1 and ICL2 in MSD1, ICL3 and ICL4 in MSD2). On the cytoplasmic side, it features two nucleotide-binding domains (NBDs) and a regulatory (R) domain, which contains phosphorylation sites for protein kinase A (PKA) and protein kinase C (PKC) (Figure 1.2) [24].

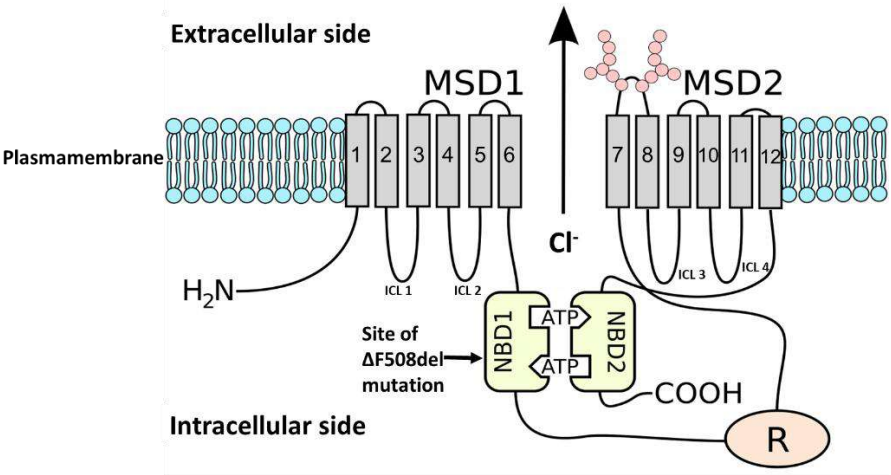

Figure 1.2. *2D representation of CFTR in the cell membrane*. NBD1: first nucleotide binding domain; NBD2: second nucleotide binding domain; ICL1-4: intracellular loops; R: R domain; MSD1: Membrane-Spanning Domain 1; MSD2: Membrane-Spanning Domain 2; 1-12: transmembrane domains. Adapted from M. P. Rogan et al. Chest. Vol. 139, Issue 6, 2011, doi:10.1378/chest 10-2077.

Cryo-electron microscopy (cryo-EM) structural analysis of human CFTR shows that in its dephosphorylated state; the R domain may inhibit channel activity by obstructing NBD dimerization [24]. CFTR activation is driven by cAMP-mediated phosphorylation of the R domain via PKA, along with ATP binding to the NBDs, both of which promote channel opening. In the ATP-bound conformation [25], phosphorylation displaces the R domain from the NBD interface, allowing the structural rearrangements necessary for channel function.

Functionally, CFTR conducts chloride and bicarbonate ions and modulates the activity of various other ion channels and transporters [26-28]. It plays a critical role in controlling transepithelial

fluid and electrolyte transport across epithelial tissues. Like many membrane glycoproteins, CFTR is glycosylated in the endoplasmic reticulum (ER) and Golgi apparatus before insertion into the plasma membrane (PM), undergoing strict quality control during its transit through the secretory pathway [29-34]. This surveillance involves key interactions beginning in the ER and continuing in the Golgi, PM, and endosomes after CFTR exits the ER. Along this pathway, numerous components of the proteostasis network influence CFTR folding, stability, degradation, and surface expression [35-42]. A significant fraction of CFTR fails to mature fully and is instead targeted for ER-associated degradation (ERAD) [34, 43, 44], in which misfolded proteins are recognized by molecular chaperones, ubiquitinated, and delivered to the proteasome for degradation. At the plasma membrane, while some wild-type CFTR persists, most misfolded proteins that evade ERAD but lack stabilization signals are internalized and degraded through the lysosomal pathway [45-47] (Figure 1.3).

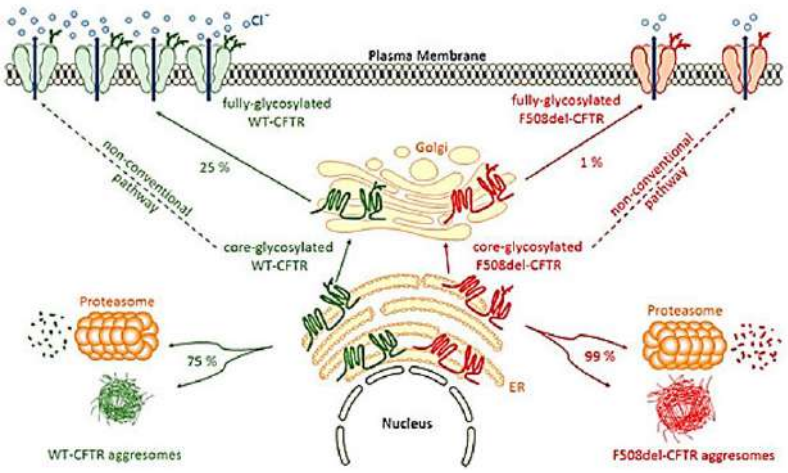

Figure 1.3. *WT- and F508del-CFTR biogenesis*. After synthesis in the Endoplasmic Reticulum (ER), the main part of core-glycosylated CFTR can form aggresomes or be recognized by the Endoplasmic Reticulum Quality Control (ERQC) system and directed to the proteasome to be degraded. CFTR escaped from ERQC, undergoes different steps of glycosylation in the Golgi before being transported to the plasma membrane, where it regulates ion channels. F508del-CFTR at the plasma membrane is less abundant and has only low activity compared to WT-CFTR. A non-conventional trafficking of the CFTR protein can be activated when the conventional trafficking is blocked, allowing expression of core-glycosylated CFTR at the plasma membrane. From Simon S et al, Int. J. Mol. Sci. 2021, 22(8), 4252; https://doi.org/10.3390/ijms22084252.

Given CFTR multidomain organization, proper folding depends on precise intramolecular interactions between TMDs and NBDs post-translation [48-51]. Various heat-shock proteins play essential roles in CFTR biosynthesis, particularly during early folding stages, through interactions with both ER and cytosolic factors [34]. Two major ATP-dependent chaperones involved in this process are Hsc70/Hsp70 and Hsp90 [52-56] (see paragraph 1.3.4). Among the lectin chaperones, calnexin and calreticulin are key players. They bind immature N-linked glycans and, together with

glycan-modifying enzymes, contribute to ER-based quality control that impacts CFTR maturation [57-60].

At the cell surface, CFTR is further regulated by peripheral quality control mechanisms, which mediate its internalization via clathrin-coated vesicles. This process is facilitated by a tyrosine-based motif (YXXΦ, where Φ denotes a hydrophobic residue) in CFTR C-terminus [61], and by adaptor proteins like AP2 and Dab2 [62-64]. Once internalized, CFTR may either be recycled back to the membrane or directed toward lysosomal degradation [46, 63]. Several Rab GTPases are involved in these trafficking decisions [46, 65], and this peripheral quality control ensures the clearance of misfolded or aged CFTR, often via ubiquitin-mediated lysosomal targeting [47, 66]. Surface levels of CFTR are influenced by its folding efficiency, trafficking, membrane stability, and residence time. Several regulatory factors enhance CFTR surface expression and function. For instance, vasoactive intestinal polypeptide modulates its secretion in the gastrointestinal tract [67-70], while cytokines such as IL-1β, IL-4, TNF-α, IL-10, and IL-13 upregulate CFTR in the airways, in contrast to TGF-β, which suppresses its expression [71, 72]. cAMP, a primary CFTR activator, also promotes surface expression by activating EPAC1 (Exchange Protein Activated by cAMP 1) [73], which recruits cytoskeletal regulators near CFTR [74]. In the respiratory tract, extracellular adenosine and ATP levels modulate CFTR activation to maintain airway surface liquid homeostasis [75]. Adenosine stimulates A2B receptors, raising intracellular cAMP and enhancing CFTR phosphorylation, while ATP activates P2Y2 receptors, increasing intracellular Ca^{2+} to activate TMEM16A, a calcium-dependent chloride channel. P2Y2 receptor activation also positively influences CFTR activity. Numerous kinases, including PKA, PKC, tyrosine kinases, and casein kinases [76-87], along with phosphatases like protein phosphatases 1, 2A, and 2B [76, 77, 88-93], regulate CFTR's phosphorylation status, directly impacting its gating properties. Notably, phosphorylation of the R domain by PKA in a cAMP-dependent manner is critical for full channel activation [80, 87, 94-96].

The most common pathogenic variant leading to CF, F508del-CFTR, is believed to have originated around 5,000 years ago within the Bell Beaker population during the transition from the late Neolithic to early Bronze Age [97]. This deletion of phenylalanine at position 508 in the 1,480-amino acid of the CFTR protein leads to misfolding, degradation, and impaired protein processing and function [98]. Loss of functional CFTR disrupts airway surface hydration, leading to mucus buildup, impaired mucociliary clearance, and chronic infections [27].

Ongoing advances in genetic testing, especially next-generation sequencing, continue to reveal new variants. Indeed, a recent study using UK Biobank data [99] identified approximately 4,000 CFTR mutations, including ancestry-specific variants across six ethnic groups. Of these, around 1,000 have been confirmed as disease-causing [100], typically affecting CFTR synthesis, processing,

or function, with F508del being the most prominent. These mutations are classified into six functional categories based on their effects on CFTR biogenesis and activity (Figure 1.4) [101-104]:

- Class I: premature stop codons (nonsense mutations) prevent protein synthesis. People with Class I variants lack CFTR protein production, resulting from disruption of the CFTR coding sequence (e.g., frameshift mutations). The Class I variant transcripts are either unstable due to premature termination (Class IA) or code for a truncated, dysfunctional protein product (Class IB). Class IA includes large deletion mutations with no mRNA synthesis [101, 105] . Class IB includes mostly nonsense mutations resulting in a premature termination codon and the production of unstable mRNA. The abnormal mRNA is rapidly recognized and eliminated by the nonsense mRNA decay (NMD) surveillance system [106, 107]. CFTR protein fragments synthesized by class IB mutations are recognized and degraded in the proteasome before they can be inserted into the apical membrane. About 10% of CF patients carry these mutations
- Class II: it results in misfolded CFTR targeted for degradation, leading to minimal surface expression and poor chloride transport. The CFTR structural defect is recognized by the cell quality-control system, which will ubiquitinate the abnormal protein in the ER and direct it to the proteasome for degradation (a process known as endoplasmic-reticulum-associated degradation or ERAD) before it can be transported to the apical membrane. The most common class II allele is the F508del mutation, and approximately 90% of CF patients worldwide have at least one F508del allele, and ~50% are homozygous
- Class III: involves impaired gating of the CFTR channel. Although the protein is structurally intact and migrates correctly to the apical membrane, where it is stable, CFTR proteins with gating mutations (such as G551D and S1251N) have an open probability that is decreased up to 100-fold compared to wild-type CFTR [108]. The gating defect is due to abnormal ATP-binding to the nucleotide-binding domains (NBD1 and NBD2) and a lack of ATP hydrolysis. The resulting dysfunction of CFTR is severe and causes classical manifestations of CF disease. These mutations allow membrane localization but impair channel opening in response to cAMP [109]. G551D is the most common, affecting ~4% of patients [110, 111]
- Class IV: it causes a conduction defect in which the anion selectivity of CFTR is altered, leading to decreased chloride and bicarbonate conductance. Because partial chloride or bicarbonate conductance is preserved, individuals with class IV mutations will often express milder CF disease. Mutations like R117H and R347P reduce chloride conductance. R117H is the most frequent in this class (~1.3%) [112]

- Class V: it results in greatly reduced amounts of functional CFTR at the apical membrane due to promoter mutations, alternate splicing defects, or missense mutations resulting in abnormal mRNA transcripts [113]. The severity of clinical manifestations within this class can vary between patients and within different organs of the same patients, but it is generally mild
- Class VI: produce functional CFTR protein, which migrates to the plasma membrane but is unstable [104]. Plasma membrane CFTR endocytosis or turnover is accelerated, thus reducing CFTR density and function [114].

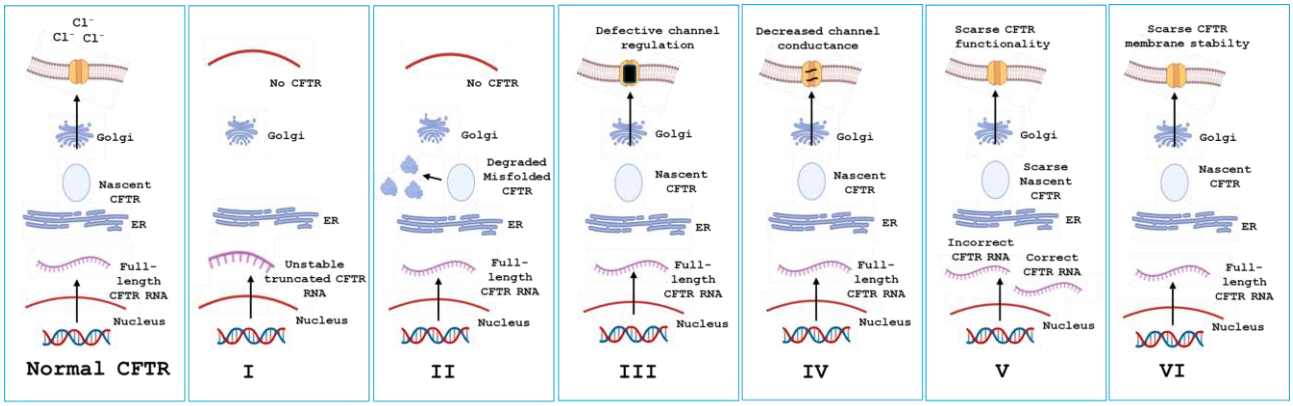

Figure 1.4. *CFTR mutation classes*. **Class I**: nonsense, frameshift, canonical splice; specific mutations: Gly542X, Trp1228X, Arg553X. **Class II**: missense, amino acid deletion; specific mutations: Phe508del, Asn1303Lys, Ile507del. **Class III**: missense, amino acid change; specific mutations: Gly551Asp, Gly178Arg, Gly551Ser. **Class IV**: missense, amino acid change; specific mutations: Arg117His, Arg347Pro, Arg117Cys. **Class V**: splicing defect, missense; specific mutations: 3849+10KbC→T, 2789+5G→A. **Class VI**: missense, amino acid change; specific mutations: 4326delTC, Gln1412X, 4279insA.

Despite differing mechanisms, all pathogenic CFTR mutations ultimately lead to deficient CFTR function, causing disrupted salt and water transport, thick mucus accumulation, impaired clearance, and increased infection risk. Increasing evidence underscores that class-specific mutation effects influence disease severity and treatment outcomes [115]. To better address this variability, the concept of theratyping has emerged [116]. This precision medicine approach uses functional assays combined with CFTR modulators to evaluate mutation-specific drug responsiveness, even for rare variants [117]. Accordingly, CFTR modulator therapies, including potentiators and correctors, have shown efficacy across multiple mutation classes [118], representing a major advance in personalized treatment for CF.

1.3. The treatment of Cystic Fibrosis disease

1.3.1. Multidisciplinary approach for treatment of CF

CF causes thick, sticky mucus that clogs the airways, leading to chronic inflammation, recurrent infections, and long-term damage such as bronchiectasis and lung parenchyma injury [10]. A persistent cough and daily sputum are hallmark symptoms. Respiratory treatment focuses on maintaining lung function and slowing disease progression [119].

Clearing that mucus is crucial. Airway clearance therapy (ACT) helps move mucus out of the lungs, reducing infection risk, improving breathing, and clearing airway blockages [10, 120-122]. The CFF recommends beginning ACT in infancy [119]. Most people with CF (pwCF) perform ACT at least twice daily, increasing frequency during pulmonary exacerbations (PEx), though ideal timing and duration remain uncertain [119, 123, 124]. Techniques of ACT include:

- Manual chest percussion and postural drainage (especially in infants)
- Autogenic drainage
- Positive expiratory pressure (PEP) and high-pressure PEP
- High-frequency oscillation vests
- Other vibrating or oscillating devices.

No single method has proven superior [119, 125] and older patients tend to favor self-administered options. Though ACT can offer short-term improvements in mucus clearance and lung function, quality evidence for long-term benefit is limited and often underpowered, especially in younger children [119, 123, 124]. Personalization based on age, needs, and preference is essential, and early training encourages consistency in daily care. Exercise supports ACT but should not replace it [125]. In CF, dehydrated airway surfaces hinder natural mucus removal. Mucolytic agents help by thinning mucus and reducing its stickiness, potentially reducing exacerbations and stabilizing lung function [126, 127]. Common options include:

- Dornase alfa (Pulmozyme®): a once-daily treatment that breaks down DNA in thick mucus. It's recommended for children ≥6 years by both the U.S. and European CF societies, and has shown benefits in lung function, LCI (lung clearance index), and reducing exacerbations in children under 12 [119, 125, 126, 128, 129]. A Cochrane review found dornase alfa may

improve percent predicted forced expiratory volume in one second (ppFEV1) more than hypertonic saline in moderate-to-severe cases after 3 months [130]

- Hypertonic saline (3–7%): an inhaled, low-cost therapy that hydrates airways to aid clearance. It is recommended for people over 6 [130, 131]. A study showed improved percent predicted ppFEV1 and fewer exacerbations with 7% saline in children over 6 [132], and recent trials suggest LCI improvement even in younger children and infants [133, 134]. However, a Cochrane review found no significant long-term lung function benefit over 48 weeks and highlighted better utility during acute exacerbations rather than as daily maintenance [130]
- Mannitol: a dry inhaled powder that draws water into the airways, helping to loosen mucus [135]. It's approved for adults with CF in UE, and for children aged ≥6 in Australia.

PwCF frequently develop acute pulmonary exacerbations, episodes of worsened respiratory symptoms (more cough, congestion, sputum), systemic effects like fatigue, malaise, or weight loss, along with lung exam findings (crackles), decreased ppFEV1 [136] and infections. Proactive infection control is crucial [137]. This includes regular respiratory cultures (sputum or throat swab) to detect pathogens early, and ensuring labs know the patient's CF status [10]. The types of pathogens change with age:

- in young children, common bacteria include *Haemophilus influenzae* and both methicillin-sensitive and resistant *Staphylococcus aureus*
- in adolescents and adults, opportunistic bacteria such as *Pseudomonas aeruginosa*, *Stenotrophomonas maltophilia*, *Achromobacter xylosoxidans*, and *Burkholderia cepacia complex* become more prevalent. *P. aeruginosa* often becomes dominant in adulthood and is linked to faster decline and increased mortality [10].

Early *P. aeruginosa* can sometimes be eradicated using inhaled tobramycin [138]. If chronic colonization occurs, defined by the modified Leeds criteria (positive cultures in >50% over 12 months, or three positive cultures over 6 months, each at least a month apart), long-term inhaled antibiotics like tobramycin, aztreonam lysine (Cayston), colistimethate sodium, or levofloxacin may be used alone or in rotation to reduce bacterial density, inflammation, and frequency of exacerbations [139-143]. Other pathogens of concern include members of the *Burkholderia cepacia* complex, nontuberculous mycobacteria (e.g., *Mycobacterium avium complex*, *M. abscessus*), and fungi such as *Aspergillus fumigatus*. CF patients may also develop allergic bronchopulmonary aspergillosis

(ABPA), a hypersensitivity reaction requiring corticosteroid treatment due to its detrimental effects on lung function [144].

CF involves a vicious cycle of infection and inflammation. Routine steroids (inhaled or oral) are not recommended unless there's a specific inflammatory condition like asthma or ABPA [119]. Instead, inflammation is usually managed with a high dose of Ibuprofen or Azithromycin [145]. Ibuprofen shows lung function benefits, but its use is limited by side effects and the need for monitoring, [146] whereas Azithromycin (taken three times weekly), although it improves lung function and reduces exacerbations, may encourage resistance in undetected mycobacterial infections, making screening necessary before treatment [119, 147]. While lung decline is a major complication in CF, poor growth often presents earliest due to a combination of reduced intake, malabsorption, and increased metabolic needs. Malnutrition significantly worsens CF outcomes (CFF recommendations: children should reach weight-for-length ≥50th percentile by age 2; children and adolescents (2–20 years) should maintain a body mass index (BMI) ≥50th percentile) [15, 148].

Persistent guidance on nutrition includes enteral feeding planning when needed [149]. Infants should be breastfed when possible, using standard formula otherwise. Salt supplementation (¼ teaspoon/day for 6 months) compensates for losses [15]. Fecal elastase testing for exocrine pancreatic function should occur after diagnosis, since ~85% of pwCF are pancreatic insufficient (fecal elastase <200 μg/g) [5]. Pancreatic Enzyme Replacement Therapy (PERT) is provided with every meal/snack for those diagnosed with insufficiency or known CFTR mutations linked to it. Doses of lipase typically range from 2,000 to 2,500 units/Kg per meal, up to a maximum of 10,000 units/Kg/day [150, 151]. Immobilized lipase cartridges may be used for continuous feeding. Excess dosing offers no benefit and can cause fibrosing colonopathy, a serious complication [152]. Adequate dosing supports growth [153]. CF also impairs the absorption of fat-soluble vitamins (A, D, E, and K):

- Vitamin A: deficiency can cause night blindness and skin issues [10]
- Vitamin D: deficiency contributes to rickets and bone weakness (goal 25-hydroxyvitamin D ≥30 ng/mL) [154]
- Vitamin E: can lead to neuropathy, muscle issues, haemolysis
- Vitamin K: deficiency causes clotting problems and bone disease [10].

Vitamin supplementation should begin promptly after diagnosis, with annual monitoring of vitamins A, D, and E [15].

A substantial understanding of the genetic basis of CF and its resulting pathophysiology has enabled the development of CFTR modulators, small molecules designed to correct and/or potentiate

dysfunctional CFTR protein, producing clinically meaningful outcomes with daily administration [155] (see paragraph 1.3.2). However, a significant unmet need remains for individuals with CF who cannot benefit from modulators due to specific CFTR variants, intolerable side effects, or limited access (accounting for 10%–20% of patients) [156, 157]. While modulator therapies can enhance trafficking and gating in minimal-function Class II–VI CFTR proteins, they are ineffective for individuals with Class I mutation, where no functional CFTR protein is produced. This group represents the most underserved segment of the CF population, typically experiencing the most severe disease. For these patients, gene therapy, introducing a functional CFTR gene into target cells, offers a potential therapeutic solution. Despite the identification of the CFTR gene over three decades ago, CF gene therapy has yet to progress beyond clinical trials, primarily due to challenges in achieving sustained efficacy and long-term improvements in lung function. Nonetheless, recent advancements in understanding CFTR expression and function in relevant cell types, novel delivery strategies targeting airway cells, and more sensitive clinical measures, particularly in young children and patients with milder disease who may benefit most from early intervention, are promising developments toward a clinically viable gene therapy.

CF has long been considered an ideal candidate for gene therapy since the discovery of its genetic cause in 1989 [158, 159]. The lungs, being relatively accessible, are particularly suitable for gene therapy delivered via inhalation or bronchoscopy, approaches that could directly address the most severe manifestations of the disease and extend life expectancy. However, over 20 clinical trials aimed at delivering genetic material to airway epithelial cells using modified or synthetic vectors have failed to reach therapeutically meaningful expression levels [160]. These shortcomings are largely due to factors such as insufficient potency, lack of cell specificity, and the presence of CF-specific mucosal and immune barriers. Earlier lung-directed gene therapies were administered as liquid boluses to the airway epithelium via nasal infusion or bronchoscopy [161, 162]. More recently, aerosol delivery has been optimized to generate smaller droplets capable of reaching the distal lung regions using nebulizers [163-165]. This technique has been employed in testing both viral and non-viral gene therapy vectors for CF. Nevertheless, barriers persist, including mucus obstruction and limited access to basal progenitor cells or basolateral receptors. To address this, chemical conditioning agents such as lysophosphatidylcholine and polidocanol, as well as physical disruption techniques, have been used to enhance transduction in animal models. However, their clinical applicability remains limited due to safety concerns, particularly the risk of facilitating systemic entry of antibiotic-resistant bacteria [166, 167].Even when transduction is successful, low-level expression of the CFTR transgene can limit therapeutic benefit. Proteasome inhibitors like doxorubicin have shown potential to enhance gene transfer and expression when combined with viral or non-viral

vectors. Though the precise mechanisms remain unclear, improvements may stem from enhanced viral uncoating, increased nuclear translocation, improved second-strand synthesis, or reduced degradation of recombinant proteins. Another challenge in gene delivery is the immune response, which may be mitigated by co-administering corticosteroids such as prednisone. Steroids can be administered before, during, or after gene therapy dosing, particularly in response to elevated liver enzymes, a common issue with systemic delivery. While preclinical studies suggest that prophylactic corticosteroids may enhance transduction and transgene expression with systemic delivery [167], it remains uncertain whether the same holds for lung-directed gene therapy. Pulmonary exacerbations remain a concern for pwCF and may be triggered by gene delivery vectors. However, the clinical utility of corticosteroids in managing such exacerbations is still debated [168]. It is also possible that CFTR gene therapy may be administered alongside existing modulator treatments. This could be due to ethical concerns around discontinuing effective therapies or to achieve additive benefits through complementary mechanisms. Since CFTR modulators act systemically while gene therapy would primarily target the lungs, patients with suitable mutations may prefer to continue modulators to manage extra-pulmonary symptoms. To date, CF gene therapy has shown encouraging signs of temporary stabilization or modest improvement in lung function [160, 169], but has yet to demonstrate sustained, long-term efficacy.

Figure 1.5 summarizes the multidisciplinary approaches to treat Cystic Fibrosis described above.

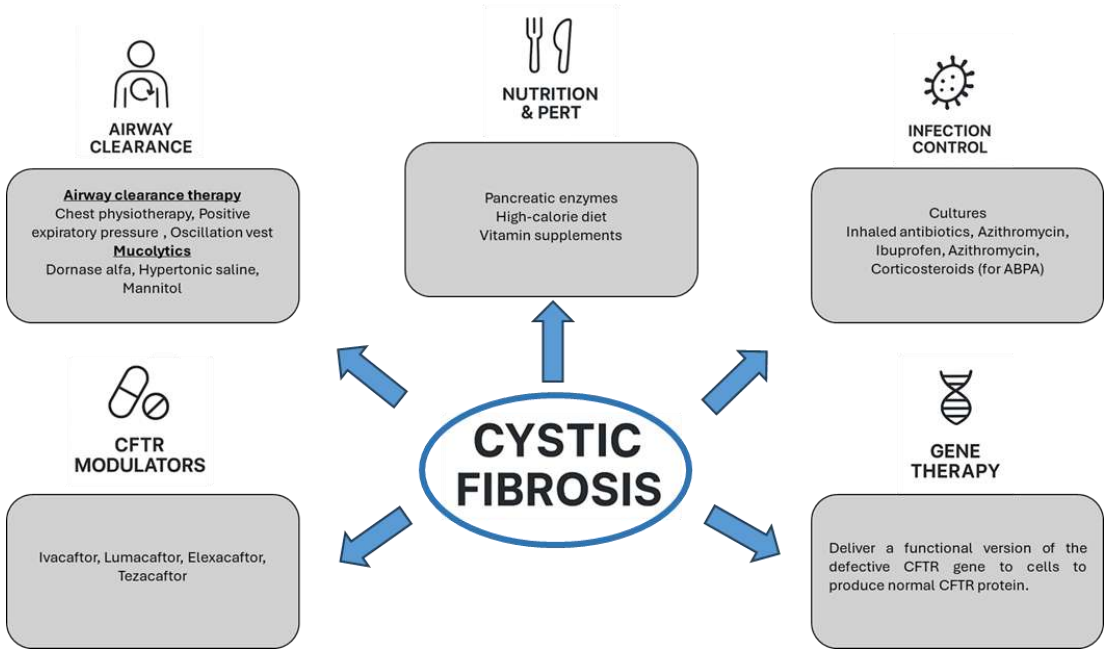

Figure 1.5. *Schematic representation of multidisciplinary approaches for Cystic Fibrosis clinical treatment.*

1.3.2. CFTR modulator therapy

Until the early 2010s, the standard of care for pwCF focused on a multidisciplinary approach to slow the progression of lung disease. This included the use of inhaled and/or systemic antibiotics, physiotherapy and/or inhaled mucoactive drugs to enhance mucus clearance, nutritional interventions such as pancreatic enzyme replacement and specific diets, and the treatment of CF-related complications [170] (as reported in paragraph 1.3.1). In the past decade, the landscape of CF management has been transformed by the introduction of small molecules known as CFTR modulators, which partially restore the function of the defective CFTR protein. These therapies, while not curative, offer substantial disease-modifying benefits and represent the current best therapeutic option for individuals with responsive CFTR mutations. Based on their mechanisms of action, CFTR modulators are classified into different categories: potentiators, which enhance ion transport through CFTR channels already present on the apical membrane and are effective in patients with Class III and IV gating mutations; correctors, which improve CFTR folding, processing, and trafficking to the cell surface and are effective in Class II mutations; amplifiers, which increase CFTR mRNA expression and protein synthesis; read-through agents, which promote ribosomal bypass of premature termination codons (PTCs) associated with Class I mutations to increase full-length CFTR protein production; NMD suppressors, which inhibit nonsense-mediated mRNA decay; and stabilizers, which increase the stability of CFTR protein at the plasma membrane [171, 172].

Currently, four CFTR modulators are approved for their use in therapy: Ivacaftor (IVA or VX770), Lumacaftor (LUM or VX809), Tezacaftor (TEZ or VX661), and Elexacaftor (ELX or VX445) (Figure 1.6). IVA, a potentiator (commercially available as Kalydeco®), improves CFTR channel gating in patients with gating mutations by increasing channel opening frequency and ion conductance [173, 174]. Initially approved for patients with at least one G551D mutation, IVA demonstrated significant improvements in respiratory symptoms, lung function, and weight gain in both adolescents and children aged 6 to 11 [175-177]. Additional studies led to the approval of IVA for other gating and residual function mutations [178, 179]. Despite initial optimism, the DISCOVER trial showed that IVA had no impact on lung function or exacerbation rates in patients homozygous for the F508del-CFTR mutation [180]. However, real-world data demonstrated that IVA benefits are sustained over time, with improved survival, reduced frequency of exacerbations, and lower prevalence of lung transplantation, *Pseudomonas aeruginosa*, and *Staphylococcus aureus* [181-185]. Longitudinal studies also indicated that early initiation of IVA yields better long-term outcomes [186]. Following IVA's success, the development of CFTR correctors became a priority.

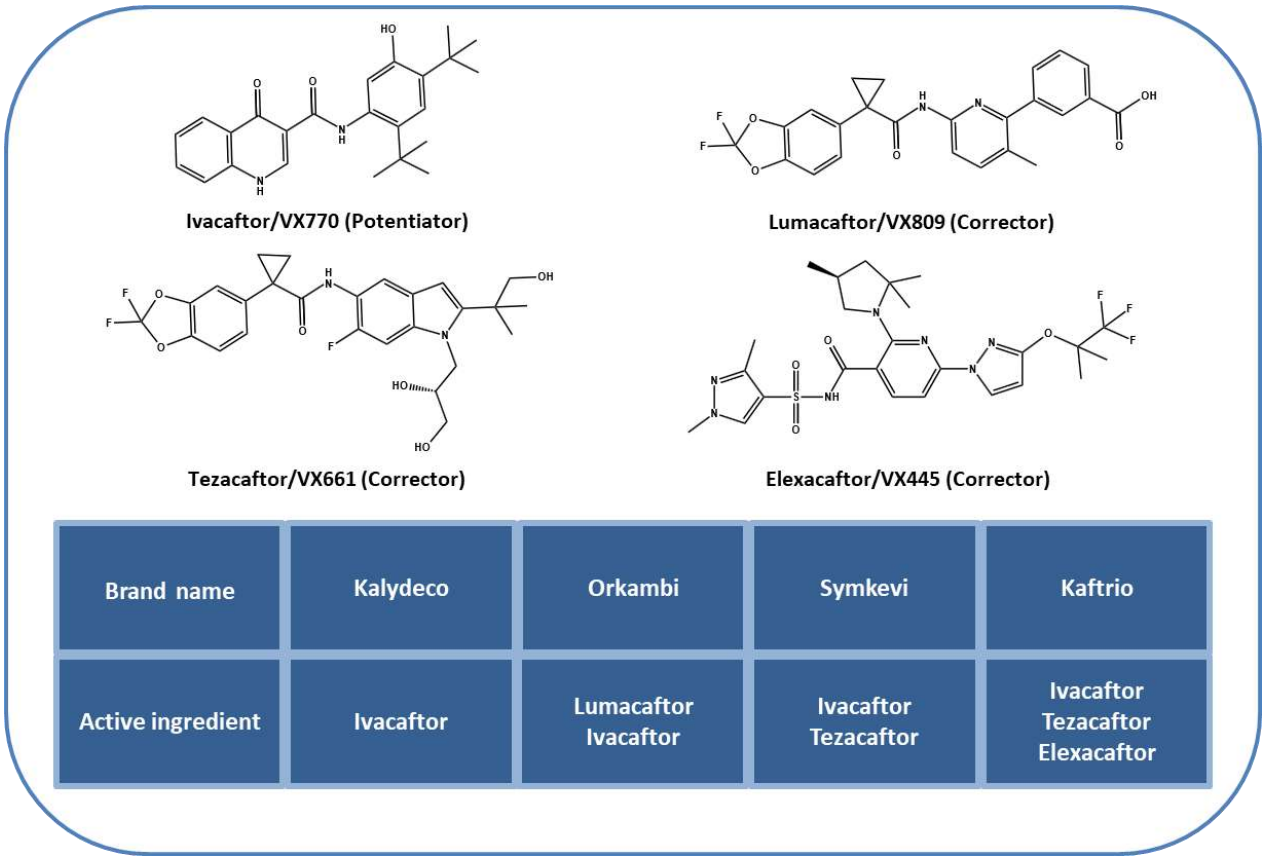

Brand name	Kalydeco	Orkambi	Symkevi	Kaftrio
Active ingredient	Ivacaftor	Lumacaftor Ivacaftor	Ivacaftor Tezacaftor	Ivacaftor Tezacaftor Elexacaftor

Figure 1.6. *Currently approved modulators for clinical therapy of CF.*

LUM, TEZ, and ELX are correctors whose mechanisms, better described in paragraph 1.3.3, are believed to improve protein folding, trafficking, and stability. Correctors are typically used in combination with IVA to address both folding and gating defects, especially in patients with the F508del-CFTR mutation. Both LUM/IVA (commercially available as Orkambi®) and TEZ/IVA (commercially available as Symkevi®) combinations are approved for individuals homozygous for F508del-CFTR [187, 188], and TEZ/IVA is also approved for patients with one F508del-CFTR mutation and a residual function mutation [189].

The triple combination ELX/TEZ/IVA (commercially available as Kaftrio® or Trikafta®) was approved in 2020 for patients aged 12 years and older who are either homozygous for F508del-CFTR or carry one F508del-CFTR mutation combined with a minimal function, gating, or residual function mutation [190-192]. About 90% of pwCF carry at least one F508del-CFTR mutation and are eligible for ELX/TEZ/IVA, which has demonstrated superior efficacy in improving lung function, reducing exacerbation rates, increasing body weight, and enhancing quality of life [174, 193-195]. In contrast to the significant improvements seen with IVA in gating mutations, the clinical benefits of LUM/IVA and TEZ/IVA were more modest. Worldwide studies showed higher discontinuation rates

for LUM/IVA (18.2–24%) due to respiratory adverse events, particularly in patients with advanced disease, compared to clinical trials where discontinuation was 5% or less [156, 196, 197]. These adverse effects were more pronounced with LUM than with TEZ [198]. Although LUM/IVA and TEZ/IVA were effective for F508del-CFTR homozygous individuals, variability in clinical response and limited benefit in those with advanced lung disease highlighted the need for better therapies [199]. Furthermore, these combinations were ineffective in patients heterozygous for F508del-CFTR with a minimal function mutation [195], leading to the development of next-generation correctors such as ELX. TEZ was favoured over LUM for its better pharmacokinetic and safety profile, including lower CYP3A activation and fewer pulmonary side effects [200].

The triple combination ELX/TEZ/IVA demonstrated the most substantial clinical benefits to date: in patients homozygous for F508del-CFTR, ppFEV1 improved by 10% points, and symptoms were significantly reduced [190]; in patients with one F508del-CFTR and a minimal function mutation, a 14-point increase in ppFEV1 and significant symptom relief were observed. Pulmonary exacerbation rates fell by 60% [191], with similar findings in open-label extension studies and randomized controlled trials [201, 202]. Patients with advanced lung disease showed comparable improvements: ppFEV1 increased by 15.1 points, body weight by 4.2 Kg, and the need for oxygen therapy, non-invasive ventilation, and enteral feeding dropped by 50%, 30%, and 50%, respectively. A concurrent decrease in lung transplants was also observed [203]. Martin et al. confirmed these findings, showing that many patients previously listed for transplant no longer met the criteria after one year of treatment, along with reduced healthcare resource utilization [204, 205]. The PROMISE study, conducted across 56 U.S. CF Foundation Therapeutics Development Network sites, reported similar benefits in ppFEV1 and BMI, even among patients previously treated with other modulators [205, 206].

The use of CFTR modulators has been expanded to younger children: IVA is now approved for infants as young as 4 months with gating or residual function mutations [206], while LUM/IVA and TEZ/IVA are approved for children aged 2 and 6 years and older, respectively, who are homozygous for F508del-CFTR [207-209]. A multicentre phase 3 study of ELX/TEZ/IVA in children aged 6-11 showed improvements in ppFEV1 and lung clearance index [210], findings that were confirmed by a placebo-controlled trial in children with one F508del-CFTR and a minimal function mutation [211].

Another study demonstrated greater benefit from ELX/TEZ/IVA compared to either IVA alone or TEZ/IVA in patients with F508del-CFTR combined with gating or residual function mutations [193]. In the United States, the FDA (Food and Drugs Administration) has expanded approval of ELX/TEZ/IVA to pwCF aged ≥6 years with at least one responsive mutation based on in

vitro data, resulting in approval for 178 mutations [212]. Europe has not yet adopted this strategy. CFTR modulators have shown significant effects beyond the lungs. Pancreatic insufficiency, which begins in utero in severe mutations [213], has not been reversed in older patients, but initial treatment with IVA has improved fecal elastase-1 in young children [206, 211], with benefits maintained for up to 84 weeks [209]. Case reports of similar outcomes with LUM/IVA further support early initiation [214-216]. While IVA may reduce pancreatitis in those with residual pancreatic function [217, 218], cases of pancreatitis following modulator initiation have also been reported. Although CFRD increases with age, IVA use may reduce its incidence [219, 220], and LUM/IVA and ELX/TEZ/IVA have also shown improved glycemic profiles in small studies [221-224], though many patients remain insulin-dependent. Improvements in chronic rhinosinusitis and nasal polyps have been noted with IVA and ELX/TEZ/IVA but not with LUM/IVA or TEZ/IVA [175-177, 225-229]. Modulators are associated with weight and BMI gains [187-191, 210, 230], with ELX/TEZ/IVA increasing both fat-free and fat mass [231]. However, new concerns include obesity and cardiovascular risk factors such as hypertension and hypercholesterolemia [232-236], prompting calls to revise dietary guidelines. Liver disease may also benefit from IVA and LUM/IVA [235-237], though evidence is limited, and two ongoing trials (RECOVER and PROMISE) are assessing ELX/TEZ/IVA effects [237]. Fertility has increased, particularly in women, with over 600 pregnancies reported in 2020 compared to fewer than 200 per year previously [238-240]. Maternal and neonatal outcomes are encouraging [239, 240], and neonatal benefits have been observed in infants exposed to modulators in utero or through breastfeeding [241].

Although the currently approved CFTR modulators, particularly IVA and ELX/TEZ/IVA, have demonstrated therapeutic benefits, they do not fully restore CFTR function in the lungs and other affected organs. Moreover, not all pwCF have access to drug therapies with ETI and other approved modulators, e.g. patients carrying CFTR "orphan mutations". Those mutations (such as G551D, S13F, R31C, G85E, E92K, V520F, M110K, N1303K) are extremely rare and lack sufficient clinical, functional, or epidemiological data to allow clear classification of their pathogenicity or response to CFTR-modulator therapy.

In general, there is a high degree of variability in response to ELX/TEZ/IVA treatment [242], for reasons that are not yet fully understood, and some of which are listed below.

CFTR modulators, in particular ELX for its hydrophobic structure, require the intake of fat with the diet to ensure proper absorption: insufficient fat intake due to the presence of restrictive or avoidant eating disorders, which have been reported in up to 13.5% of adolescents and young adults with CF [243] can lead to reduced bioavailability and subtherapeutic drug levels, thus compromising the overall efficacy of the therapy. Additionally, these drugs (mostly IVA) are metabolized by the

cytochrome P450 enzymes CYP3A4 and CYP3A5, which can be inhibited by several medications commonly co-administered in pwCF [244]. Therefore, this aspect may limit the therapeutic efficacy of such drugs. Moreover, the CFTR modulators themselves can affect the metabolism of other medications, thus causing side effects. For example, LUM has been shown to alter concentrations of CYP3A and P-glycoprotein (P-gp) substrates [245].

It has been described that most CF patients involved in clinical trials with the FDA-approved CFTR modulators reported adverse events (AE) [155, 190]. Most of these AE were mild or moderate in severity and consistent with CF symptoms or common pediatric infections. To evaluate these possible side effects, careful monitoring during CFTR modulator therapy is necessary, especially of liver function, as elevated transaminases have been observed in approximately 10–26% of children [246] and 5% of adults [247] undergoing ELX/TEZ/IVA therapy. Some studies have also shown that ELX/TEZ/IVA can significantly increase serum cholesterol levels by enhancing its absorption, as evidenced by the correlation between serum cholesterol and phytosterol levels [248, 249]. These metabolic changes, along with the rising prevalence of overweight and obesity in pwCF (from 10% to 21% in children and from 18% to 42% in adults) [250] could increase the risk of comorbidities, such as metabolic disorders and cardiovascular disease, especially with chronic use in the pediatric population. Finally, although rare, some serious adverse events have also been reported, such as increased intracranial pressure [246, 251], neuropsychiatric effects on mental health [252, 253], drug reactions with eosinophilia and systemic symptoms (DRESS), musculoskeletal lesions, or severe thrombocytopenia [254].

1.3.3. Classification of correctors

As already mentioned in paragraph 1.3.2, correctors are used in combination with potentiators, which target the channels once they reach the membrane. They are small molecules that directly bind to and enhance the conformational stability of the CFTR, allowing it to pass through the Endoplasmic Reticulum Quality Control System smoothly and facilitating its trafficking to the cell membrane [255].

Correctors have been classified into three categories based on their mode of action: type I correctors that stabilize the NBD1-TMD1 and NBD1-TMD2 interfaces, type II correctors that target NBD2, and type III correctors that directly stabilize NBD1 [256]. The structures of some Type I correctors developed so far are reported in Table 1.1.

In a high-throughput screening of 164,000 compounds, Van Goor et al. identified the quinazolinone corrector VRT-325 (Table 1.1), which improved trafficking of F508del-CFTR (EC_{50}:

3.3 μM) [257]. VRT-325 appears to bind directly to CFTR at the NBD1 region and promotes stabilization of the NBD1-TMD1/TMD2 interface, thereby partially recovering inter-domain interactions [258-261]. However, at elevated concentrations, the compound suppresses chloride currents, acting as an inhibitor of CFTR gating [262]. These limitations prevented its advancement into clinical development. Subsequent optimization efforts by Vertex Pharmaceuticals led to VRT-768, which increased F508del-CFTR maturation 2.5-fold (EC_{50}: 16 μM) and enhanced chloride transport (EC_{50}: 7.9 μM) in Fisher Rat Thyroid (FRT) cells compared with vehicle controls.

Table 1.1. *Structure of type I correctors developed.*

Type I Correctors	
Compound	Structure
VRT325	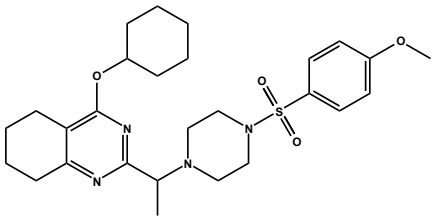
VRT768	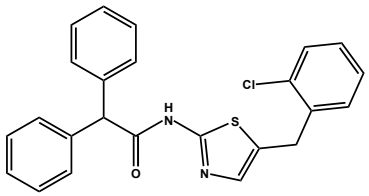
Lumacaftor (VX809)	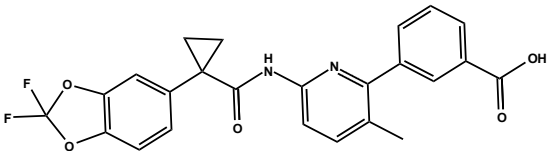
Tezacaftor (VX661)	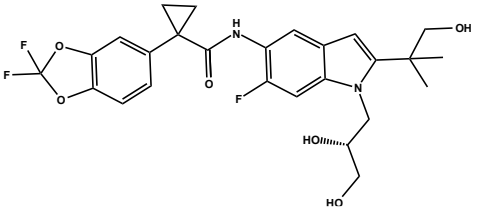
ABBV-2222 (Galicaftor)	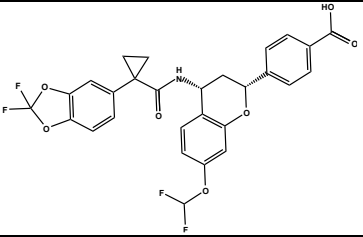

ARN23765	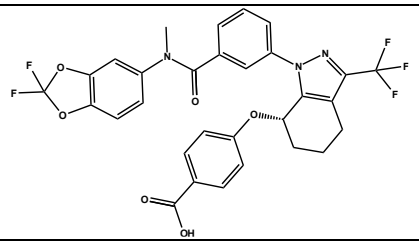
b2	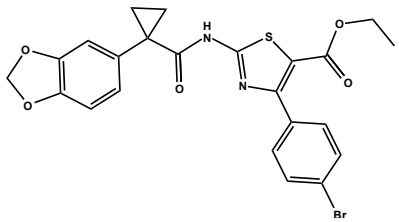

Retention of the central amide group in VRT-768, combined with systematic modification of the amine and carboxylic acid moieties, resulted in Lumacaftor (LUM or VX809), featuring a 1-(benzo[d][1,3]dioxol-5-yl)cyclopropane-1-carboxamide (BCC) head group [263]. VX809 displayed superior potency relative to VRT-768, correcting F508del-CFTR folding defects and boosting chloride conductance. In human bronchial epithelial cells derived from patients homozygous for F508del-CFTR, VX809 improved ER processing and restored chloride secretion to ~14% of non-CF levels (EC_{50}: 81 nM).

VX809 also produced additive benefits when combined with Corr-4a or VRT-325, consistent with distinct binding sites [264]. Cryo-EM studies established that VX809 targets TMD1. The BCC head inserts into hydrophobic cavities within TMD1, while its variable substituents engage lipid molecules. The head group fits the pocket in a “lock-and-key” manner, stabilizing partially folded TMD1 during domain assembly and reinforcing the membrane integration of transmembrane helices [265-267]. VX809 also enhances CFTR trafficking to the plasma membrane and shows selective benefits for different CFTR mutations [268] . Its co-administration with Ivacaftor (IVA or VX770) produces synergistic effects, and the dual regimen is marketed as Orkambi®, the first FDA-approved therapy addressing the underlying defect caused by F508del-CFTR in patients ≥12 years [269]. In Phase III trials, Orkambi® improved ppFEV1 by 2.6–4.0% from baseline at week 24 and reduced pulmonary exacerbation rates by 30–39% in patients homozygous for F508del-CFTR. Dosing schedules involved once- or twice-daily VX809 with VX770 given twice daily (NCT01807923, NCT01807949). However, VX809 induces CYP3A4, creating a risk of drug–drug interactions [270], and is not available as monotherapy (NCT00865904).

Another type I corrector developed by Vertex Pharmaceuticals is Tezacaftor (TEZ or VX661), which also features a BCC head, binds at the same TMD1 site as Lumacaftor, as confirmed by cryo-EM [265]. When combined with VX770, VX661 demonstrated a more favourable safety profile, causing fewer side effects compared with VX809 [188, 271]. In Phase III testing, the VX661/VX770

combination showed efficacy but was not significantly superior to VX770 monotherapy; the least-squares mean ppFEV1 improvement versus VX770 alone at week 8 was 0.3 percentage points (NCT02412111) [272]. Greater benefit was observed in triple therapy regimens that included VX661, VX770, and VX445 (Kaftrio® or Trikafta®), which provided superior clinical outcomes compared with earlier combinations [191, 273, 274].

ABBV-2222 (GLPG-2222, Galicaftor) was designed by retaining the BCC scaffold while screening modifications at the amine position. A 2-phenylbenzodihydropiperan derivative emerged as the lead compound, and SAR studies highlighted the importance of para-substitution on the distal phenyl ring for potency. Compared to VX809, Galicaftor showed much higher potency (EC_{50}: 5 nM) with similar efficacy, along with low clearance across preclinical species and minimal CYP interaction, suggesting reduced risk of drug–drug interactions [275]. Despite good tolerability, however, clinical trials failed to demonstrate improvements in lung function (NCT03045523, NCT03119649). A trial of ABBV-2222 with the potentiator ABBV-3067 has since been terminated (NCT03969888) [276].

Another notable type I corrector is ARN23765, a tetrahydroindazole derivative first reported by Fondazione FIBROSI CISTICA and now under development by Sionna Therapeutics. It is exceptionally potent (EC_{50}: 38 pM), highly suitable for combination regimens, and exhibits durable corrective effects. Structurally, ARN23765 retains the benzo[d][1,3]dioxole motif of BCC but incorporates a reversed amide configuration with a shortened carbon linker, positioning the amide nitrogen directly at the 5-position of the benzene ring [277].

A Quantitative structure-activity relationship (QSAR) analysis by Millo et al., based on F508del-CFTR correctors, informed the design of hybrid molecules combining the BCC group of Lumacaftor with the aminoaryl thiazole (ATT) scaffold of type II correctors. In CFBE41o- bronchial cells expressing F508del-CFTR, several hybrids displayed strong corrective activity. Compound b2 surpassed Lumacaftor in potency (EC_{50}: 0.087 μM and 0.3 μM, respectively) [278]. Co-treatment with Lumacaftor produced no additive benefit, consistent with a shared binding site involving the benzodioxole unit.

Unlike the correctors mentioned above, Corr-4a, developed by Pedemonte (through the screening of approximately 150,000 compounds), falls within corrector class II (Table 1.2). It is a bis(aminomethyl)bithiazole corrector [279]. It directly associates with F508del-CFTR, improving its folding and trafficking to the plasma membrane. This action increases channel density at the cell surface and produces a more substantial recovery of chloride currents compared to cryo-salvage. In addition, Corr-4a enhanced CFTR-dependent chloride secretion up to 8% when compared to non-cystic fibrosis epithelia [260, 279]. Although Corr-4a has been suggested to interact with both NBD2

and the transmembrane domains, its precise site of binding and mechanism of action remain unresolved [261, 280, 281].

From the same screening campaign, Corr-2b was identified as another lead compound, belonging to the amino-aryl thiazole (ATT) family of correctors [279].

Besides its corrective effect, some ATT derivatives, such as EN277I, also act as potentiators of class III CFTR mutants. In G1349D-CFTR cells, prolonged EN277I treatment markedly improved channel activity, leading to frequent simultaneous multichannel openings. Specifically, EN277I enhanced the open probability of CFTR channels by nearly 25-fold and tripled the apparent channel number [84]. Early molecular docking predicted two binding sites for Corr-2b within CFTR NBD1, which could account for both its corrective and potentiating activities [282, 283].

Table 1.2. *Structure of type II CFTR correctors*.

Type II Correctors	
Compound	Structure
Corr-4a	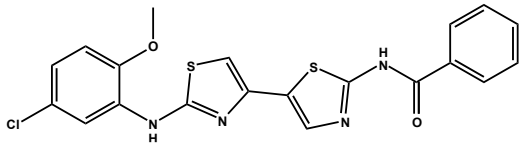
Corr-2b	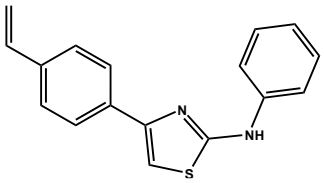
EN277I	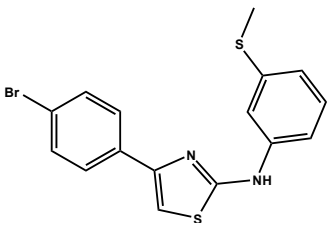

ATT-4a (FCG)	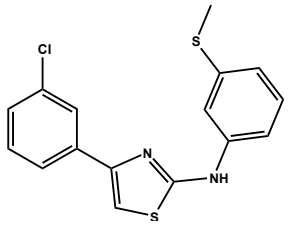
3151	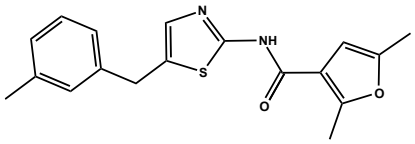

To probe structure-activity relationships, a series of EN277I analogues was generated. ATT-like correctors were subdivided into three structural components: the aminothiazole core, the substituent at C-4, and the substituent at N-2. Since modifications to the latter two regions were less feasible, most efforts focused on altering the phenyl group at the thiazole 4-position. Replacing the para-bromine on the phenyl ring with chlorine at the meso-position yielded FCG (ATT-4a; EC_{50}: 5.3 μM), whereas substituting bromobenzene with a 2-thiophene group gave rise to ATT-9d (EC_{50}: 8.5 μM) [283]. Both showed enhanced correction of F508del-CFTR and displayed some potentiation. In Human highly transfectable embryonic kidney (HEK-t) cells, FCG not only elevated the total expression of F508del-CFTR but also promoted its maturation [284]. Although initial docking studies suggested binding of ATT-like correctors within an NBD1 pocket [283], more recent biochemical analyses indicated that FCG interacts with NBD2. Virtual docking further predicted binding at the same NBD2 site as Corr-4a (PDB ID: 6UK1) [284], providing a rationale for the stabilization of NBD2 by type II correctors. Moreover, Lukacs et al. identified an aminothiazole compound type II corrector, named 3151 (EC_{50} 4.2 μM in CFBE41o- cells), with structural similarity to the investigational type II correctors C4 and D-01 that require NBD2 for corrector action [256, 279, 285].

Type III correctors, on the other hand, are molecules that directly stabilize NBD1 and thereby facilitate the maturation of F508del-CFTR (in Table 1.3 some of them developed are reported). The first examples of this group were 5-bromoindole-3-acetic acid (BIA) and its analogue 5-bromo-4-ethoxyindole-3-acetic acid (BEIA), both of which require concentrations above 0.5 mM to be effective [286]. In a screen of 600,000 compounds, Veit et al. identified pyrazole-like correctors, with compound 4172 as a representative hit. In CFBE41o- cells, 4172 corrected F508del-CFTR function with an EC_{50} of 3.1 μM. These pyrazole analogues restored CFTR activity both independently and in combination with Lumacaftor, by binding CFTR directly and stabilizing NBD1 [287].

Subsequently, Vertex Pharmaceuticals developed "next-generation correctors" such as VX445 and Bamocaftor, which act synergistically with VX661 and VX770. Even though other groups demonstrated that VX445 interacts with TMD2 of CFTR, suggesting that it may have different binding sites [288, 289], it has been proposed as a type III corrector due to its ability to stabilize NBD1 [290, 291] and its additive/synergistic effect on F508del-CFTR functional rescue [292]. Triple-combination regimens demonstrated superior in vivo efficacy compared with Orkambi® [192, 273, 293, 294]. In a Phase III study, patients receiving VX445 (200 mg qd) with VX661 (100 mg qd) and VX770 (150 mg q12h) showed a reduction in sweat chloride by 46.2 mmol/L, compared with only 3.4 mmol/L for the VX661/VX770 group. This triple therapy (Kaftrio® or Trikafta®) has been FDA-approved for patients ≥12 years carrying at least one F508del-CFTR allele [191].

Table 1.3. *Structure of the type III correctors.*

Type III Correctors	
Compound	Structure
BIA	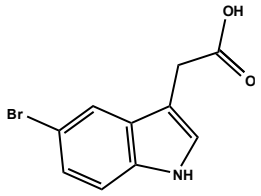
4172	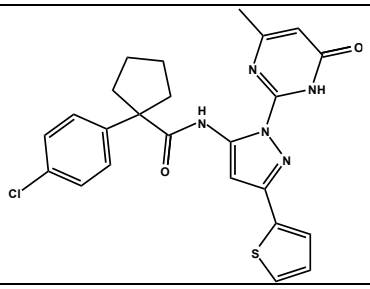
Elexacaftor (VX445)	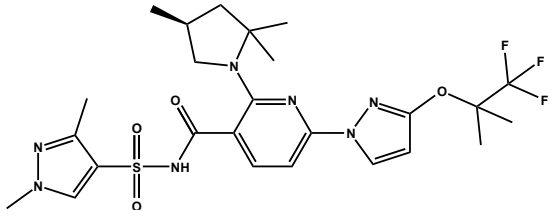
Bamocaftor (VX659)	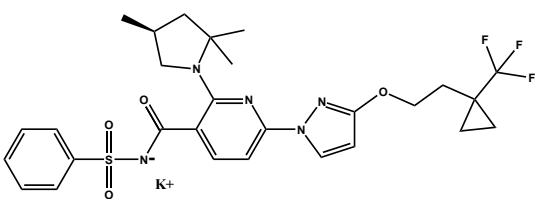

Vanzacaftor (VX121)	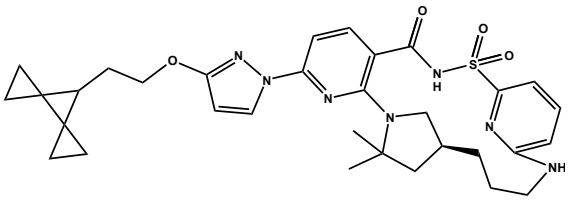
PP028	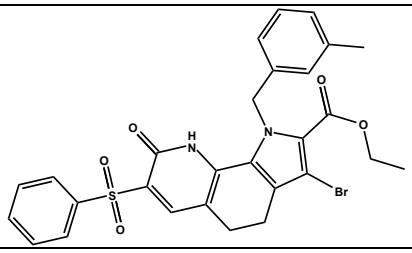

In homozygous HNE, the combination of VX661 and VX445 restored chloride channel activity to ~62% of wild-type CFTR when VX770 was also present [290, 295]. This partial rescue likely reflects the potentiating effect of VX445 in addition to its corrective role. Notably, VX445 also enhances the channel function of class III mutants, such as G551D [288, 289]. Cryo-EM studies revealed that VX445 binds at a distinct site from VX661, engaging TM11 of the pyrazole-sulphonamide region through electrostatic and van der Waals interactions, and making contacts with TM2, TM10, and the lasso motif. These interactions stabilize the NBD1–TMD interface [291], consistent with its designation as a type III corrector. Structurally related compounds, Bamocaftor and Vanzacaftor, fall into the same class. However, clinical trials testing Bamocaftor in combination with VX661 and VX770 were discontinued (NCT03460990, NCT03447262, NCT03447249, NCT03633526). Vanzacaftor, which contains a macrocyclic arylamino–methylpyrrolidine structure, is currently in Phase III trials in combination with VX661 and Deutivacaftor (NCT05444257).

Another type III molecule, PP028 (a tricyclic pyrroloquinoline derivative), displayed strong synergy with LumacaftorVX809 and VX661 (EC_{50}: 1.1 μM), but not with VX445, and antagonized the effect of 4172, supporting its classification within this group [296].

1.3.4. The HSP family and their role in CF

Proteins do not always attain their correct three-dimensional conformation on their own. To achieve proper folding and functional activity, they rely on molecular chaperones, specialized proteins that operate within the broader chaperone system, a complex cellular network dedicated to ensure correct protein folding and function. These chaperones are vital for maintaining protein homeostasis (proteostasis) by guiding the folding process, preventing incorrect configurations, and facilitating the refolding of misfolded proteins when needed [297, 298]. In collaboration with the

ubiquitin-proteasome system, they form the cellular quality control machinery, which detects improperly folded proteins and directs them toward degradation pathways. Misfolded proteins can interact aberrantly, forming aggregates that can be toxic to cells. Alternatively, the ubiquitin-proteasome system may degrade these defective proteins, preventing them from reaching their designated cellular compartments. Such failures in protein folding and degradation are associated with a group of disorders known as proteinopathies, which include neurodegenerative diseases like Huntington's, Parkinson's, Alzheimer's, and Creutzfeldt-Jakob diseases, as well as metabolic and inherited disorders such as Gaucher's disease and CF [299]. Molecular chaperones function as part of multi-component assemblies, interacting with each other and with various cofactors. The chaperone system comprises core chaperones, co-chaperones, receptors, and chaperone-interacting proteins [300, 301].

A significant subset of molecular chaperones includes Heat Shock Proteins (HSPs), which are upregulated in response to various cellular stresses, including heat shock. HSPs are classified into families based on their molecular mass in kilodaltons (kDa), encompassing small HSPs (15–30 kDa), Hsp40, Hsp60, Hsp70, Hsp90, and Hsp100 [302]. Therapeutic strategies aimed at modulating chaperone systems, particularly HSP networks, form the basis of pharmacological chaperone therapy, which has been investigated in cancer, neurodegenerative, and inflammatory diseases [303-305]. Notably, targeting HSPs represents a promising avenue for managing airway disorders, including CF, where overexpression of certain HSPs, such as Hsp90, Hsp70, and Hsp60, has been observed in affected lung tissues, particularly in relation to the misfolded CFTR–protein. HSPs are essential elements of the protein quality control (PQC) system within cells and play a crucial part in the biosynthesis of wild-type CFTR.

The PQC machinery can drive CFTR either toward proper folding and maturation or toward degradation, depending on which pathway predominates. Both wild-type CFTR and its mutant form fail to fold efficiently (up to 70% for the wild-type protein and an even higher proportion for mutant CFTR), being eliminated via ERAD [306]. HSPs can significantly influence this outcome. For example, Hsc70, in conjunction with the Hsp40 co-chaperone Hdj-2, has been shown to assist in the early stages of CFTR folding [307]. In contrast, the Hsc70–CHIP complex plays a role in CFTR ubiquitination, promoting its degradation [308]. The duration of interaction between Hsp70 and CFTR may also affect whether the protein is marked for degradation [309]. Other members of the Hsp40 family, such as cysteine string protein (Csp/DNAJC5) and DNAJB12, have also been implicated in CFTR degradation, as demonstrated in yeast models [310, 311]. On the other hand, Hsp90 is required for the correct folding of CFTR; when it is absent, CFTR cytosolic domains fail to assemble correctly, resulting in degradation early in the protein life cycle [52].

Using proteomic analyses, Balch and colleagues explored the CFTR "interactome," highlighting differences in how cochaperones associate with wild type (WT) versus mutant CFTR. One key finding was that the Hsp90 cochaperone Aha1, which stimulates Hsp90's ATPase activity, might act in a pro-degradative manner by disrupting the Hsp90-CFTR interaction, leaving CFTR unprotected and susceptible to degradation [312]. Balch's team proposed a multi-step model for CFTR folding. Initially, Hsc70 and Hsp40 recognize and bind the newly synthesized CFTR to prevent early misfolding. The cochaperone HOP then links this complex to Hsp90 in its ADP-bound form. Next, p23 joins the complex in the presence of ATP, displacing Hsc70, Hsp40, and HOP, and forming the mature Hsp90–p23–CFTR complex. This complex undergoes ATP hydrolysis cycles, promoting proper folding and maturation of CFTR. Expression levels of cochaperones such as FKBP8 and p23 appear to influence whether CFTR achieves a functional state or is targeted for degradation [312]. While Hsp60 is less well-studied in this context, it has been identified in the CFTR interactome. Interestingly, it is upregulated in IB3.1 cells that have undergone chemical or genetic rescue [313], suggesting a potential, though yet unconfirmed, role in CFTR processing. As such, therapeutic agents capable of modulating the folding, stabilization, and degradation of CFTR may hold promise for addressing the unmet clinical needs of complex disorders like CF.

Efforts to restore CFTR function have led to the development of small-molecule modulators. Over the past decade, substantial progress has been made in identifying CFTR-targeted compounds, culminating in the approval of potentiators like Ivacaftor and correctors such as Tezacaftor, Elexacaftor, and Lumacaftor, as well as combination therapies like Orkambi® and Trikafta® [255, 296, 314-320] (see paragraph 1.3.2). In this therapeutic landscape, targeting molecular chaperones (especially Hsp70 and Hsp90) may represent an alternative or complementary strategy, given their central roles in CFTR folding, stability, and intracellular trafficking.

1.3.5. Hsp70 modulators in CF

The Hsp70 chaperone system comprises 13 isoforms, including the constitutively expressed heat shock cognate 70 (Hsc70), glucose-regulated protein 78 (GRP78, also known as Bip or HspA5), the stress-inducible form Hsp70 (Hsp72 or HspA1), and mortalin (GRP75 or HspA9) [321]. These isoforms are distributed in distinct cellular compartments based on their roles: Hsc70 is primarily found in the cytoplasm, mortalin resides in mitochondria, and GRP78 is localized in the ER [322].

Hsc70, the most prevalent non-inducible Hsp70 in the cytosol, plays a critical role in preserving cell function by managing protein transport across membranes, ensuring proper protein folding, and preventing protein aggregation under stress. It also participates in chaperone-mediated

autophagy and assists in dismantling clathrin-coated vesicles. In contrast, inducible Hsp70 helps combat proteotoxic stress from misfolded proteins and exerts protective effects by blocking apoptosis and stabilizing IAPs (Inhibitor of Apoptosis Proteins) [321]. Although Hsc70 primarily manages protein quality control under normal conditions, both Hsc70 and Hsp70 are upregulated in response to stress, working together to provide a coordinated heat shock response [322, 323].

GRP78 plays a significant role in protein quality control in the ER by participating in the unfolded protein response (UPR). In the absence of stress, GRP78 binds to three ER-resident stress sensors: ATF6 (activating transcription factor 6), IRE1 (inositol-requiring kinase 1), and PERK (protein kinase-like ER kinase). When unfolded proteins accumulate in the ER, GRP78 releases these sensors, triggering downstream UPR signalling cascades.

Mortalin (GRP75) primarily localizes to mitochondria, although it may also be found in the cytoplasm and perinuclear region when overexpressed. It collaborates with Hsp60 and Hsp10 to assist mitochondrial protein folding, particularly under stress conditions [321].

All members of the Hsp70 family share a conserved structure, featuring two key domains: the N-terminal nucleotide-binding domain (NBD), responsible for ATP binding and hydrolysis, and the C-terminal substrate-binding domain (SBD), which interacts with client proteins (Figure 1.7) [324]. In cytosolic and nuclear isoforms, a conserved EEVD motif (Glu-Glu-Val-Asp) at the C-terminal end mediates interactions with other chaperones and co-chaperones. Hsp70 activity cycle involves conformational changes regulated by ATP binding and hydrolysis (hydrolysis increases substrate affinity, while ADP release facilitates client protein dissociation). This cycle is further modulated by co-chaperones and other proteins such as Hsp40, Bag-1, Hsp110, HOP, CHIP, Hsp90, Hip, and HspBP1 [321, 322, 324].

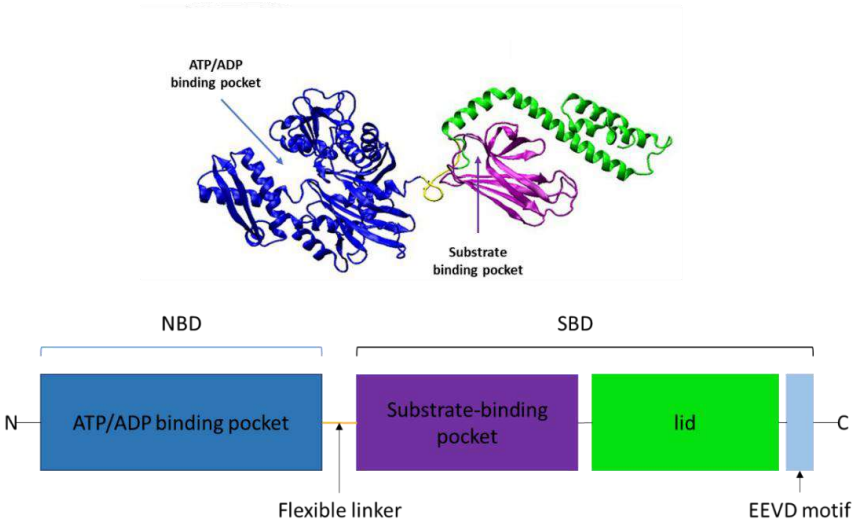

Figure 1.7. *The Hsp70s protein.* The Hsp70s consist of two highly conserved functional domains, including a Nucleotide-Binding Domain (NBD) and a C-terminal Substrate-Binding Domain (SBD), as well as an EEVD-motif at the C-terminal. The NBD contains

the ATP/ADP pocket that binds and hydrolyses ATP. The SBD contains a substrate-binding pocket that interacts with extended polypeptides as a substrate, and an α-helical subdomain from the C-terminal side of SBD forms a flexible lid. EEVD-motif participates in binding to co-chaperones and other HSPs.

Thanks to its structural adaptability, the Hsp70 family can bind a wide variety of client proteins, positioning it as a key player in maintaining proteostasis and responding to cellular stress [325]. Research has extensively examined cytosolic Hsp70 in correcting misfolded ion channels [326-329], including CFTR. The Hsc70/Hsp70 complex has been shown to influence both folding and degradation of CFTR (Figure 1.8), making it an important focus of CF research.

Hutt and colleagues found that silencing BAG3, a nucleotide-exchange factor specific to Hsp70, enhanced the stability and trafficking of the F508del-CFTR variant [330]. Additionally, interaction between Hsc70 and co-chaperone DNAJA1 supports CFTR folding at the ER. Reducing DNAJA1 levels decreases both the immature (band B) and mature (band C) forms of CFTR, suggesting a pro-folding role [331]. However, overexpressing DNAJA1 does not impact CFTR maturation but instead increases CHIP-mediated degradation of F508del-CFTR. Co-expression of DNAJA1 and Hsc70 reduces CFTR aggregation, suggesting a holdase-like function [308]. At the same time, the Hsc70/CHIP complex is involved in both lysosomal degradation of misfolded CFTR and ubiquitination of its immature form (band B) [332, 333].

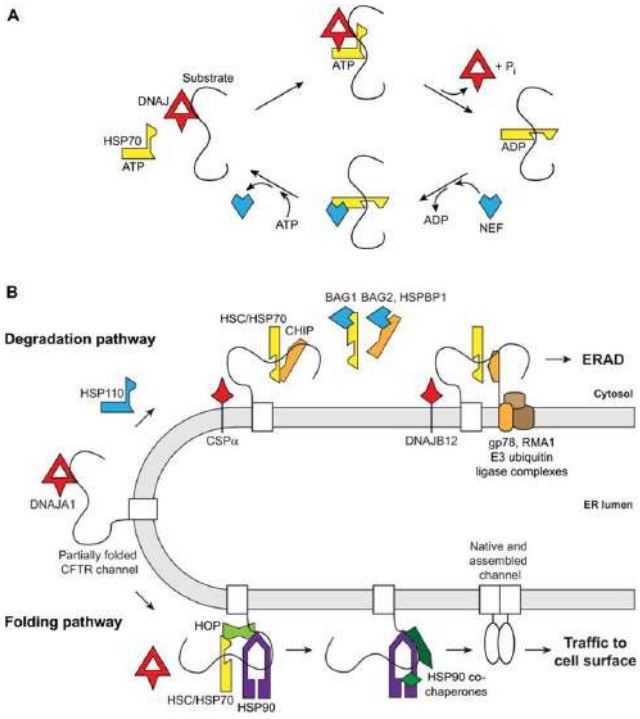

Figure 1.8. *Mechanisms of Hsc70/Hsp70 functional interaction with substrate polypeptide.* (A) The Hsp70 ATPase cycle. Clockwise, starting from left in the ATP-bound state, Hsp70 does not bind substrate polypeptide. A substrate-binding DNAJ co-chaperone contacts

HSP70 to stimulate ATP hydrolysis. In the ADP-bound state, Hsp70 binds substrate tightly, and the DNAJ dissociates. An NEF co-chaperone promotes the exchange of ADP for ATP and dissociates, returning Hsp70 to the ATP-bound state. (B) Chaperone-assisted folding and ERAD of CFTR. CFTR follows chaperone-mediated pathways for degradation (top) as well as folding (bottom). In the folding pathway, starting from the left, DNAJA1 (red) activates the binding of Hsc/Hsp70 (yellow) to CFTR to initiate folding; co-chaperone HOP (light green) transfers CFTR from Hsc/Hsp70 to Hsp90 (purple) and its co-chaperones (dark green) to complete folding and allow trafficking to the cell surface. In the degradation pathway, the Hsc/Hsp70 co-chaperone (orange) is an E3 ubiquitin ligase that promotes degradation of misfolded CFTR. CHIP functions in parallel to membrane-anchored E3 ubiquitin ligases gp78 and RMA1 and associated components (brown), which do not depend on Hsc/Hsp70. The DNAJ co-chaperones (red) CSPα and DNAJB12 promote CFTR degradation by CHIP, and by gp78 and RMA1, respectively. The NEFs (blue) BAG2, BAG1, and HSPBP1 interfere with CHIP activity, BAG1 by causing Hsc/Hsp70 to release substrate, BAG2 and HspBP1 by binding directly to CHIP. The NEF Hsp110 also promotes CFTR degradation. Hsp110 is homologous to Hsc/Hsp70 in the ATP-bound state. From Jason C. Young, Disease Models & Mechanisms (2014) 7, 319-329 doi:10.1242/dmm.014001.

Given their dual roles in promoting CFTR folding and mediating its degradation [54, 334-336], targeting Hsc70/Hsp70 offers a potential therapeutic approach for enhancing mutant CFTR trafficking, despite the specific contribution of each of the two proteins, Hsc70 and Hsp70, in favouring the folding or degradation of the mutated CFTR, has not yet been fully explained. It has been demonstrated that suppression of Hsc70 leads to stress-induced Hsp70 upregulation, aiding in F508del-CFTR rescue [337]. As Hsc70 is always present at baseline, its inhibition activates a compensatory stress response that boosts Hsp70 levels. Sodium 4-phenylbutyrate (4PBA), originally studied for its ability to induce Hsp70 in leukemia cells [338, 339], has been shown to promote F508del-CFTR folding and transport by increasing Hsp70 expression and its binding to CFTR [328, 332, 340]. Treatment of IB3-1 cells (a CF bronchial epithelial cell line heterozygous for F508del and W1282X mutations) with 2 mM 4PBA led to a 1.35-fold increase in forskolin-stimulated chloride secretion [340]. This improvement results not only from reduced Hsc70 expression [341-343] and weakened Hsc70-F508del-CFTR interaction [342], but also from enhanced Hsp70 expression and its increased binding to the mutant protein [279, 344].

A similar mechanism is seen with matrine, a natural alkaloid that downregulates Hsc70, thereby increasing both F508del-CFTR levels and its exit from the ER [332, 341]. In FRT cells expressing F508del-CFTR, 30 μM matrine raised CFTR activity by 53% compared to untreated controls [345].

Another compound, 8-cyclopentyl-1,3-dipropylxanthine (CPX), an adenosine receptor antagonist, supports F508del-CFTR trafficking by both binding directly to its NBD1 and upregulating Hsp70. CPX increased forskolin-induced chloride efflux 2.5-fold, with an EC_{50} of 58 μM [328, 346].

The imidazole-based molecule Apoptozole (Az), discovered through a screen for apoptosis-inducing agents [347], also modulates Hsc70 activity. Indeed, Az interacts with Hsc70/Hsp70 and inhibits Hsc70 function, restoring cAMP-stimulated CFTR activity in F508del-CFTR HEK cells at

200 nM, yielding an average current density of 40 ± 7.8 pA/pF [348]. In detail, mechanistic studies show that Az binds to the ATP-binding site of Hsc70/Hsp70, blocking nucleotide access and locking the protein in an open conformation [347, 349]. Az also reduces F508del-CFTR polyubiquitination by disrupting its association with Hsc70 and CHIP, rescuing it from ERAD [348]. Similarly, the adamantyl-modified lipid adaSGC appears to inhibit ATP hydrolysis by Hsc70 triggered by Hsp40, thus preventing the binding of misfolded CFTR to Hsc70 during low-temperature glycerol rescue. Iodide efflux assays in F508del-CFTR BHK cells treated with 50 μM adaSGC showed significantly enhanced chloride channel function [350]. All these results seem to indicate that the inhibition/regulation of Hsc70 activity, and the likely Hsp70 upregulation, play a pivotal role in the F508del-CFTR rescue. Conversely, more recently, Hsp70 allosteric inhibitors MKT-077 and YK5 have been developed. When MKT-077 (0–30 nM) was combined with the corrector Lumacaftor (VX809, 3 μM), a 40% increase in mature CFTR (band C) was observed. In HeLa cells expressing F508del-CFTR, this combo also doubled iodide efflux, thus MKT-077 supported CFTR rescue by preventing its ER-associated degradation and allowing accumulation of functional protein, while VX809 corrected its trafficking [331]. Despite its low toxicity in normal human cells, MKT-077 was withdrawn from Phase I clinical trials due to poor metabolic stability [351]. To address these limitations, further studies sought new allosteric Hsp70 inhibitors [352, 353] and molecular docking studies led to the discovery of aminoarylthiazoles (AATs) as promising analogues of MKT-077 [354]. These compounds were synthesized and tested for their Hsp70-modulating activity in conjunction with CFTR correctors VX809, showing their ability to enhance CFTR rescue [354].

1.4. Aim of the thesis

Although currently approved CFTR modulators, particularly IVA and ELX/TEZ/IVA (Kaftrio® or Trikafta®), have shown therapeutic benefits, they do not fully restore CFTR function in the lungs and other affected organs. Experimental studies have demonstrated that these treatments fail to completely correct CFTR protein stability, trafficking defects, and channel gating abnormalities in several variants, including F508del-CFTR and G551D [290, 292, 355-357]. In models such as intestinal organoids and primary nasal epithelial cells, ELX/TEZ/IVA treatment leads to only about a 50% improvement in CFTR function, highlighting the potential for further enhancement [358]. Consequently, pwCF continue to experience a gradual decline in lung function and other complications, although the progression is slower [359].

In addition, many CFTR variants show only partial (sub-therapeutic) or no response to current modulators. Individuals with these genotypes are likely to be “poor” or only “moderate” responders,

for whom disease progression remains relatively rapid [360]. Therefore, the development of new molecules for the treatment of CF fits into this general context aimed at filling the gaps in currently available therapies, and my thesis work was born in line with this need.

To pursue the goal of my thesis, my scientific research was organized in two complementary objectives:

1. synthesizing new correctors based on the thiazole scaffold and investigating their mechanism of action
2. finding new allosteric inhibitors of Hsp70, analogous of MKT-077, to be used in combination with CF correctors.

For the first aim, new molecules able to rescue the F508del-CFTR processing were developed staring both from the structure of the already used correctors VX809 (see Part. 1 of the Results) and from the active compounds (mentioned in paragraph 1.3.3) FCG, Corr-4a and 3151 (see Part. 2 of the Results) combining *in silico* and *in vitro* studies to improve the interaction with the target. Both their activity and mechanism of action were evaluated in F508del-CFTR cells using fluorescence-based methods and biochemical techniques.

To achieve the second objective, which represents an indirect method to target CFTR protein, new potential allosteric inhibitors of Hsp70 were synthesized, since it has highlighted the usefulness of such compounds to improve the functioning of correctors in CF (see paragraph 1.3.5). The activity of the designed compounds was evaluated *in vitro* over the human recombinant Hsp70 (hrHsp70), combining a biochemical technique (the colorimetric assay based on Malachite green reagent) and a biophysical one (Thermal Shift Analysis). Finally, their efficacy in rescuing mutant F508del-CFTR, when tested alone or in combination with the already clinically approved correctors, was evaluated in CFBE41o- cells stably expressing this type of mutation (see Part 3 of the Results).

2. Results

Part 1. Evaluation of the mechanism of action of three VX809-based hybrid derivatives as potential correctors of the F508del CFTR protein

2.1. In silico structure-based studies assessment

To identify in silico the CFTR most probable binding regions affected by the action of the compounds investigated in this first part of my thesis (i.e. **1a**, **2a**, **3a**; Table 2.1), the structural information associated with the Protein Data Bank (PDB) codes 8EIG, 8EIO, and 8EIQ [291] for F508del-CFTR in the presence of corrector VX445 alone (8EIG) or in combination with one or two other CFTR modulators (8EIO and 8EIQ) was used.

Table 2.1. *Chemical structure of compounds **1a**, **2a,** and **3a**.*

Compound	Structure
1a	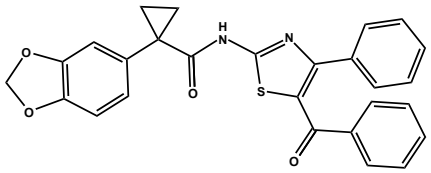
2a	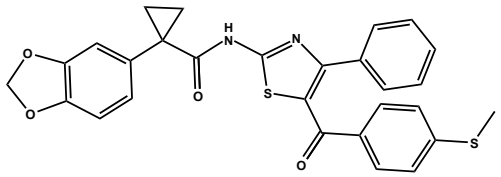
3a	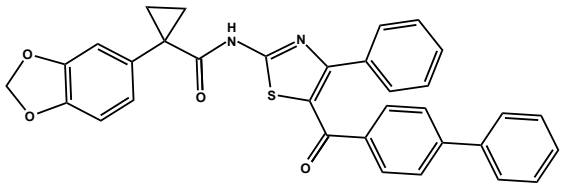

These information were endowed with: (i) comparable or better resolution values than the previous ones reported with the Protein Data Bank codes 6O2P, 7SV7, 7SVD, 7SVR, (ii) key data about the binding mode featured by different classes of CFTR correctors, such as VX445, VX661, and VX809, (iii) recurrent presence of VX445 in all of them to preliminarily explore the putative

stability of the CFTR-VX445 complex, in the presence or not of further modulators. The superimposition of the F508del-CFTR structures of the 8EIG, 8EIO, and 8EIQ PDB files and the position of their co-crystallised ligands were shown in Figure 2.1 [361].

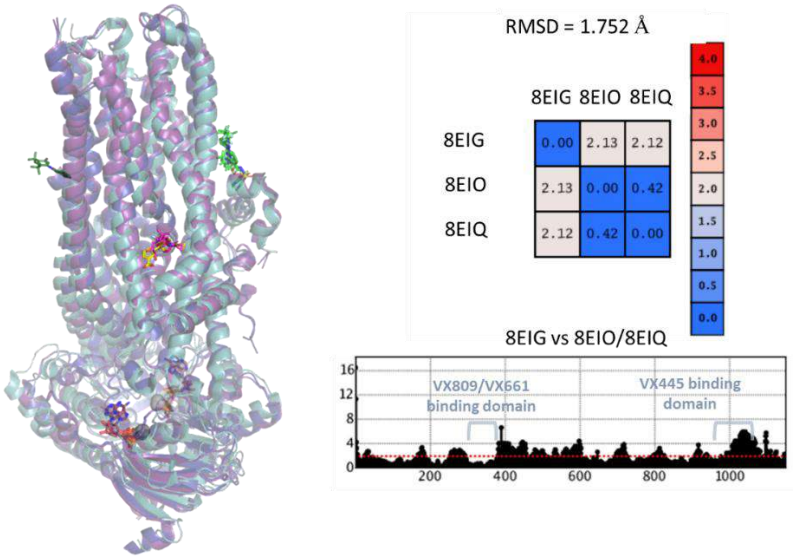

Figure 2.1. *Superimposition of the 8EIG, 8EIO, and 8EIQ.* Data obtained after superimposition of the 8EIG (ribbon in light cyan), 8EIO (ribbon in blue), and 8EIQ (ribbon in violet) (left). Both the calculated carbon atom root mean square deviation (CA RMSD) values and the overall RMSD variation trend are shown in the figure [361].

In the presence of additional modulators, a modest increase in CFTR flexibility was observed compared to that of CFTR in the presence of VX445 alone. Indeed, as shown by the table in Figure 2.1, the calculated carbon atom root means square deviation (CA RMSD) values of the distances between the 8EIG pair and 8EIO/8EIQ (CA RMSD = 2.12–2.13Å) were higher than those observed between the 8EIO and 8EIQ data (CA RMSD = 0.42Å).

Interestingly, when the three PBD structures were considered separately, a different positioning of the protein cavity surrounding compound VX445 was observed. This is probably because the 8EIG structure included only the corrector VX445, whereas the 8EIO and 8EIQ PDBs also included the CFTR modulators VX809, VX661, and VX770. The effect, played out in terms of RMSD variations along the whole protein, revealed much more protein flexibility around the VX445 cleft than near the VX809/VX661 binding pocket (Figure 2.1). These results support the hypothesis of an allosteric behaviour of class I CFTR correctors (VX809 and VX661) with respect to the binding site of VX445, which was found to be located on the solvent-exposed surface area of the protein [362]. Accordingly, the VX445 binding positioning on the CFTR surface, as well as the protein-ligand interactions, were slightly different from the 8EIG to the 8EIO, 8EIQ data. Indeed, the 8EIG PDB code suggested key H-bonds involving the dimethyl-substituted imidazole group H-bonded and

Arg21, Arg25. The CF3-alkyl group and the pyrrolidine ring were projected outside the surface protein (Figure 2.2).

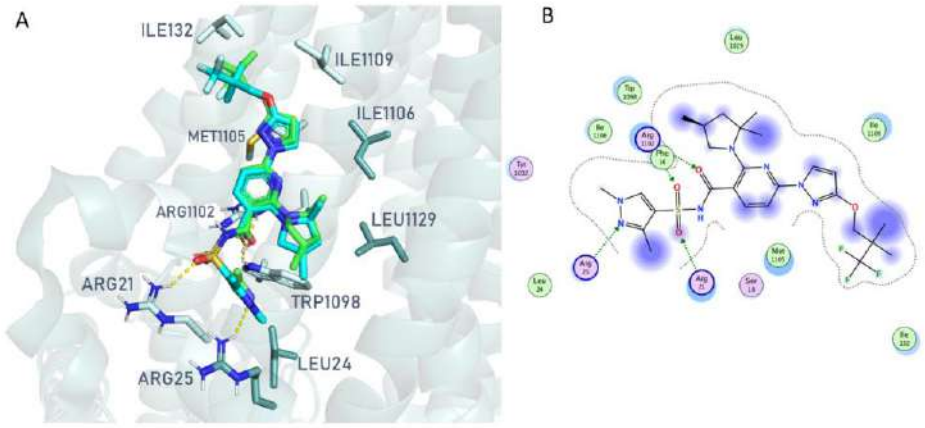

Figure 2.2. *Docking pose of VX445 at the 8EIG PDB code*. On the left side (A), the docking pose of the modulator VX445 (C atom; green) at the 8EIG PDB code is reported, with respect to the experimental positioning (C atom; cyan). In the ligplot shown (right) as a schematic representation of the main protein-ligand contacts (B), polar and hydrophobic residues are coloured in pink and green, respectively, while the portion of the ligand to be developed outside the protein surface is highlighted in blue [361].

Conversely, the pyrrolidine and imidazole substituents at positions 2 and 5 of the pyridine ring of VX445 rotated much closer to the folded surface of CFTR in the presence of the co-crystallised class I modulators, VX809 and VX661, as shown in 8EIO and 8EIQ rather than in 8EIG. This allowed the compound to move the main pyridine ring and the tethered sulphonamide group in proximity to Arg21, Trp1098, and Arg1102, revealing additional H-bonds and cation-π stacking within the 8EIO/8EIQ experimental data. Based on the interactions mentioned, the presence of VX809 rather than VX661 proved to stabilize the positioning of VX445 on the protein surface, thus gaining more contact with the biological target. In any case, the protein cavity containing corrector VX445 was the same in all PDB codes and was referred to here as pocket A.

Regarding the specific binding behaviour of the CFTR class I correctors, the co-crystallised pose of VX809 and CFTR within the 8EIO PDB code experienced H-bonds involving the terminal carboxylic group and the CFTR residues, Lys68 and Arg74, with the benzodioxole portion involved in π-πstacking with Phe81 and Trp361 (not shown). This positioning allowed the compound to fit properly into the CFTR cavity on the channel surface. Similarly, the experimental data on VX661 showed that the π-πstacking between the benzodioxole group and the previously mentioned Phe81 and Trp361 was maintained, while the substituents at indole positions 1 and 2 were H-bonded to Asn71 and Arg74, respectively (not shown). This behaviour was expected to ensure the correct CFTR-ligand binding mode, albeit at the expense of a salt-bridge with Lys68, as previously described

for VX809. However, the binding cavity of VX809 and VX661 was the same in both the PDB codes and was designated as pocket B. This positioning allowed the compound to fit properly into the CFTR cavity at the channel surface.

Notably, mutual allosteric behaviour could be noticed between VX445 and VX809/VX661, being the latter two CFTR modulators better stabilised at the protein cavity when combined with VX445 rather than alone, based on the experimental poses. As shown in the PDB codes, 7SVD and 7SV7, VX809 and VX661 featured limited H-bond contacts or polar interactions with the CFTR protein when they are the only bound modulators to CFTR.

*2.2. Molecular docking studies of the VX809-hybrids **1a**, **2a,** and **3a***

Considering the PDB codes 8EIG, 8EIO, and 8EIQ reported above (see paragraph 2.1), molecular docking studies were performed with the VX809-hybrid derivatives **1a**, **2a,** and **3a** to evaluate, *in silico*, by using the experimental data obtained from these three PDB codes, the putative hybrid binding ability to the VX445 and VX809/VX661 binding cavities. To evaluate preliminarily the reliability of the docking protocol to be used for hybrid docking simulations, a re-docking of the three X-ray protein-ligand co-crystallised complexes was performed following a previously applied procedure [363, 364]. As shown in Figure 2.3, correctors VX445, VX809, and VX661 were properly re-docked to the corresponding CFTR binding site as defined by the experimental data reported in paragraph 2.1.

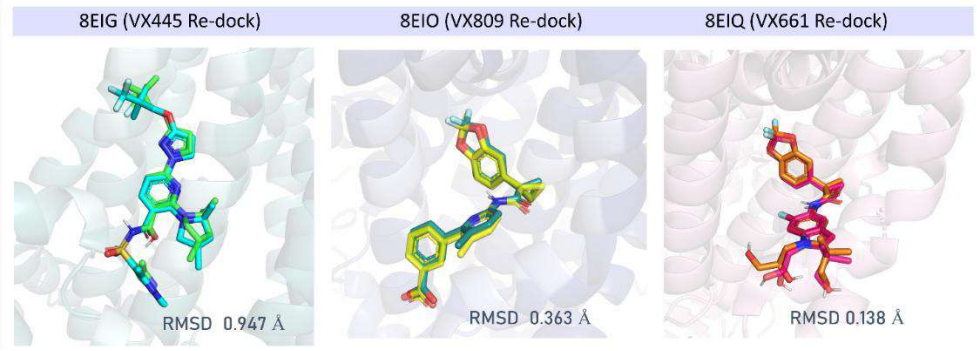

Figure 2.3. *RMSD (calculated via DockRMSD) as a parameter of re-docking performances of the docking pose, referring to 8EIG, 8EIO, and 8EIQ, respectively [361].*

The MOE Dock tool was used to perform template-based docking calculations (see Materials and methods). As ten poses were calculated for each re-docked compound, it was possible to evaluate whether the applied final scoring exploited for the conformer ranking efficiently scores the lowest

RMSD-based poses as the top ones. The MOE S score (affinity dG) was able to correctly select the bio-active pose in accordance with the experimental data in 7/10 cases for each ligand, with the best-scored conformers VX445 (S = -6.5860 Kcal/mol), VX661 (S = -9.9823 Kcal/mol), and VX809 (S = -8.7534 Kcal/mol), as endowed with RMSD values < 1Å.

On this basis, the same docking protocol was applied to the **1a**, **2a**, and **3a** VX809-hybrid compounds. To evaluate in silico the most probable binding site for each compound at the 8EIO, 8EIG, and 8EIQ CFTR-ligand complexes, the following parameters were considered: (i) comparison of the obtained scoring functions for each pocket (A and B), (ii) number of different clusters (CLs) containing only comparable poses, taken as a measure of the reproducibility of the best-scored poses (Table 2.2).

Table 2.2. *Best-ranked docking poses*. The best-ranked docking poses of the hybrids **1a**, **2a,** and **3a** and of the CF drugs VX809, VX661 and VX445 are listed via MOE Dock. The number of different conformer clusters (CLs) obtained during molecular docking calculations are reported (CLN) in tandem with the corresponding best S-score values (affinity ΔG; Kcal/mol) of CL1. The population of CL1 defined as the one containing the highest score pose, is also reported [361].

	8EIG-VX445 binding site (pocket A)			**8EIO-VX809 binding site (pocket B)**			**8EIQ-VX661 binding site (pocket B)**		
Compounds	**CL1 S value**	**CL1 Population**	**CLN**	**CL1 S value**	**CL1 Population**	**CLN**	**CL1 S value**	**CL1 Population**	**CLN**
VX445	-6.5860	8	2	-7.3970	8	2	-7.9867	3	5
VX809	-5.4008	5	3	-8.7534	5	2	-9.0052	6	2
VX661	-5.8536	8	3	-9.7202	9	2	-9.9823	8	2
1a	-4.4228	3	5	-7.8760	7	3	-8.3534	6	2
2a	-4.6130	4	4	-8.5604	6	2	-8.5864	4	4
3a	-5.5739	5	4	-10.3685	6	3	-8.8892	6	4

The binding of VX445 (S = -6.5860 Kcal/mol) to CFTR pocket A was predicted as more likely than that of VX809 (S = -5.4008 Kcal/mol) and VX661 (S = -5.8536 Kcal/mol), in agreement with the experimental data. Conversely, the ability of CFTR correctors, VX809 (S = -9.0052 to -8.7534 Kcal/mol) and VX661 (S = -9.9823 to -9.7202 Kcal/mol), to bind CFTR pocket B was calculated to be more likely than that of VX445 (S = -7.9867 to -7.3970 Kcal/mol).

All three hybrids, **1a** (EC_{50} = 0.087 μM), **2a** (EC_{50} = 0.10 μM), and **3a** (EC_{50} = 0.070 μM), showed recurrent docking poses at the 8EIO-VX809 binding site (pocket B) with comparable

interactions with the CFTR protein (Figure 2.4A–C). In particular, the corresponding S values ranging from -10.3685 to -7.8760 Kcal/mol agreed with those of the reference compounds, VX809 (S = -8.7534 Kcal/mol) and VX661 (S = -9.7202 Kcal/mol), and were also more promising than that of VX445 (S = -7.3970 Kcal/mol) at pocket B. As shown in Figure 2.4 A and C, both the prototype **1a** (EC_{50} = 0.087 μM) and the optimised **3a** compound (EC_{50} = 0.070 μM) moved the benzoyl-based group towards Arg74 and Phe78, with π-πstacking and cation-π contacts. Further cation-π interactions were also experienced by the phenyl substituent of **1a** and **3a** and the Arg74 residue.

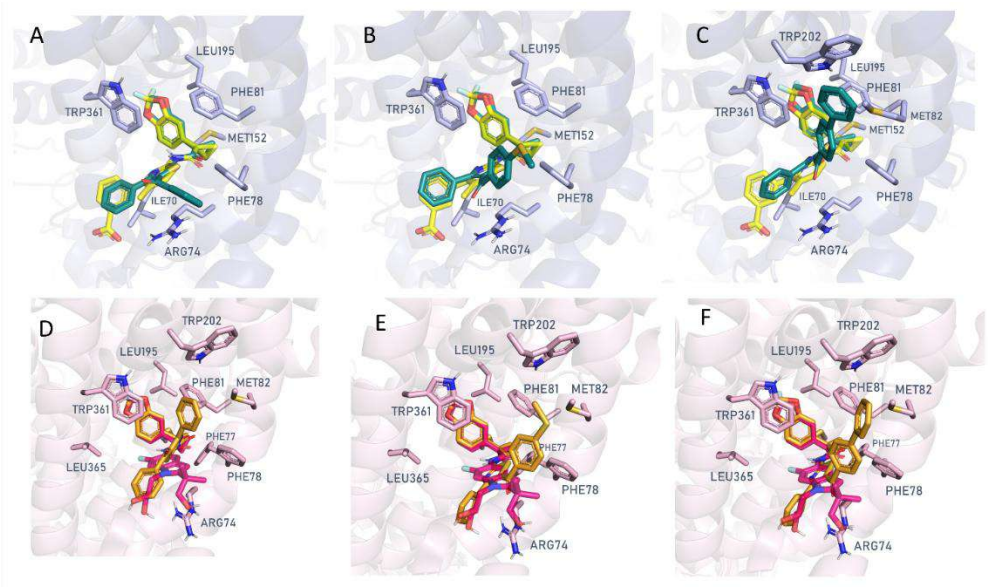

Figure 2.4. Docking pose at the 8EIO/VX809 binding site (pocket B) of compound: (A) **1a** (C atom; green), (B) **2a** (C atom; green), and (C) **3a** (C atom; green) compared to the experimental pose of VX809 (C atom; yellow). Figures D, E, and F represent the docking pose of **1a** (C atom; orange), **2a** (C atom; orange), and **3a** (C atom; orange) at the 8EIQ/VX661 binding site (pocket B), respectively. The experimental pose of VX661 is also depicted (C atom; magenta) [361].

The thiazole ring of the two in-house modulators proved to be the bioisostere of the VX809 pyridine ring, efficiently superimposing on the reference bioactive conformation. This behaviour was also correctly maintained for the benzodioxol group. Comparable information can be derived for the corresponding docking pose of **2a** (EC_{50} = 0.10 μM) (Figure 2.4B). Further molecular docking studies performed on the 8EIQ-VX661 binding site (pocket B) confirmed the previously mentioned interactions, despite the different chemo-type used as a template in the molecular docking calculations (see Materials and methods for details). In particular, the benzodioxole substituent of **1a** (EC_{50} = 0.087 μM) and of **3a** (EC_{50} = 0.070 μM) were involved in π-π stacking with Trp361, while the benzoyl-based group and the phenyl ring of the two hybrids were projected in proximity to Arg74 and Phe81, as observed for the VX661 indole-substituted portion (Figure 2.4D, F).

The final docking pose obtained for the analogue **2a** (EC_{50} = 0.10 μM) is also reported (Figure 2.4E). The calculated S values of **1a**, **2a,** and **3a**, ranging from -8.8892 to -8.3534 Kcal/mol, support the effectiveness of these compounds as CFTR-targeting ligands, in agreement with those of VX809 (S = -9.0052 Kcal/mol) and VX661 (S = -9.9823 Kcal/mol).

As a result, pocket B is predicted in silico as the most promising binding cavity for the **1a**, **2a,** and **3a** VX809-hybrids. Accordingly, the estimated S values of **1a**, **2a** and, **3a** (S = -5.5739 to -4.4228 Kcal/mol) at the 8EIG-VX445 site (pocket A) were too high, as were those of the class I correctors VX809 and VX661 (S = -5.8536 to -5.4008Kcal/mol), when compared to VX445 (S = -6.5860 Kcal/mol), taken as a pocket A binder.

2.3. Synthesis of the VX809-hybrid compounds

The VX809-hybrid derivatives developed **1a**, **2a,** and **3a** were synthesized by exploiting the formation of an amide bond between 1-(benzo[d][1,3]dioxol-5-yl) cyclopropanecarboxylic acid (a VX809 portion common to all three compounds aforementioned) and the appropriate 2-amino-arylthiazole (Scheme 2.1).

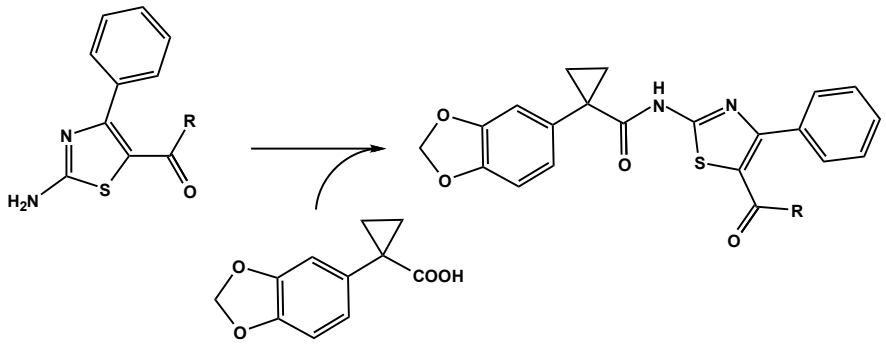

Scheme 2.1. *Synthetic approach used to synthesize VX809-hybrid compounds **1a**, **2a,** and **3a***. The reaction involves the formation of an amide bond through condensation between 1-(benzo[d][1,3]dioxol-5-yl) cyclopropanecarboxylic acid and 2-aminothiazole. Reaction conditions: HATU, N,N-Diisopropylethylamine (DIPEA), N,N-dimethylformamide (DMF), 50 °C, up to 24 hours. Compound **1a**: R=C_6H_5; **2a**: R=C_6H_4-*p*-SCH_3; **3a**: R=C_6H_4-C_6H_5.

While compounds **2a** and **3a** share a common strategy in obtaining the 2-aminothiazole intermediate, compound **1a** exploits a different synthetic route based on condensation between thiourea and 2-bromo-1,3-diphenylpropane-1,3-dione (Scheme 2.2).

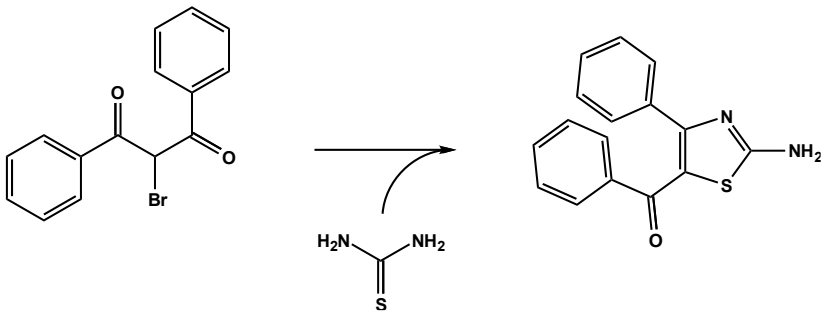

Scheme 2.2. *Synthetic strategy to obtain 2-aminothiazole derivative necessary for **1a***. The reaction involves the formation of thiazolic ring through condensation between thiourea and 2-aminothiazole. Reaction conditions: thiourea, EtOH, reflux, 24 hours.

The synthetic pathway to obtain the 2-aminothiazole for the compounds **2a** and **3a** was more complex, as shown in Scheme 2.3.

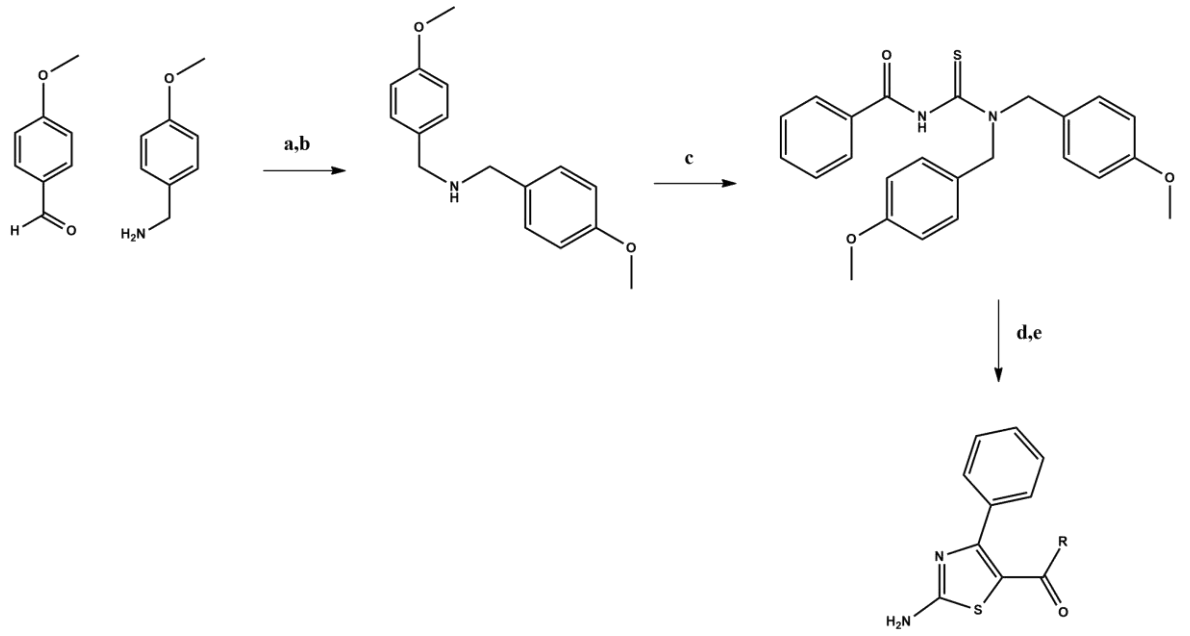

Scheme 2.3. *Reagents and conditions to obtain 2-aminothiazole for the synthesis of compounds **2a** and **3a***. (a) methanol, reflux, 3 hours; (b) $NaBH_4$,0 °C to rt,10 hours; (c) Benzoylisothiocyanate, acetone, 0 °C, 1 hours; (d) $RCOCH_2Br$, DMF, 85 C, 3 hours; (e) TFA, 80 °C, 36 hours.

Bis((4-(methoxy) phenyl)methyl)amine was obtained by heating in refluxing methanol a mixture of 1-[4 (methoxy)phenyl]methanamine and 4-(methoxy)benzaldehyde. Protected carbamothioyl amide was then obtained by condensation of benzoylisothiocyanate and bis ((4-(methoxy) phenyl) methyl) amine in high yield. Condensation of protected carbamothioyl amide and a haloketone, followed by deprotection, afforded the thiazolic derivatives, which were then further

condensed with 1-(benzo[d] [1,3] dioxol-5-yl)cyclopropanecarboxylic acid to produce the desired analogues **2a** and **3a** [365].

2.4. Evaluation of cytotoxicity of the VX809-hybrid compounds

To evaluate the potential cytotoxicity of the newly synthesized VX809-hybrid derivatives **1a**, **2a,** and **3a**, a Trypan blue survival test on HEK-t, FRT, and CFBE41o- cells with the three compounds was performed (Table 2.3).

Table 2.3. *Cell viability after treatment with the compounds under investigation*. The viability of HEK-t, FRT, and CFBE41o- cells was assessed by Trypan blue exclusion test, after 24 hours incubation with **VX661**, **VX445**, **1a**, **2a,** and **3a** at the following concentrations: 10, 5, 3, 2, 1, 0.5, 1, 0.5, 0.25, 0.125, and 0 (vehicle, DMSO) μM. TD_{50} is the concentration required to achieve the half maximum toxicity, whereas TD_{max} is the maximum toxicity. Data are presented as means ± standard error of the mean (SEM) of at least four independent experiments [361].

	HEK-t		FRT		CFBE41o-	
Compound	**TD_{50} (μM)**	**Tox_{Max} (μM)**	**TD_{50} (μM)**	**Tox_{Max} (μM)**	**TD_{50} (μM)**	**Tox_{Max} (μM)**
VX661	27.15 ± 17.88	0.42 ± 0.30	11.09 ± 3.22	0.59 ± 0.08	7.51 ± 2.22	0.62 ± 0.06
VX445	9.60 ± 2.25	0.75 ± 0.04	4.29 ± 0.32	0.79 ± 0.01	11.75 ± 3.42	0.60 ± 0.07
1a	2.44 ± 1.03	0.78 ± 0.04	9.24 ± 2.25	0.56 ±0.06	10.11 ± 1.80	0.44 ± 0.06
2a	1. 40 ± 0.20	0.86 ± 0.01	5.76 ± 0.89	0.68 ± 0.03	9.78 ± 3.35	0.51 ± 0.10
3a	1.59 ± 0.36	0.86 ± 0.01	6.13 ± 2.75	0.70 ± 0.07	11.97 ± 2.87	0.49 ± 0.08

In the test also the toxicity of the known correctors VX661 and VX445, already used in CF therapy, was also evaluated to compare their own cytotoxicity concentration with the values obtained by testing the VX809-hybrid derivatives. The Trypan blue survival test yielded half maximum toxicity (TD_{50}) values of 27.15 ± 17.88 μM, 11.09 ± 3.22 μM, 7.51 ± 2.22 μM for corrector VX661, and 9.60 ± 2.25, 4.29 ± 0.32, 11.75 ± 3.42 μM for corrector VX445 in HEK-t, FRT, and CFBE41o- cells, respectively. The cytotoxicity of **1a**, **2a,** and **3a** resulted in mildly higher than that of correctors VX661 and VX445. In particular, **3a** was the most toxic compound in all three cell lines (TD_{50} values of 1.40 ± 0.20 μM, 5.76 ± 0.89 μM, and 9.78 ± 3.35 μM in HEK-t, FRT, and CFBE41o- cells,

respectively), while **1a** resulted the least toxic in HEK-t (TD_{50} 2.44 ± 1.03 μM) and FRT (TD_{50} 9.24 ± 2.25 μM) cells and 7a (TD_{50} 11.97 ± 2.87 μM) in CFBE41o- cells (Table 2.3).

The mildly higher TD_{50} values obtained for the three hybrids with respect to the VX661 and VX445 correctors were mitigated by their low maximum toxicity values (TD_{Max}) in all three cell lines. Considering the cytotoxicity values resulted from Trypan blue survival test, the subsequent experiments were performed with VX661 and VX445 at 3 μM and **1a**, **2a,** and **3a** at 2 μM, i.e., the concentrations that gave ≥90% cell viability in all three cell lines tested.

2.5. Western blot evaluation of VX809-hybrid compounds and of VX445 and VX661 on full-length WT and F508del-CFTR expression in HEK-t cells

To test the effects of VX445 and VX661 and of the newly synthesized hybrids **1a**, **2a,** and **3a** on the expression of full-length WT and F508del-CFTR, WT and F508del-CFTR transiently transfected HEK-t cells were treated for 24 hours with 3 μM VX661, 3 μM VX445, 2 μM **1a**, 2 μM **2a**, 2 μM **3a**, or DMSO as a control vehicle. As shown in Figure 2.5, the Western blot analysis on whole cell extracts, the monoclonal antibody MM13-4, raised against the N-terminus of the CFTR protein, detected both on WT and F508del-CFTR whole cell extracts two bands of approximately 160 and 180 kDa. The lower one at 160 kDa corresponded to the immature, core glycosylated, and endoplasmic reticulum (ER)-entrapped form of CFTR commonly named band B, whereas the 180 kDa band represented the mature, fully glycosylated, and fully processed isoforms of CFTR commonly known as band C.

The highly expressed band in the lysates of the WT CFTR-transfected HEK-t cells was the band C (first lane of the upper panel in Figure 2.5A), whereas the whole cell extract of HEK-t cells expressing F508del-CFTR predominantly showed the band B, according to the severe folding and trafficking defects caused by the mutation (first lane of the upper panel of Figure 2.5B).

Treatment of full-length WT CFTR transfected cells with VX661, VX445, **1a**, **2a**, and **3a** did not modify either the total expression of WT CFTR, defined as the sum of bands B and C, or the maturation of WT CFTR, expressed as the ratio of the mature, fully glycosylated (band C) to total (B + C bands) isoforms of the protein (plots of Figure 2.5A). Conversely, VX661, VX445, **1a**, **2a,** and **3a** significantly increased F508del-CFTR total protein and maturation rate (plots of Figure 2.5B). Compared to the untreated isoform, the correctors VX661 and VX445 increased the total expression of F508del-CFTR of approximately 2.61- and 3.11-fold, and its maturation rate of 2.10- and 2.50-fold, respectively. Among the newly synthesized VX809-hybrids, **2a** was the most effective by increasing F508del-CFTR total expression and its maturation rate of 2.48- 2.15-fold, respectively, whereas **1a** resulted to be the least effective both on F508del-CFTR total expression and protein

maturation rate (2.09- and 1.42-fold, respectively) when compared to the untreated control isoform (Figure 2.5B, left and right panels). The CFTR polypeptide was not detected in non-transfected HEK-t cells.

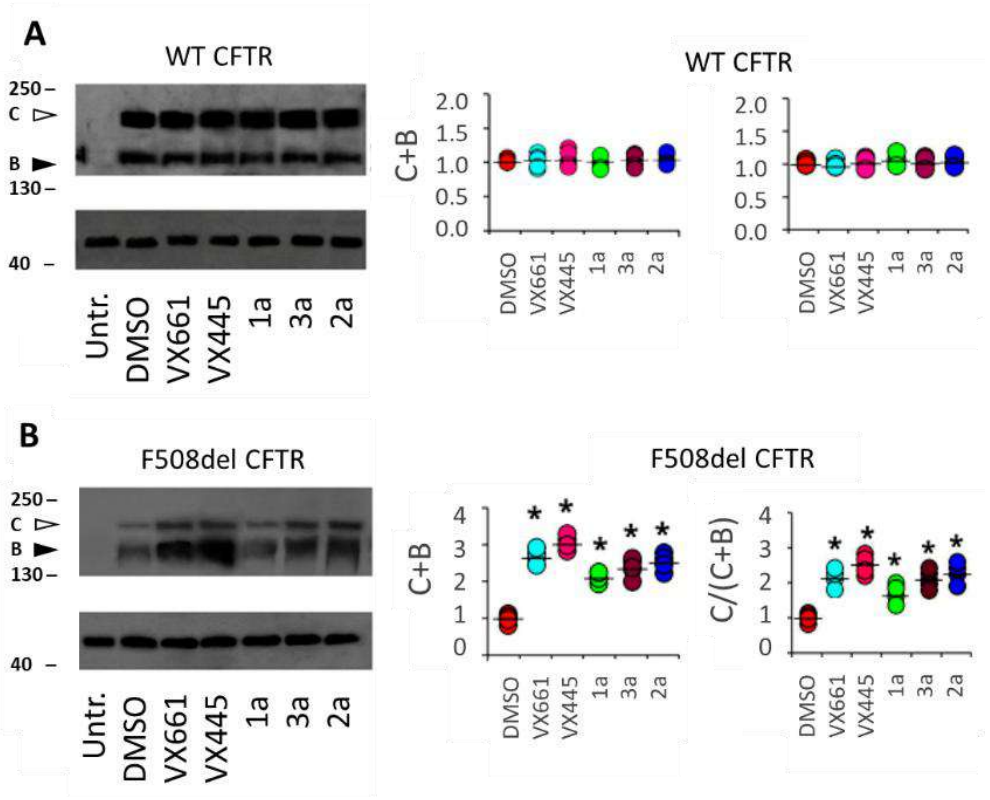

Figure 2.5. *Western blot results for the detection of the full-length WT and F508del proteins in HEK-t cells.* On the left side of the figure, the expression of WT (A) and F508del-CFTR (B) in whole cell lysates of untransfected (untr.) and transiently transfected cells is shown after treatment with DMSO (control), VX661, VX445, **1a**, **2a,** and **3a** (upper panels). The molecular weight of the proteins in the SDS-PAGE molecular weight marker is indicated on the left of each blot. The level of expression of the housekeeper protein actin in the samples (lower part of each panel) was used for the normalization of each band, whose position in Western blot analysis is indicated by black and white arrowheads, respectively. The graphs on the right side show the quantification of total (sum of bands B and C) and mature (expressed as the ratio of C/(C + B) bands) WT (A) or F508del (B) CFTR. For each condition, at least 4 independent experiments were performed, and the resulting black horizontal lines represent the mean ± SEM, while the coloured circles the individual measurements. *$p < 0.05$ compared to control, DMSO-treated samples, was determined by performing Dunnett's post hoc multiple comparison test (all groups versus control) [361].

2.6. Assessing the impact of VX661, VX445 and VX809-hybrid compounds on CFTR single domain expression

Based on the results reported in the previous paragraph, Western blot analysis of whole cell lysates from HEK-t cells transiently transfected with MSD1, WT, and F508del NBD1, R domain, MSD2, and NBD2 was performed to assess on which specific(s) CFTR domain(s) the compounds

under investigation could have caused an increase in expression. As expected [257, 267, 284, 366, 367], treatment with VX661 generated a 2.19-fold increase in the expression of MSD1 (molecular weight of ~45 kDa) in HEK-t cells, which was not observed with VX445 nor with any of the newly synthesized hybrids when compared to control DMSO-treated cells (Figure 2.6A).

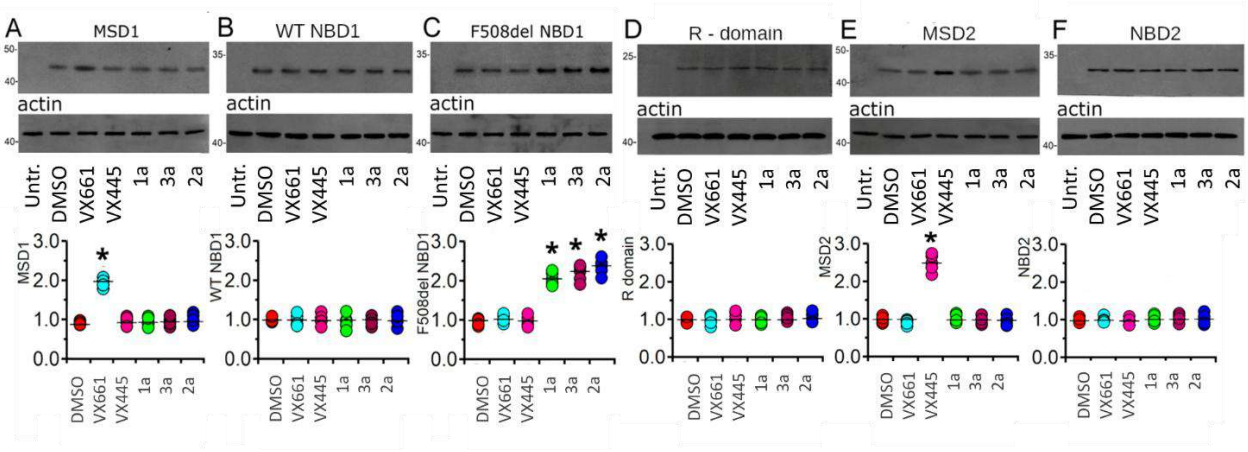

Figure 2.6. *Western blot to evaluate the effect of VX661, VX445,* ***1a****,* ***2a****, and* ***3a*** *on CFTR single domain expression*. The following CFTR domains were considered in the experiments: (A) MSD1, (B, C) WT and F508del NBD1, respectively, (D) R domain, (E) MSD2, (F) and NBD2. In the upper panels of the figure, the level of expression of B and C bands is shown in untransfected (untr) and transiently transfected HEK-t cells treated with the compounds, while the graphs at the bottom of each panel show the expression level of each domain normalised based on actin expression (lower panels). The molecular weight of the proteins of the molecular weight marker run in the SDS-PAGE is given to the left of each blot. Black horizontal lines represent the mean ± SEM, while coloured circles represent single measurements ($n \geq 4$). Dunnett's post hoc multiple comparison test was used to compare data. * $p < 0.05$ compared to control, DMSO-treated samples [361].

None of the tested compounds modified the expression level of WT NBD1 (molecular weight of ~32 kDa, Figure 2.6B). Similarly, VX661 and VX445 had no significant effect on the expression level of F508del NBD1, whereas, on the contrary, **1a**, **2a**, and **3a** induced a significant increase in its expression. **2a** was the most effective of the three hybrids, determining an increase in F508del NBD1 expression (molecular weight of ~32 kDa) of 2.32-fold with respect to that of control F508del NBD1 DMSO-treated cells (Figure 2.6C). No significant increase either in the expression level of the R domain polypeptide (molecular weight of ~22 kDa) or of NBD2 (molecular weight of ~30 kDa) was observed after treatment with all compounds under investigation (Figure 2.6D and 2.6F, respectively).

Finally, treatment with the corrector VX661, or with **1a**, **2a,** and **3a,** did not change the expression of MSD2 (molecular weight of ~47 kDa). On the contrary, as observed elsewhere [291, 366], VX445 increased 2.51-fold the expression of this domain when compared with its expression

in untreated HEK-t cells (Figure 2.6E). Controls in untransfected HEK-t cells showed that the specific primary antibodies used in these experiments did not detect any CFTR single domain on the blots.

2.7. Evaluation of F508del-CFTR channel activity on FRT and CFBE41o- after incubation with correctors

The YFP functional assay was performed to evaluate whether the increase in protein expression, specifically on NBD1 domain, induced by treatment with the compounds under investigation (see paragraphs 2.5- 2.6) correlated with an increase in F508del-CFTR channel activity. To achieve this aim, FRT and CFBE41o- cells stably co-transfected with F508del-CFTR and the iodine-sensitive YFP were used. The iodide influx, mediated by F508del-CFTR channels, was measured as the initial quenching rate (QR) of the fluorescence of the YFP. Figure 2.7 panels A–D show that treatment with either the correctors VX661 and VX445 or hybrids **1a**, **2a,** and **3a** significantly increased the iodide influx in both FRT and CFBE41o- cells. In detail, VX661 evoked an increase in the QR, which was 1.63- and 1.46-fold higher when compared to the control condition in FRT and CFBE41o- cells, respectively, whereas VX445 increased the same parameter of 1.78-fold in FRT cells and of 1.55-fold in CFBE41o- cells with respect to the relative control, untreated cells (Figure 2.7). The VX809-hybrids also caused a significant increase in iodide influx in FRT and CFBE41o- cells. In both cell preparations, the effect of the hybrids on QR was **2a** > **3a** > **1a**.

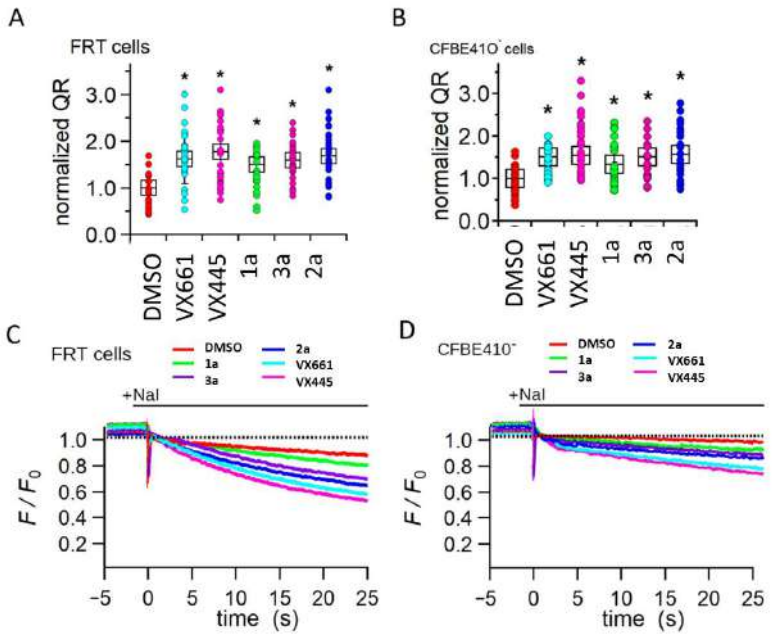

Figure 2.7. *YFP assay.* YFP assay to assess the F508del-CFTR channel functioning, which is expressed in terms of initial fluorescence quenching rate (QR) of YFP in permanently transfected FRT (A) and CFBE41o- (B) cells with the yellow fluorescence protein gene.

While coloured circles represent single measurements (n≥10), black boxes represent the mean ± SEM. The time course of fluorescence decay in FRT (C) and CFBE41o- (D) cells incubated with DMSO (vehicle control), 3 μM VX661, 3 μM VX445, 2 μM **1a**, 2 μM **2a**, 2 μM **3a**. * $p < 0.05$ compared to control, DMSO-treated samples [361].

2.8. Effect of the tested compounds on the stability of F508del NBD1

Since **1a**, **2a,** and **3a** seemed to mainly affect the expression of F508del NBD1, the potential effect on the stability of this polypeptide was evaluated after incubation of F508del NBD1-HEK-t cells with the newly synthesised VX809-hybrids. For comparison, the effect of the treatment with VX661 and VX445 on the half-life of the F508del NBD1 polypeptide was also assayed on the same cells (Figure 2.8). Time-course experiments showed that the expression of F508del NBD1 decreased to 63% after 2 hours, and to 43% and 23% after 4 hours and 6 hours from the beginning of the treatment with cycloheximide (time=0) in control DMSO untreated cells, respectively (Figure 2.8A).

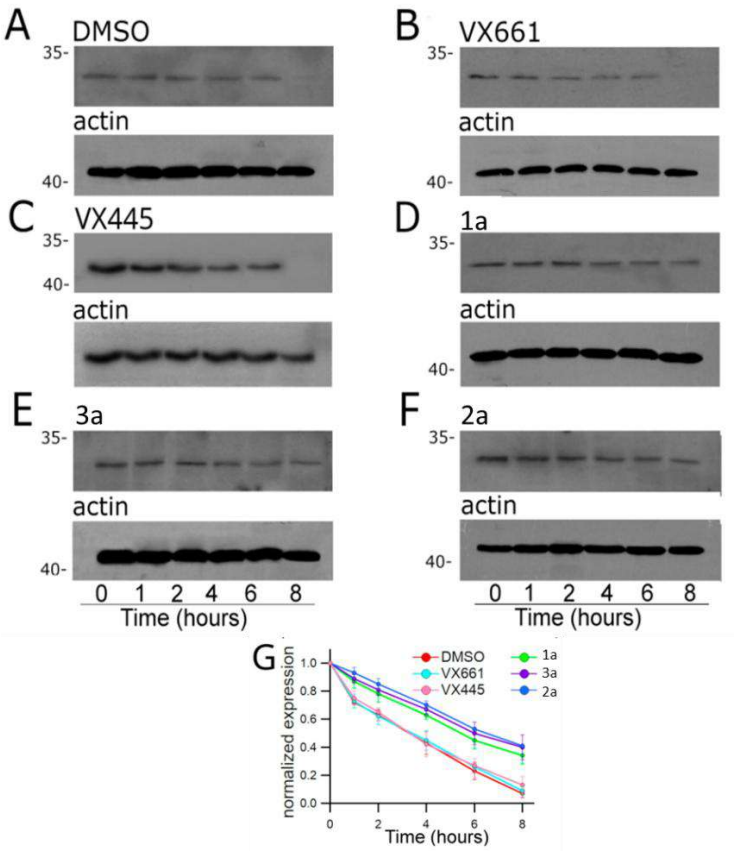

Figure 2.8. *Results of the cycloheximide chase assay on F508del NBD1*. The immunoblot panels show the F508del NBD1 expression in HEK-t cell lysates after treatment with (A) DMSO, (B) VX661, (C) VX445, (D) **1a**, (E) **3a**, and (F) **2a**, and subjected to protein synthesis inhibition by incubation with cycloheximide. The lower panels show the expression of actin as a housekeeping protein. The molecular weight of the proteins of the molecular weight marker run in the SDS-PAGE is indicated on the left of each blot. At the bottom of the figure (**G**), the expression of the F508del NBD1 protein at each of the six time points measured. The expression level of

F508del NBD1 was normalised to the level of actin protein detected in the same samples and expressed relative to time 0. Data are expressed as mean ± SEM of at least 4 independent experiments [361].

The time course decay of the expression level of F508del NBD1 in transfected HEK-t cells treated with VX661 and VX445 was like that observed in control DMSO untreated cells. Indeed, in VX661 and VX445 treated samples, the expression level of F508del NBD1 was 62% and 65% after 2 hours from the beginning of the incubation with cycloheximide and decreased to 45% and 42% after 4 hours and to 26% and 27% after 6 hours with respect to its time 0 expression level in VX661 and VX445 treated cells, respectively (Figure 2.8B, C).

Conversely, incubation of F508del NBD1 transfected HEK-t cells with **1a**, **2a,** and **3a** determined a significant increase in F508del NBD1 domain stability, suggesting a possible similar stabilizing effect of the whole F508del-CFTR protein. Indeed, the expression level of the defective CFTR protein resulted in 78%, 81% and 85% at 2 hours, 63%, 67% and 70% at 4 hours, and 45%, 50%, and 53% at 6 hours of its initial level from the beginning of the treatment with cycloheximide, respectively (Figure 2.8D–F).

2.9. Evaluation of the efficacy of the corrector combinations on full-length F508del-CFTR function

The YFP-based functional assay was used to investigate the effect of different combinations of the VX809-hybrid compounds with VX661 and VX445 on F508del-CFTR channel activity in FRT and CFBE41o- cells stably expressing the F508del-CFTR and YFP proteins.

As previously reported, incubation with forskolin and VX770 was used to stimulate the maximal F508del-CFTR channel activity (Figure 2.9A–D). In both FRT and CFBE41o- cells, the combination of VX661 + VX445 induced a greater increase in the F508del-CFTR iodide transport, which was significantly higher than that induced by VX661 or VX445 alone, respectively. The meaning of using different combinations of each VX809-hybrid with the combo of the already approved correctors, arose from the different domains of F508del-CFTR on which they act. Indeed, as reported in paragraphs 2.5 and 2.6, VX661 and VX445 trigger on MSD1 or MSD2, respectively, whereas the newly synthesized VX809-hybrids exerted their activity on NBD1 domain of the mutated protein.

In both cell lines, the effect of the combination VX661 + **1a** on F508del-CFTR channel activity was like that induced by VX661 alone. On the contrary, the F508del-CFTR-mediated I^- transport induced by the double combinations VX661 + **3a**, and VX661 + **2a** was significantly higher than that produced by VX661 alone.

Similarly, in both FRT and CFBE41o- cells, the combination VX445 + **1a** did not modify the QR with respect to VX445 alone, whereas the hybrids **2a** and **3a** produced a significant additive/synergistic effect when combined with this corrector (Figure 2.9A–D). Further dedicated experiments should be exploited to discriminate between which of the two aforementioned effects may be.

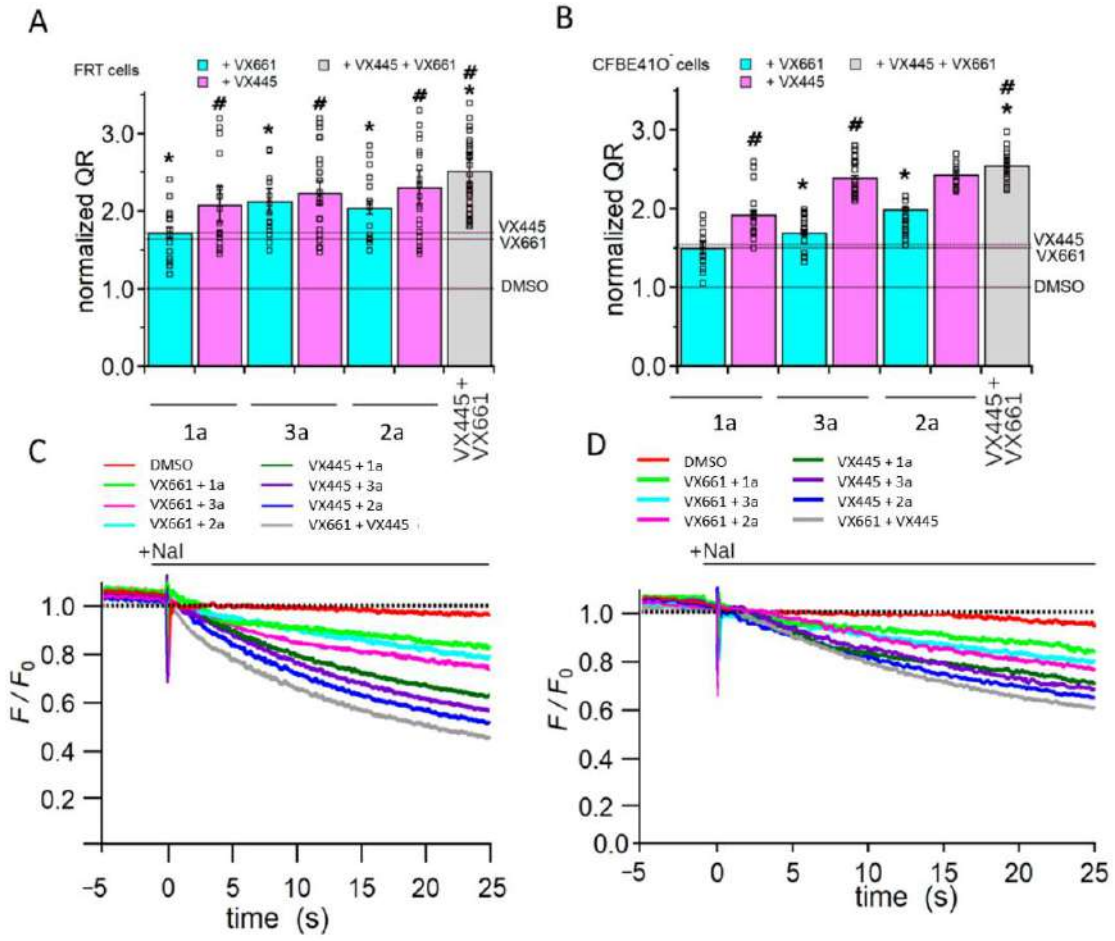

Figure 2.9. *F508del-CFTR channel function assessment after treatment with combinations of correctors*. Panels A-B show the Quenching rate (QR) of the yellow fluorescent protein (YFP) elicited by the iodide influx in FRT and CFBE41o- cells, respectively, permanently co-transfected with the YFP and the F508del CFTR proteins. In panels C-D the time course of the fluorescence decay in FRT and CFBE41o- cells is reported. The fluorescence is normalised to the initial value obtained after the addition of iodide. (A,B): black squares represent each single measurement, while the bars represent the mean ± SEM. The dashed lines stand for the QR elicited in the cell preparations incubated with DMSO, VX661, or VX445, respectively. For each condition, each measurement was repeated at least 10 times. #, * $p < 0.05$ with respect to VX661 and VX445 treated samples, respectively [361].

Part 2. Structure-guided combination of novel CFTR correctors to improve the function of F508del-CFTR in airway epithelial cells

2.10. Design of novel thiazole-based CFTR modulators and docking study

Based on the promising results achieved with the VX809-hybrid compounds (see Part.1 of Results), a new small libraries of VX809-hybrids derivatives (**4a**-**6a**) and of thiazole-based compounds (**1b**-**7b**, **1c**-**4c**) (Table 2.4) was created by applying structural variations that took into account not only the *in silico* putative mechanism of action of VX809-hybrid derivatives (mainly **1a** VX809-hybrid derivative) but also of amino-arylthiazoles (AATs) such as FCG. [368].

Table 2.4. *Structure of the new libraries of the synthesized compounds*.

Compound	Structure
4a	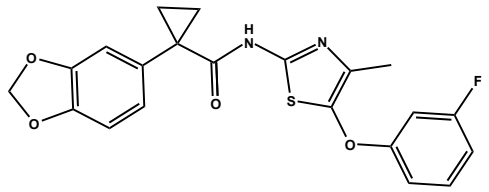
5a	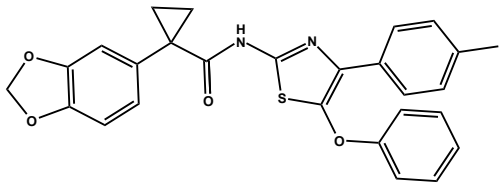
6a	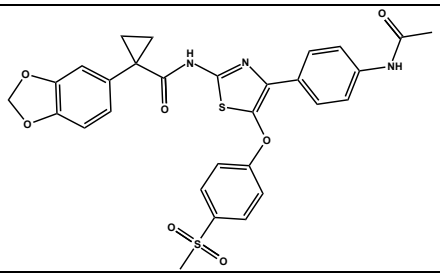

Compound	Structure
1b	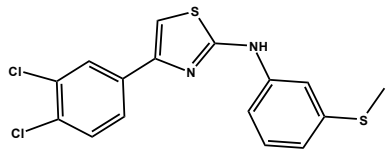
2b	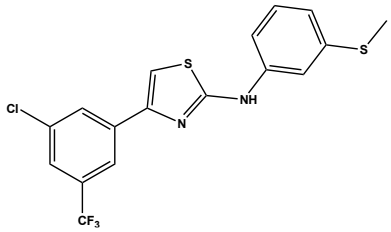
3b	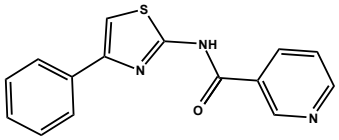
4b	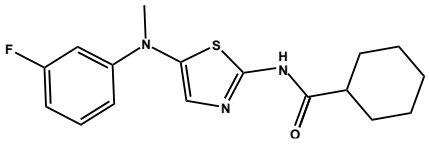
5b	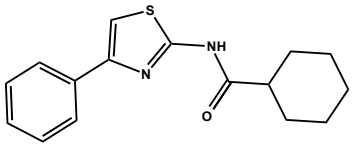
6b	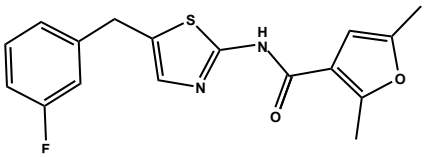
7b	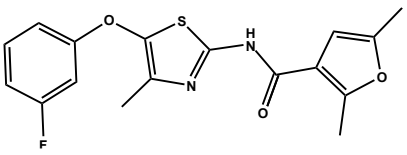

Compound	Structure
1c	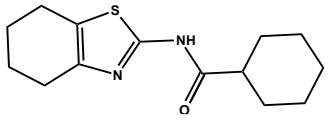
2c	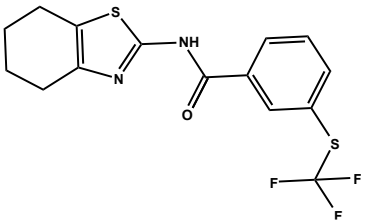
3c	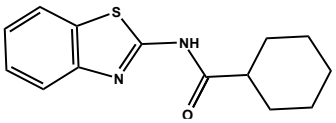
4c	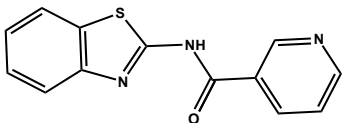

While compounds **1b**-**2b** are highly related FCG analogues, bearing bulkier and hydrophobic substituents at the thiazole position 4, compounds **3b**, **6b,** and **7b** exhibit the amide spacer as featured by 3151, a corrector belonging to the family of aminothiazole compounds (see paragraph 1.3.3). As a result, hydrophobic interactions with Leu1254, Leu1255, Leu1260, and polar contacts with Gln1291 and Arg1283 are expected to be optimized when compared to the relative compounds from which they derive. In the case of compounds **4b** and **5b**, a folded non-aromatic group has been introduced as a terminal substituent to explore the size of the F508del-CFTR protein pocket. Applying structural cyclization at the thiazole positions 4 and 5 led to compounds **1c**-**4c**. Finally, the VX809 analogues **4a**-**6a** have been designed to scout the role of the methyl group at thiazole position 4 (compound **4a**) as a bioisostere of the VX809 methyl-pyridine ring and are also VX809-hybrid analogues of 1a (see Part 1 of Results). Molecular docking studies were performed with the a-c series of compounds based on the PDB codes 8EIO and 6UK1, following the previously reported docking protocols (see Part 1 of Results). The full list of obtained a-c poses, and the related scoring functions are shown in Table 2.5.

Table 2.5. *The best-ranked docking poses of the reference derivatives Corr-4a, FCG, VX809,* ***1a,*** *and of the novel compounds are listed*. The corresponding S-score values (affinity dG; Kcal/mol) via MOE Dock at the NBD2 and 8EIO-VX809 proteins are reported, together with the population of CL1 defined as the one containing the highest docking score pose, and the number of different conformer clusters (CLs) obtained [368].

NBD2 BINDING SITE				8EIO-VX809 binding site			
Compound	Best scored pose (CL1)S value	Number of poses in CL1	Total Number CLs	Compound	Best scored pose (CL1)S value	Number of poses in CL1	Total Number CLs
Corr 4a	-4.9158	5	1	**VX809**	-8.7534	5	1
FCG	-4.4587	4	2	**1a**	-7.8760	5	1
1b	-4.1908	4	2	**4a**	-8.2353	4	2
2b	-5.0959	5	1	**5a**	-9.3012	5	1
3b	-4.8290	4	2	**6a**	-7.8137	4	2
4b	-4.3341	3	2				
5b	-4.0847	3	2				
6b	-4.1746	4	2				
7b	-4.5398	5	1				
1c	-4.8843	4	2	**1c**	-4.9912	3	2
2c	-4.5406	4	2	**2c**	-7.9827	4	2
3c	-3.5907	3	2	**3c**	-3.9125	3	3
4c	-3.9338	3	2	**4c**	-4.7819	3	2

According to the molecular docking calculations, **1b**-**7b** poses agreed with those of FCG and Corr-4a, suggesting for all of them a putative CFTR class II corrector behaviour. Among them, the most promising derivatives were **2b**, **3b,** and **7b**. As shown in Figure 2.10A, the thiazole ring and the di-substituted phenyl group at the thiazole position 4 of **2b** properly overlapped the 2-aminophenyl thiazole moiety of Corr-4a. Thus, several hydrophobic contacts involving the Leu1255, Pro1290, and Gln1291 side chains were detected. The thiomethyl-substituted phenyl ring of **2b** was projected in proximity to the reference compound carboxamide and thiazole group, featuring cation-π contacts and Van der Waals interactions with Arg1283 and Leu1258. A comparable docking positioning was also observed for the analogue **1b**, maintaining a di-substituted phenyl ring tethered to the thiazole position 4. The introduction of bulkier groups at the thiazole positions 4 and 5, combined with a carboxamide spacer at the thiazole position 2 allowed to design of compound **7b**, which better mimicked the Corr-4a positioning (Figure 2.10B). Indeed, the methyl group and the phenoxy moiety were superposed onto the Corr-4a methyl ring and 2-aminothiazole ring, featuring hydrophobic contacts with the Leu1255, Leu1260, and Gln1291 side chains. The carboxamide group tethered to the terminal furan ring was H-bonded to Val1288, being the furan oxygen atom engaged in one H-bond with Ser1362. Similarly, **3b** moved the pyridine carboxamide portion near the reference compound phenyl carboxamide group, being H-bonded to Val1288. Conversely, compound **4b**

featured a reversed docking mode due to the cycloaliphatic group. The aliphatic terminal moiety moved near Leu1255, Pro1290, while the aromatic substituent at the thiazole position 5 displayed Van der Waals contacts with Leu1258, Gln1291.

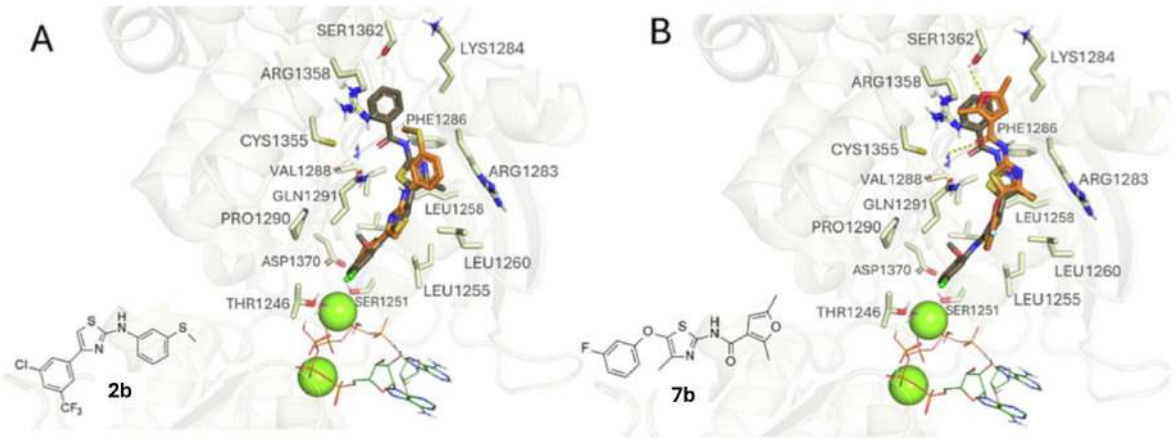

Figure 2.10. Docking pose of **2b** (C atom, orange) (A) and **7b** (C atom, orange) (B) in the NBD2 domain (PDB code 6UK1) are representative of the newly designed class II correctors **1b**-**7b**. The experimental poses of ATP (C atom, green) and Mg^{2+} (green) and the docking pose of Corr-4a (C atom, grey) are shown. (For the interpretation of colour references in the legend of this figure, please refer to the web version of this article) [368].

As regards the newly developed VX809-hybrid compounds **4a**-**6a**, the analogues **4a** and **5a** proved to be the most interesting class I derivatives of this series. As shown in Figure 2.11, the carboxamide benzoxazole group of the two compounds overlapped that of VX809, featuring hydrophobic contacts and π–π stacking with Met152, Phe81, Phe191, and Trp361. The folded thiazole core and phenoxy group engaged in polar contacts and cation-π interactions with Arg74 and in π–π stacking with Trp361 (**4a**) or additional polar contacts with Lys68 (**5a**). Finally, the putative docking mode of compounds **1c**-**4c** has been evaluated at the 6UK1 and 8EIO PDB codes (Table 2.5), suggesting a limited number of interesting derivatives (**1c**), herein resulting as class II corrector, or **2c** as dual corrector. Indeed, the bicyclic ring of **1c** was surrounded by Leu1260, displaying hydrophobic contacts as featured by **7a**, while the terminal cyclohexyl substituent was projected towards Pro1290. Maintaining a terminal aromatic core, as by **2c,** allowed the compound to mimic the behaviour of the Corr-4a benzamide group and to detect polar contacts with Arg1358, as a class II corrector. At the 8EIO/VX809 binding site, the (trifluoromethyl)thio substituted phenyl ring of **2c** was bioisostere of the VX809 benzodioxole group. As a result, key contacts with Arg74, Phe77, and Trp361 were maintained as displayed by class I correctors.

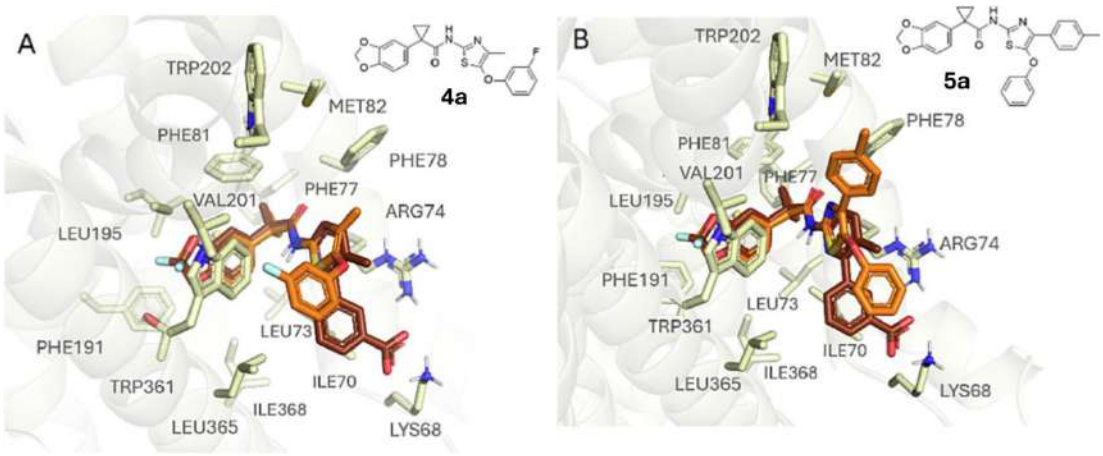

Figura 2.11. Docking pose of: (A) **4a** (C atom, orange) and (B) **5a** (C atom, orange) at the 8EIO-VX809 complex, as representative of the newly developed class I correctors **4a**-**6a**. The experimental pose of VX809 (C atom, brown) is also reported (PDB code = 8EIO) [368].

2.11. Synthesis of the new potential correctors

A simple synthetic strategy for the preparation of phenyl ether analogues **4a**, **5a**, **6a**, and **7b** (Scheme 2.4) was applied by relying on a reaction between a substituted thiazole in position 5 and a carboxylic acid derivative.

The 4-arylthiazol-2-amines portion, like 4-(p-tolyl)thiazol-2-amine for **5a** or N-(4-(2-aminothiazol-4-yl)phenyl)acetamide for **6a** and 4-methylthiazole-2-amine for **4a** and **7b,** were commercially available and were brominated with N-bromosuccinimide using procedures previously described. Bromination in position 5 of the thiazole ring, followed by a nucleophilic addition with different phenols, formed 4-aryl-5-aryloxythiazol-2-amines.

The thiazolic derivatives were then further condensed with 1-(benzo[d][1,3]dioxol-5-yl)cyclopropanecarboxylic acid to produce the desired analogues **4a**, **5a,** and **6a** or with 2,5-dimethylfuran-3-carboxylic acid to obtain **7b**. This last synthetic step was achieved by reaction of the 2-amino-thiazole with the carboxylic group of carboxylic acid derivatives, with uronium salt activation in anhydrous solvents [278] (Scheme 2.4).

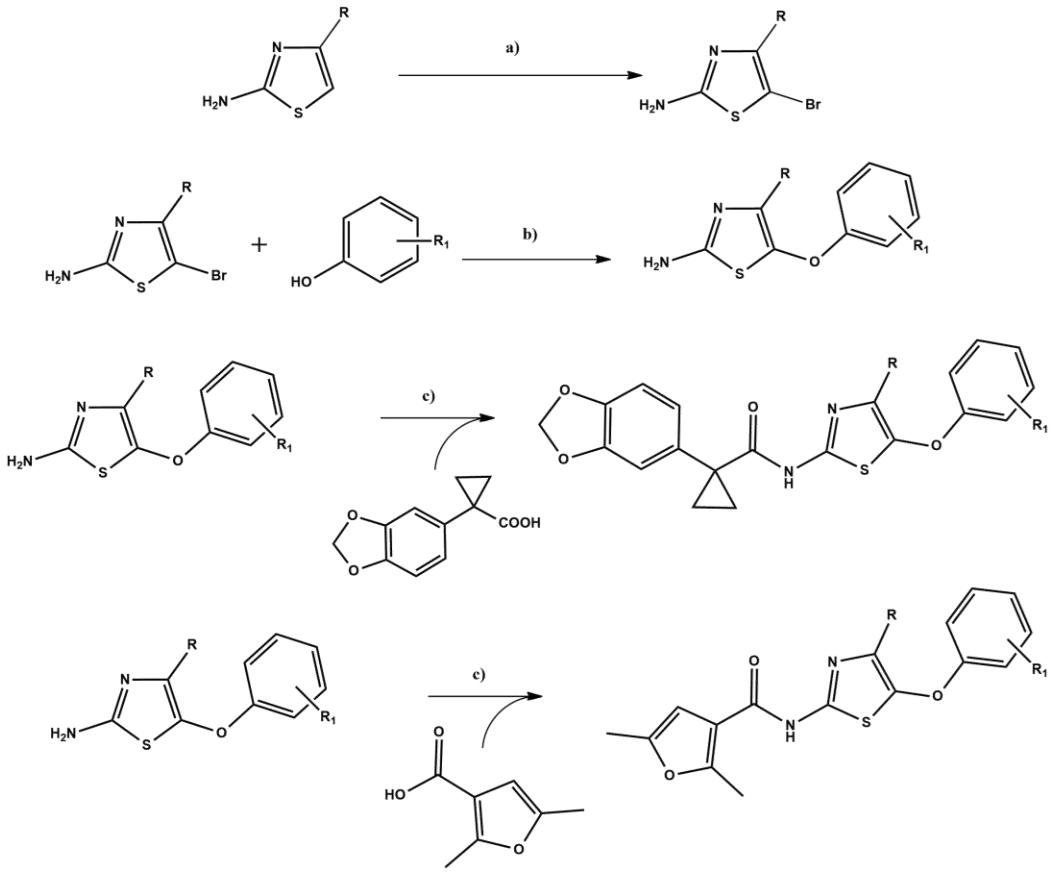

Scheme 2.4. *Protocol used to synthesize compounds **4a-6a** and **7b***. The synthetic protocol involves bromination of position 5 of 2-aminothiazole followed by a reaction of substitution with a phenol derivative and a final step of conjugation with the proper carboxylic acid. Reaction conditions: a) N-bromosuccinimide, acetic acid, 2 hours, r.t. (or N-bromosuccinimide, THF, 5 hours, 40 °C); b) Cs_2CO_3, acetonitrile, 70 °C, 1 hour; c) HATU, DIPEA, DMF, 50 °C. Compound **4a**: R= CH_3, R_1= *m*-F; **5a**: R= C_6H_4-p-CH_3, R_1=H; **6a**: R=C_6H_4-*p*-$NHCOCH_3$, R_1=p-SO_2CH_3; **7b**: R= CH_3, R_1= *m*-F.

The derivatives **1b** and **2b** were synthesized in the same method previously published (Scheme 2.5) [283]. Briefly, both the compounds were synthesized through a condensation reaction between the 1-(3-(methylthio)phenyl)thiourea and the proper haloketone, the commercially available 2-bromo-3',4' dichloro-acetophenone, as regards **1b** synthesis, and the 2-bromo-1-(3-chloro-5-(trifluoromethyl)phenyl)ethenone (obtained by α-bromination with N-bromosuccinimide and trimethylsilyl trifluoromethanesulfonate (TMS-OTf) in acetonitrile) as regards compound **2b.** 1-(3-(methylthio)phenyl)thiourea was synthesized by condensation between 3-methylthioaniline with benzoyl isothiocyanate, followed by saponification to remove the benzoyl group.

For the compound **4b,** 3-fluoro-N-methylaniline reacted with brominated thiazole under basic conditions (cesium carbonate) to give an aminic intermediate. Coupling this portion with cyclohexanecarboxylic acid affords the final compound (Scheme 2.6).

For **1c**, **3c,** and **5b,** the cyclohexanecarboxylic acid moiety was condensed with different thiazolyl cores, respectively, 2-amino-4,5,6,7-tetra-hydrobenzothiazole, 2-aminobenzo[d] thiazole, or 4-phenylthiazol-2-amine to furnish the final structures (Scheme 2.7).

On the contrary, a different carboxylic portion containing a pyridinic core was used for **3b** and **4c**. For **3b,** the reaction takes place with 2-amino-4-phenylthiazole, while for **4c,** with 2-aminobenzo[d]thiazole and the nicotinic acid. For the compound **2c,** the same thiazole portion of **1c** was condensed with 3-((trifluoromethyl)thio) benzoic acid, while in **6b,** a 5-(3-fluorobenzyl)thiazol-2-amine was conjugated with 2,5-dimethylfuran-3-carboxylic acid. The synthesis of all the amide derivatives of 2-aminothiazoles was achieved by reaction of thiazole portions with suitable carboxylic derivatives with HATU/DIPEA activation in anhydrous DMF (Scheme 2.7).

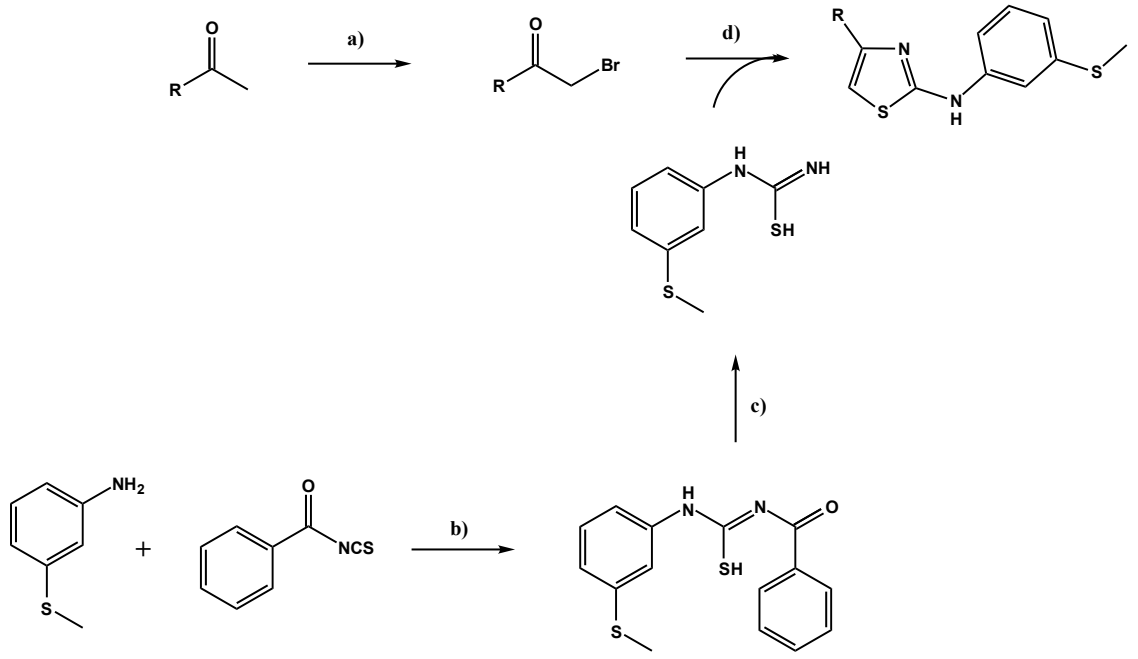

Scheme 2.5. Reagents and conditions for the synthesis of compound **2b**. (a) N-bromosuccinimide, TMS-OTf, acetonitrile, 40 °C, 24 hours; b) anhydrous Tetrahydrofuran (THF), 25 °C, overnight; c) EtOH absolute, NaOH 1M, 40 °C, 8-10 hours; (d) EtOH absolute, reflux, 24 hours. **1b** was synthesized using the same protocol except the reaction a), which was not carried out because such a reaction started directly from the commercial haloketone [283]. Compound 1b: R=3,4 -Cl; 2b R=3 -Cl, 5 -CF_3.

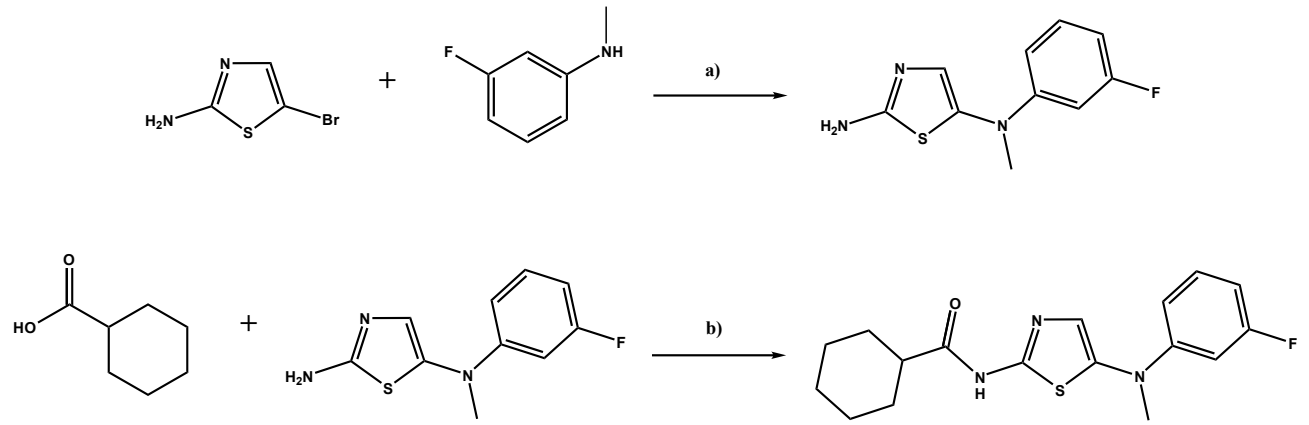

Scheme 2.6. The synthesis of compound **4b** involved a preliminary step to obtain 2-aminothiazole intermediate through reaction between a 5-brominated thiazole and 3-fluoro-N-methylaniline. The conjugation with cyclohexane carboxylic acid gave the compound **4b**. Reaction conditions: a) Cs_2CO_3, acetone, 55°C, 8 hours; b) HATU, DIPEA, DMF, 50°C, 24 hours.

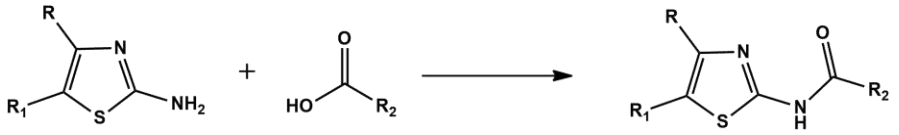

Scheme 2.7. Compounds **3b**, **5b**, **6b**, **1c**, **2c**, **3c**, and **4c** were obtained through the conjugation between a 2-aminothiazole and a carboxylic acid derivative directly.

2.12. Evaluation of the rescue of F508del-CFTR function of the newly synthesised compounds in the CFBE41o- cell line

To perform *in vitro* biological characterization, the CFTR corrector activity of these 14 newly synthesized compounds was evaluated by using a fluorescence-based membrane potential (FMP) assay in CFBE41o- cells, stably expressing F508del-CFTR. Briefly, cells were incubated for 24 hours with compounds at concentrations ranging from 0.3 to 20 μM. Then, to fully activate CFTR function in the plasma membrane, cells were stimulated with Forskolin (FSK) and the FDA-approved potentiator VX770. Dose-response measurements confirmed that these compounds were active, although with varying efficacies (Figure 2.12A). The efficacy of these compounds was compared to VX445, VX661, VX809, and only 8 compounds (**4a**, **5a**, **1b**, **2b**, **3b**, **4b**, **7b**, **1c**) showed comparable F508del-CFTR functional rescue at 10 μM (Figure 2.12B), demonstrating that molecular docking studies have enabled the development of potentially active molecules based on S scores comparable (see Table 2.5) to those of their progenitors FCG and VX809.

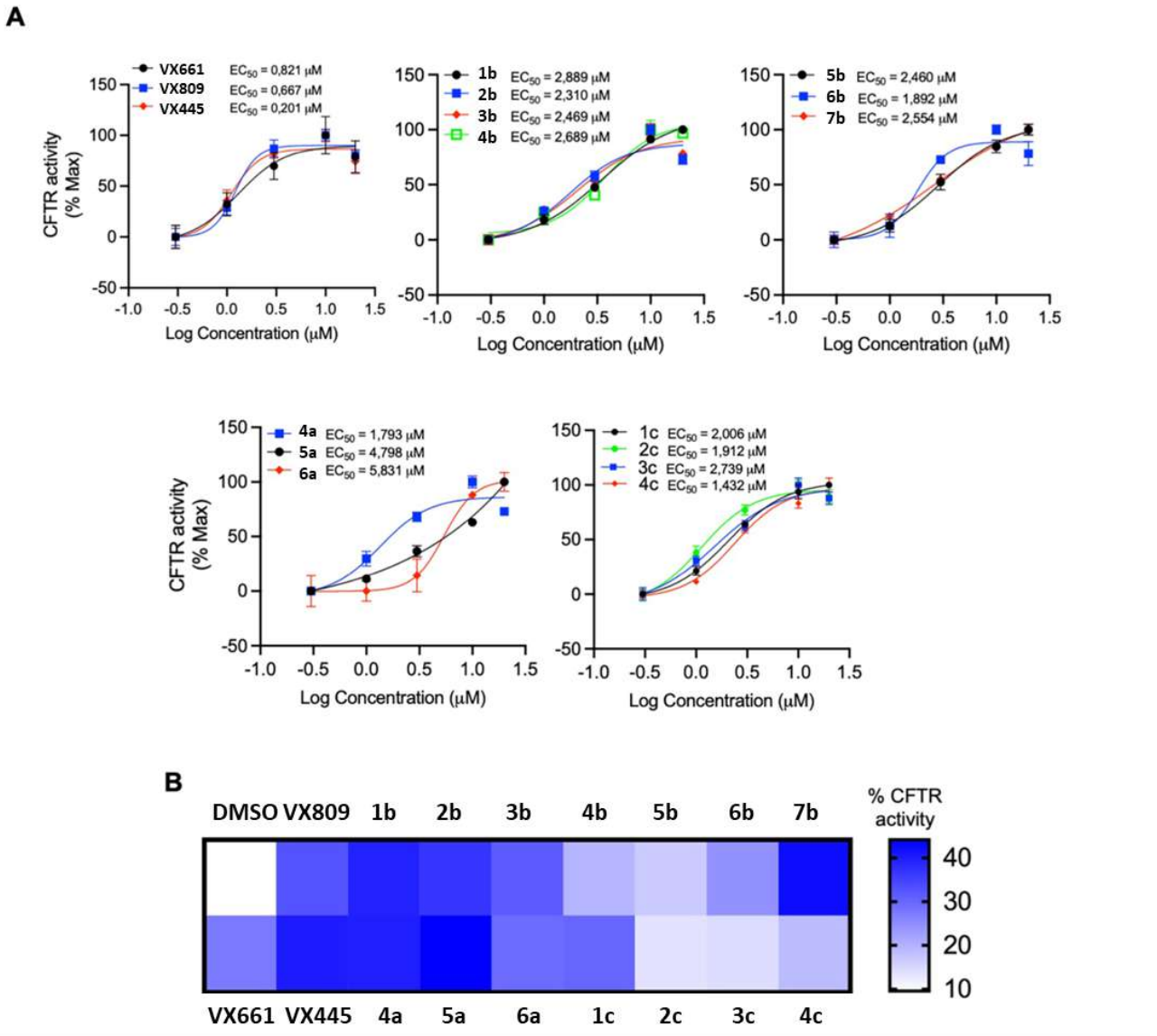

Figure 2.12. *High-Throughput Screening in F508del-CFTR bronchial cells for the identification of CFTR correctors.* The Fluorescence Membrane Potential (FMP) assay was used to measure F508del-CFTR function in CFBE41o- cells treated for 24 hours at 37 ˚C. In panel (A), function dose–response (0.3, 1, 3, 10, 20 μM) of small molecules normalized to the maximal response of each compound is reported. Data are presented as means ± SEM (n =3). (B) Heat map of corrector effect (3 μM for Vertex compounds, 10 μM, 24 hours, 37 ˚C) on F508del-CFTR in CFBE cells [368].

2.13. Evaluation of cytotoxicity of the newly synthesised compounds in the CFBE41o- cell line

The cytocompatibility of the 8 novel CFTR correctors in CFBE41o- cells after 24 hours of incubation was tested by using an MTT assay. As shown in Figure 2.13, none of the 8 compounds significantly decreased cell viability at any of the tested concentrations.

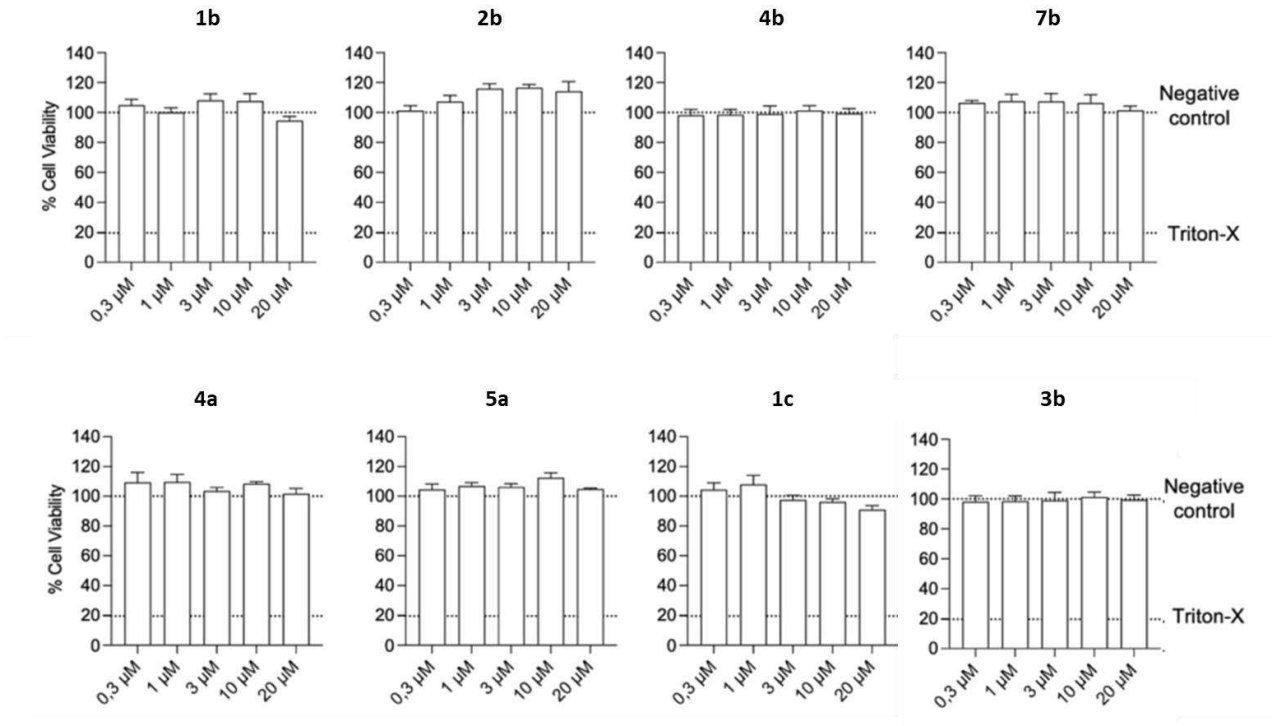

Figure 2.13. *MTT assay to assess the cytotoxicity of novel CFTR correctors*. F508del-CFTR CFBE41o- cells were treated for 24 hours with **1b**, **2b**, **3b**, **4b**, **7b**, **4a**, **5a,** and **1c** at the indicated concentrations. Untreated cells (negative control) represented 100 % viability, whereas 1 % Triton X-100 (Triton-X) was used as a positive control. Data represent the mean ± SEM of 3 biological replicates [368].

2.14. Effect of novel correctors on NBD1-ICL4 interface stabilization

Based on the ability of the 8 new compounds to restore F508del-CFTR function (see paragraph 2.13), their supposed ability to modulate the assembly and correction of F508del-CFTR by stabilizing the NBD1-ICL4 interface was subsequently evaluated in HEK293 cells transfected with F508del- or F508del/R1070W plasmid.

The R1070W (p. Arg1070Trp), located in the coupling helix of ICL4, is a second-site mutation that partially rescues the F508del mutation [256, 369] As shown in Figure 2.14, while all 8 compounds significantly rescued F508del-CFTR function, **1b**, **4b,** and **4a** did not enhance F508del/R1070W-dependent chloride efflux in HEK293 cells. This result was in line with the docking studies previously reported (see paragraph 2.10). Indeed, although structurally similar to FCG, compounds **1b** and **4b** had less comparable S score to FCG (-4.19 and -4.33 Kcal/mol, respectively, vs. -4.45 Kcal/mol for FCG) with respect to **2b**, **3b**, **7b** and **1c** compounds, resulting in lack of effect on chloride efflux restoration in HEK293 cells transfected with F508del/R1070W double mutations. Also the lack of enhance in chloride efflux on HEK293 cells transfected with these double mutations (Fig.2.14C) by compound **4a** could be possibly explained with the less comparable

S score value respect to its progenitor VX809, indicating a possible different site of interaction on CFTR protein by this compound.

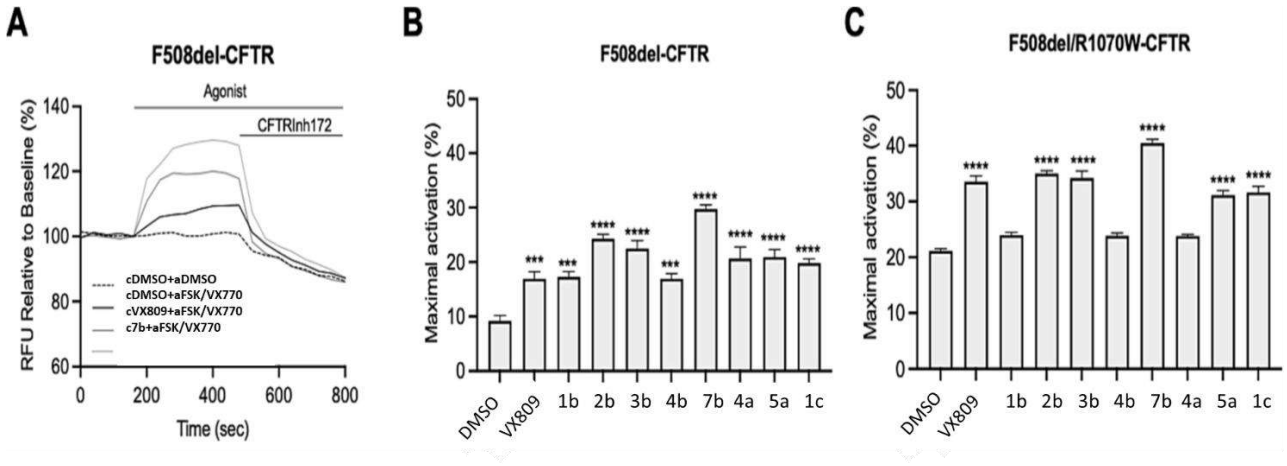

Figure 2.14. *Correctors activity in the presence of the second-site mutation R1070W*. HEK293 cells were transiently transfected with F508del or F508del/ R1070W-CFTR mutant and treated for 24 hours with 0.2 % DMSO, 3 μM VX809, 10 μM of **1b**, **2b**, **3b**, **4b**, **7b**, **4a**, **5a,** and **1c**. (A) Representative traces of F508del-CFTR function in HEK293 cells using the FMP assay. Following 5 minutes of baseline measurements, CFTR was activated by 10 μM FSK +1 μM VX770, and after 10 minutes, the CFTR inhibitor (CFTRinh-172, 10 μM) was added to deactivate CFTR. (B) and (C) represent the mean ± SEM of maximal activation of F508del-CFTR or F508del/ R1070W, respectively, in HEK293 cells (n =4). ***p <0,001; ****p <0,0001 compared to control, DMSO-treated cells [368].

2.15. CFTR corrector combinations showed robust rescue of F508del-CFTR function in airway epithelial cells

The novel 8 compounds (i.e., **4a**, **5a**, **1b**, **2b**, **3b**, **4b**, **7b**, **1c**) were individually tested, compared to FDA-approved Vertex compounds, for their potential CFTR corrector activity in bronchial epithelial cells overexpressing the F508del-CFTR mutation.

As shown in Figure 2.15 panels A and B, despite the variable efficacy, all 8 compounds significantly increased F508del-CFTR function compared to vehicle (DMSO) treatment.

Then, a combinatorial profiling of these correctors with distinct mechanisms of action, based on their structures and molecular docking results (Figures 2.10 and 2.11), was tested to investigate their possible additive/synergistic effect when combined, leaving to be demonstrated which of the two distinct phenomena can be by performing further experiments. F508del-CFTR CFBE cells were treated with different combinations (10 μM each compound) in comparison with VX809 + VX445 (3 μM each compound), which proved to be, in vitro, the most effective dual corrector combination [292]. Interestingly, CFTR corrector combinations showed a comparable VX809 + VX445-dependent CFTR rescue (Figure 2.15C, D). Surprisingly, two corrector combinations (**2b** + **5a** and **7b** + **4a**) showed approximately 20 and 29 % greater F508del-CFTR rescue than VX809 + VX445.

Furthermore, the triple combination of CFTR correctors did not exert any additive/synergistic effect, suggesting that these compounds shared a similar mechanism of action (Figure 2.15C, D). Western blot analysis showed a significant increase in F508del-CFTR protein processing (Band C/Band C+B) following treatment with the novel CFTR corrector combinations compared with DMSO treatment (Figure 2.15E, F). These findings support the improved CFTR function measured in F508del-CFTR CFBE41o- cells following the corrector combinations (Figure 2.15C, D).

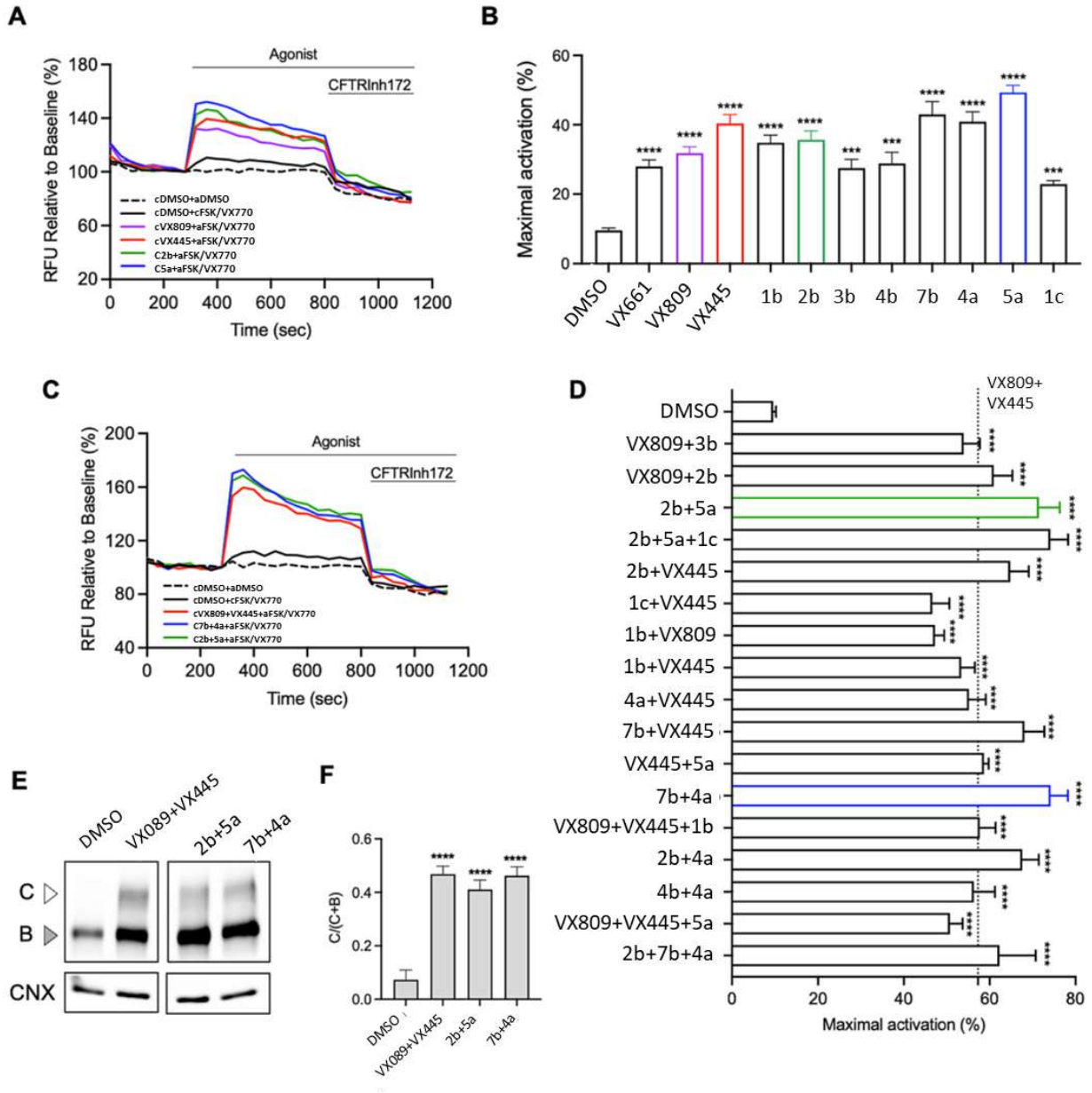

Figure 2.15. *Corrector combinations rescue the F508del-CFTR in bronchial epithelial cells*. (**A**) Representative traces of F508del-CFTR function in CFBE41o- cells using FMP assay after 24 hours of treatment with DMSO (0.2 %), 10 μM CFTR newly synthesised correctors or 3 μM VX661, VX809, and VX445. Following 5 min baseline measurements, CFTR was activated by 10 μM FSK +1 μM VX770, and after 10 minutes, the CFTR inhibitor (CFTRinh-172, 10 μM) was added to deactivate CFTR. (**B**) Bar graph represents the mean ± SEM of maximal activation of F508del-CFTR in CFBE41o- cells (n =4). The fluorescence peak changes in the presence of

CFTR agonists were normalised relative to baseline fluorescence (ΔF/F0) and expressed as %. (**C**) Representative traces of F508del-CFTR function in CFBE41o- cells using FMP assay after 24 hours of treatment with DMSO (0.2 %), 10 µM CFTR newly synthesised correctors, or 3 µM VX809 and VX445. (**D**) Bar graph represents the mean ± SEM of maximal activation of F508del-CFTR in CFBE41o- cells (n =4). The peak changes in fluorescence to CFTR agonists were normalised relative to the baseline fluorescence (ΔF/F0) and expressed as %. The dashed line represents the mean of rescued F508del-CFTR function by 3 µM VX661 +3 µM VX445 or 3 µM VX809 +3 µM VX445. (**E**) Western blot of steady-state expression of F508del-CFTR in CFBE41o- cells following the indicated treatments. (**F**) Bars represent the mean ± SEM of the ratio C/(C +B) (n =4). .***p <0,001; ****p <0,0001 compared to control, DMSO-treated cells [368].

Finally, to confirm the efficacy of these novel CFTR corrector combinations, a functional measurement of CFTR function by FMP assay in primary nasal epithelial cells was performed. To this aim, HNE cells from 4 pwCF homozygous for F508del mutation were differentiated under air–liquid interface for 18 days and were treated 24 hours before measurements by adding the compounds to the basolateral medium [370, 371]. As shown in Figure 2.16, it was confirmed that the novel CFTR corrector combinations increased FSK-activated and VX770-potentiated F508del-CFTR function compared to the VX809 + VX445- or VX661 + VX445-mediated rescue level in HNE cells. Interestingly, the two double combinations (**2b** + **5a** and **7b** + **4a**), despite patient-to-patient variability, induced F508del-CFTR functional rescue significantly higher than VX809 + VX445/ VX661 + VX445.

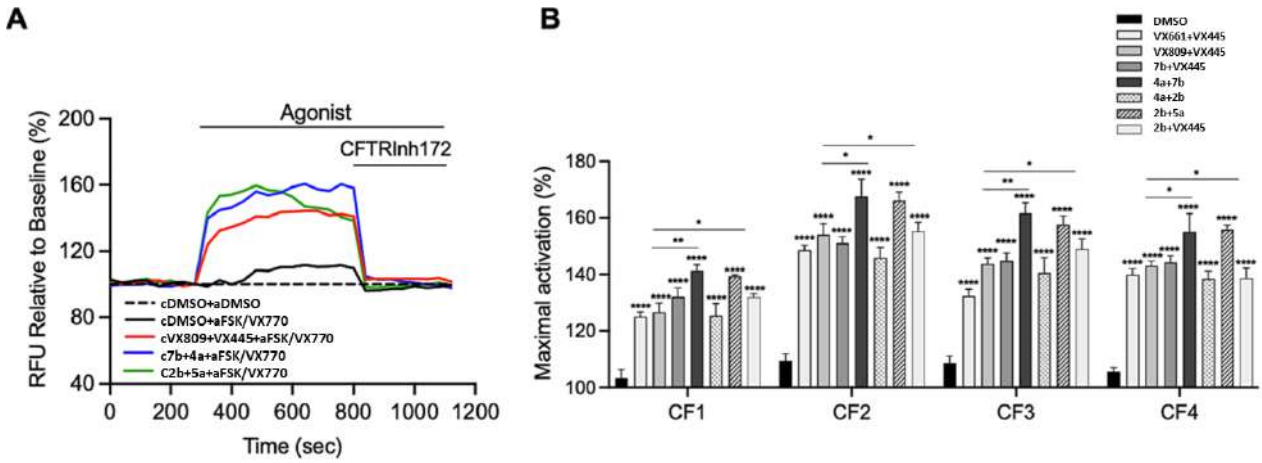

Figure 2.16. *CFTR modulators combination rescued F508del-CFTR function in primary nasal epithelial cells from 4 CF patients (CF1, CF2, CF3, and CF4)*. (A) Representative traces of F508del-CFTR function in primary nasal (HNE) cells using FMP assay after 24 hours of treatment with DMSO (0.2 %), 10 µM CFTR newly synthesised correctors, or 3 µM **VX661**, **VX809,** and **VX445**. Following 5 minutes of baseline measurements, CFTR was activated by 10 µM FSK +1 µM VX770, and after 10 minutes, the CFTR inhibitor (CFTRinh-172, 10 µM) was added to deactivate CFTR. (B) Bar graph represents the mean ± SEM of maximal activation of F508del-CFTR in HNE cells from 4 CF patients (n =3 biological replicates for each patient). The peak changes in fluorescence to CFTR agonists were normalised relative to the baseline fluorescence (ΔF/F0) and expressed as %. ****p <0,0001 compared to control,

DMSO-treated cells; CF1 and CF3: *p<0,05 **2b** + **5a** and **p<0,01 **4a** +**7b** compared to VX809 + VX445; CF2 and CF4: *p<0,05 for **2b** + **5a** and **4a** + **7b** compared to VX809+VX445 [368].

Part 3. Efficacy of new Hsp70 modulators on F508del-CFTR rescue

2.16. Design of new Hsp70 inhibitors and docking studies

As reported in paragraph 1.3.5, emerging evidence has highlighted a potential beneficial role of modulating the Hsp70 chaperone system in improving both folding and trafficking of the F508del-CFTR protein when combined with clinically approved correctors. Notably, MKT-077, an allosteric inhibitor of Hsp70, was shown by Young and colleagues to significantly enhance the stability of F508del-CFTR at the endoplasmic reticulum, reducing its degradation by approximately 12% when used in combination with the corrector VX809 [331].

Starting from this promising result, a small library of MKT-077-like compounds was synthesized by Sabbadini and co-workers [354] to explore their potential as Hsp70 inhibitors. In their study, they demonstrated that compound Ia (hereafter referred to as GR24) at 0.1 μM, when combined with 1 μM VX809, significantly improved the stability of F508del-CFTR against ER-associated degradation by approximately 8.3%, compared to VX809 treatment alone in CFBE41o- cells [354]. In the present thesis, three new MKT-077 analogues, **DL79**, **DL90,** and **AP161** (Figure 2.17), were designed based on the molecular scaffold of GR24.

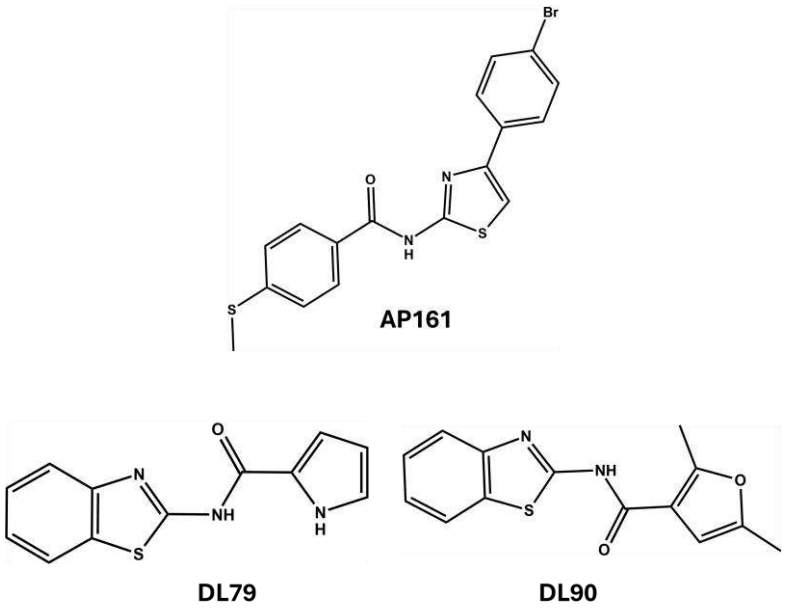

Figure 2.17. *Structure of the designed Hsp70 modulators*.

MKT-077, GR24, and the designed thiazole-based compounds (**DL79**, **DL90,** and **AP161**) have been explored *in silico* via molecular docking studies. The S score of the newly designed compounds has been analysed in comparison to both MKT-077 and GR24.

Tabella 2.6. *The best-ranked docking poses of the reference derivatives MKT-077, GR24, DL79, DL90, and AP161.* The corresponding S-score values (affinity dG; Kcal/mol) via MOE Dock (see the Materials and methods section for the detailed procedure) at the Hsp70 allosteric binding site.

Compound	S score
DL79	-120,079
MKT-077	-116,682
AP161	-115,525
DL90	-110,731
GR24	-109,821

According to Sabbabini et al. [354] the Hsp70 allosteric inhibitor MKT-077 experienced polar contacts between the carbonyl oxygen atom of the main five-membered ring, and the pyridinium ring and side chains of Arg97 and The251, respectively (Figure 2.18, the reference pose of MKT-077 in dark violet). In addition, it proved to be highly stabilized at the Hsp70 surface, thanks to polar and cation-π interactions, involving the terminal benzothiazole ring and Mg^{2+}, Lys96; cation-π contacts between the pyridinium cation group and Tyr175 sidechain.

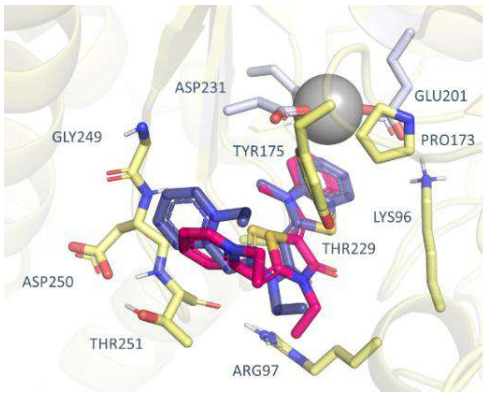

Figure 2.18. *MKT-077 previously derived docking pose at the Hsp70 allosteric binding site (C atom, dark violet)* [354]. The newly derived MKT-077 docking pose has been added (C atom, magenta). Mg^{2+} is shown as a sphere, while the surrounding stabilizing acid residues are shown in white.

Redocking of MKT-077 led to a comparable docking pose as shown in Figure 2.18 (C atom, magenta). The thiazole compound **AP161** moved the main core in proximity of the reference

compound five-membered ring, detecting hydrophobic contacts and π-π stacking with Tyr175, while the p-Br-phenyl was projected near the MKT-077 pyridinium ring (Figure 2.19; C atom, magenta).

The quite planar phenyl-amide group of **AP161** features a comparable positioning to the reference compound benzothiophene ring, exhibiting the same polar contacts with Mg^{2+}, Lys96, and hydrophobic interactions with Pro173.

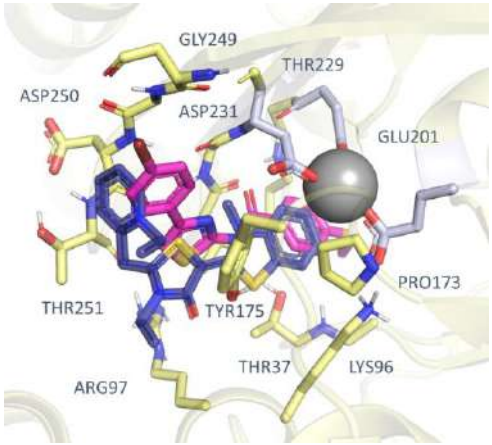

Figure 2.19. *MKT-077 previously derived docking pose at the Hsp70 allosteric binding site (C atom, dark violet)* [354]. The derived **AP161** docking pose is also reported (C atom, magenta). Mg^{2+} is shown as a sphere, while the surrounding stabilizing acid residues are shown in white.

The choice of the amide spacer group tethering a terminal bicyclic ring to a five-membered one, as featured by **DL90** and **DL79**, proved to be effective, giving conserved hydrophobic contacts with Pro173 and polar ones with Mg^{2+} and Lys96 (Figures 2.20 and 2.21, C atom, magenta).

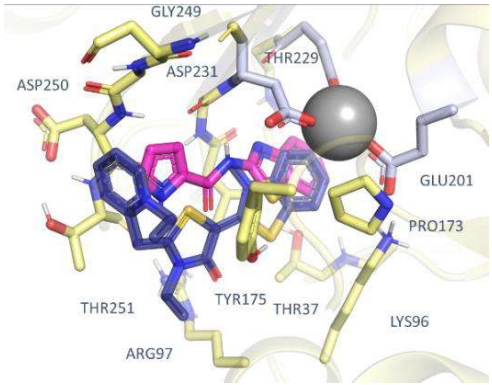

Figure 2.20. *MKT-077 previously derived docking pose at the Hsp70 allosteric binding site (C atom, dark violet)* [354]. The derived **DL90** docking pose is also reported (C atom, magenta). Mg^{2+} is shown as a sphere, while the surrounding stabilizing acid residues are shown in white.

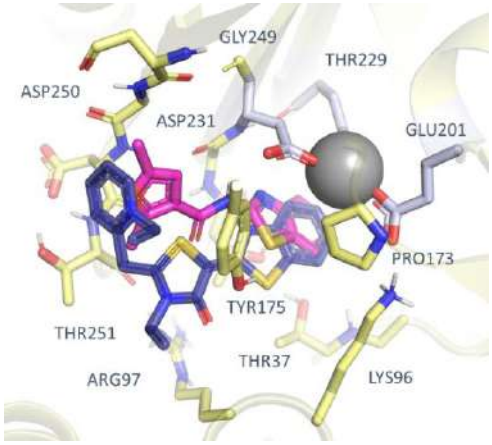

Figure 2.21. *MKT-077 previously derived docking pose at the Hsp70 allosteric binding site (C atom, dark violet)* [354]. The derived **DL79** docking pose is also reported (C atom, magenta). Mg^{2+} is shown as a sphere, while the surrounding stabilizing acid residues are shown in white.

The terminal pyrazolyl and furanoyl substituents were in proximity of the MKT-077 five-membered ring, displaying π-π stacking with Tyr175 and hydrophobic interactions with Gly249, Asp250, and Tyr175.

The synthesis of these three compounds involved a conjugation reaction between carboxylic acid and a 2-aminothiazole, as shown in the previous scheme (Scheme 2.8).

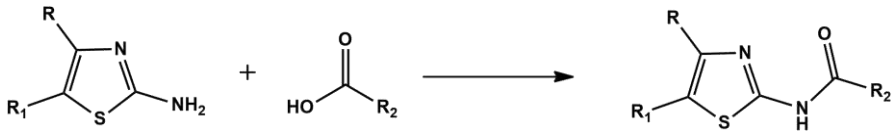

Scheme 2.8. *Scheme of reaction for the synthesis of compounds **AP161**, **DL79**, and **DL90***. Reaction conditions: HATU, DIPEA, DMF, 50 °C, up to 24 hours.

2.17. The Malachite green assay on the newly Hsp70 inhibitors

The previous shown compounds were evaluated for their ability to interact and inhibit Hsp70 activity using two different techniques, the Malachite green colorimetric assay.

The Malachite green colorimetric assay, performed on recombinant hrHsp70 protein, revealed that **DL79**, **DL90**, and **AP161** inhibited the ATPase activity of Hsp70 by 80%, 68%, and 57%, respectively (Table 2.7). These inhibitory effects exceeded those observed for the reference compounds MKT-077 (50%) and GR24 (45%) tested under the same conditions (Table 2.7), indicating a stronger ability of the newly synthesized molecules to directly interact with hrHSP70.

Table 2.7. *Malachite green assay*. hrHsp70 was incubated in the presence or absence (control) of the different compounds as described in Materials and methods section. Compounds were all tested at 300 μM. Results are the mean ± SEM of 4 experiments, where each condition was performed in quadruplicate.

	Phosphatase activity (% of inhibition)
MKT-077	50±6
GR24	45±7
DL90	68±5
DL79	80±6
AP161	57±7

2.18. Thermal Shift Assay on the newly Hsp70 inhibitors

Thermal Shift Assay (TSA) experiments further confirmed the binding of **DL79, DL90**, and **AP161** to hrHSP70. As shown in Table 2.8, **DL79** and **DL90** significantly increased the melting temperature (Tm) of the protein at all tested concentrations. This shift in Tm reflects a typical scenario in which ligand binding stabilizes the protein, thereby increasing the thermal energy required for denaturation. In contrast, **AP161** significantly increased the Tm of hrHsp70 only at the highest tested concentration (Table 2.8), consistent with its lower inhibitory activity observed in the Malachite green assay (Table 2.7).

Table 2.8. *Thermal shift analysis*. hrHsp70 was incubated in the presence or absence (control) of the different compounds as described in Material and methods section. All compounds, each at a different specific concentration, were tested in triplicate. Results are the mean ± SEM of 4 experiments. ΔTm was calculated as the difference between the Tm of hrHsp70 alone or in the presence of each specific compound.

	ΔTm (°C)	***p (t-test)***
MKT-077 300 μM	0.4±0.2	0.012
MKT-077 150 μM	0.3±0.1	0.006
MKT-077 75 μM	0.5±0.1	0.026
GR24 300 μM	0.6±0.2	0.017
GR24 150 μM	0.6±0.2	0.0006
GR24 75 μM	0.7±0.3	0.004
DL90 300 μM	0.7±0.1	0.0003
DL90 150 μM	0.6±0.2	0.0189
DL90 75 μM	0.5±0.2	0.00007
DL75 300 μM	0.8±0.1	0.00024
DL75 150 μM	0.8±0.3	0.042
DL75 75 μM	0.7±0.2	0.003
AP161 300 μM	0.4±0.1	0.001
AP161 150 μM	0.1±0.1	n.s.
AP161 75 μM	0.1±0.1	n.s

2.19. Effect of novel Hsp70 inhibitors on F508del-CFTR

Based on these results, **DL79** and **DL90** (identified as the most promising candidates) were preliminarily assessed for their efficacy in rescuing mutant F508del-CFTR trafficking, either as single agents or in combination with various correctors. As reported in Figure 2.22, both **DL79** and **DL90**, ranging between 0.025 and 10 μM, could not increase the iodide influx in CFBE41o- cells as a single compound, thus indicating the lack of activity as potential CFTR correctors. When tested in combination with 1 μM VX809, only **DL79** demonstrated a significant ability to enhance the corrective effect of VX809 on F508del-CFTR at all concentrations tested. The most pronounced effect (+39.7%) was observed at the lowest concentration of **DL79** (0.025 μM) (Figure 2.22). This level of potentiation clearly exceeded the increases previously reported for 0.011 μM MKT-077 (12%) and 0.1 μM GR24 (8.3%) when each compound was individually combined with 1 μM VX809 [360]. In contrast, none of the concentrations of **DL90** evaluated were able to enhance the corrective activity of VX809 (Figure 2.22).

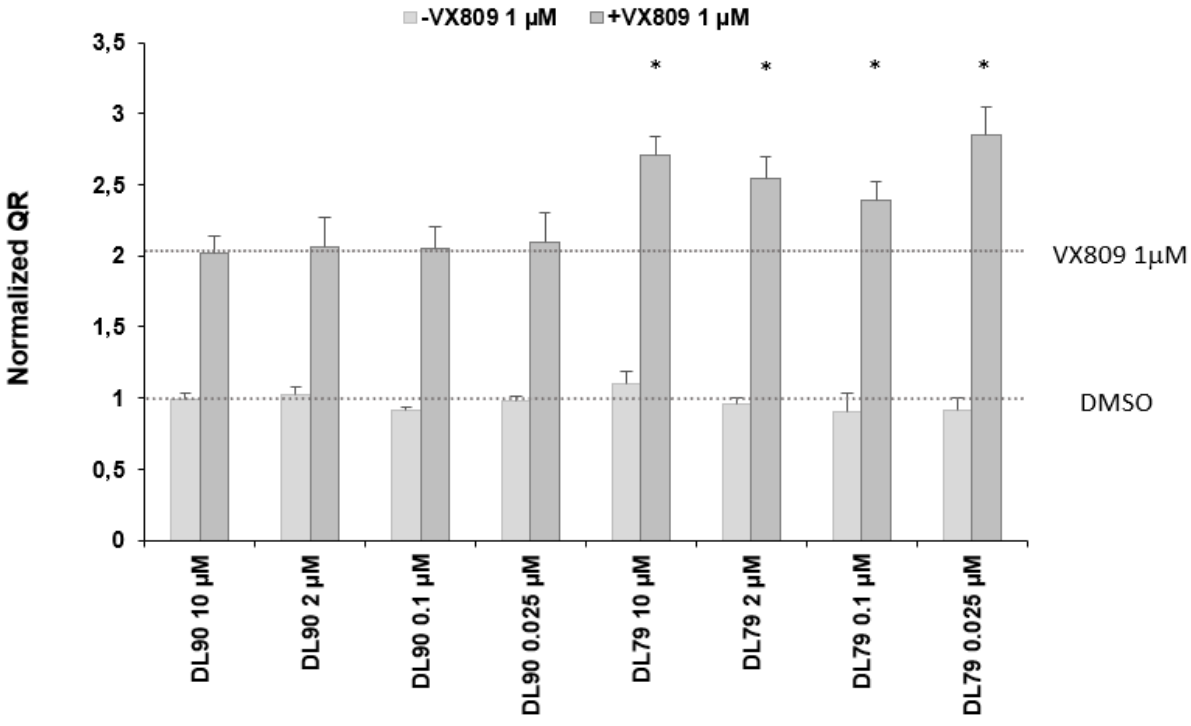

Figure 2.22. *F508del-CFTR channel function assessment after treatment with combinations of VX809 and **DL79** or **DL90***. Bars show the Quenching rate (QR) of the yellow fluorescent protein (YFP) elicited by the iodide influx in CFBE41o- cells permanently co-transfected with the YFP and the F508del-CFTR proteins. Grey bars represent the mean ± SEM of **DL79** or **DL90** at the indicated concentration in the absence of VX809; black bars represent the mean ± SEM of **DL79** or **DL90** at the indicated concentration, in combination with 1μM VX809. The black or red dashed lines stand for the QR elicited in the cell preparations incubated with DMSO

or VX809, respectively. For each condition, each measurement was repeated at least 5 times. * $p < 0.05$ with respect to VX809 in the absence of **DL79**.

By combining the concentration of **DL79** that proved most effective in enhancing VX809-mediated correction with other well-known correctors, either individually or in combination, it was observed that **DL79** was able to further increase their efficacy. Specifically, the combination of 0.025 µM **DL79** with 10 µM VX661 significantly potentiated the corrective effect of VX661 alone, resulting in a +38.1% increase in F508del-CFTR rescue (Figure 2.23).

Conversely, co-treatment with 3 µM VX445 and **DL79** led to a modest, non-significant enhancement (+13%) of corrective activity (Figure 2.24).

Notably, the triple combination of **DL79** with the combo VX661/VX445 resulted in a significant improvement (+12.3%) in F508del-CFTR rescue compared to the VX661/VX445 combination alone (Figure 2.25).

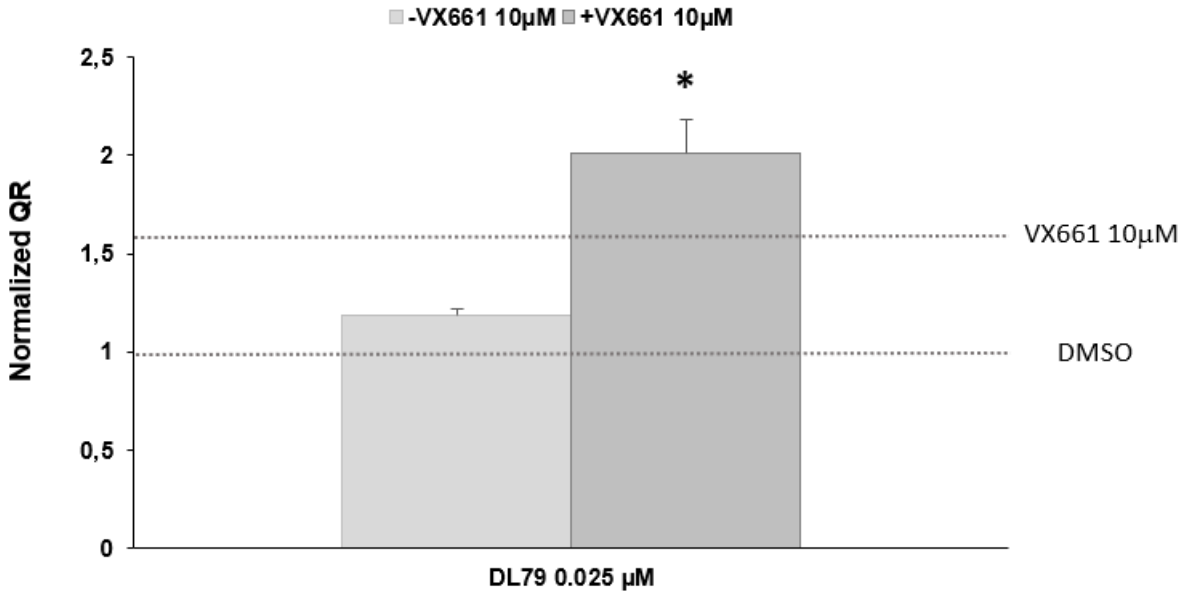

Figure 2.23. *F508del-CFTR channel function assessment after treatment with combinations of VX661 and **DL79***. Bars show the Quenching rate (QR) of the yellow fluorescent protein (YFP) elicited by the iodide influx in CFBE41o-cells permanently co-transfected with the YFP and the F508del CFTR proteins. Grey bars represent the mean ± SEM of 0.025 µM **DL79** in the absence of VX661; black bars represent the mean ± SEM of 0.025 µM **DL79** in combination with 10µM VX661. The black or red dashed lines stand for the QR elicited in the cell preparations incubated with DMSO or VX661, respectively. For each condition, each measurement was repeated at least 5 times. * $p < 0.05$ with respect to VX661 in the absence of **DL79**.

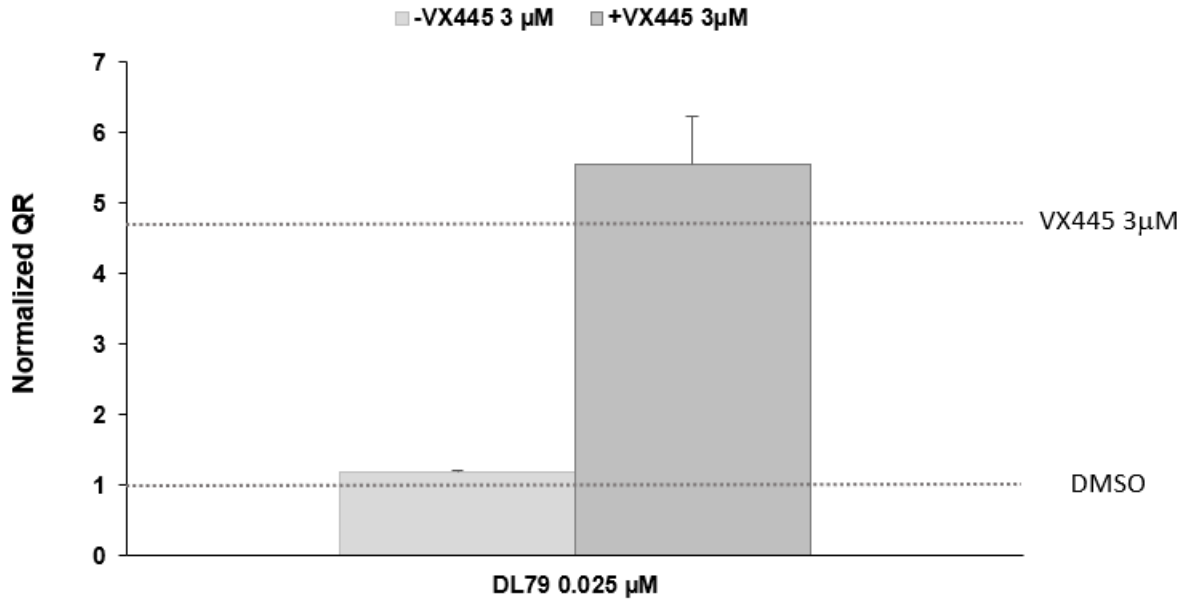

Figure 2.24. *F508del-CFTR channel function assessment after treatment with combinations of VX445 and* ***DL79***. Bars show the Quenching rate (QR) of the yellow fluorescent protein (YFP) elicited by the iodide influx in CFBE41o- cells permanently co-transfected with the YFP and the F508del-CFTR proteins. Grey bars represent the mean ± SEM of 0.025 µM **DL79** in the absence of VX445; black bars represent the mean ± SEM of 0.025 µM **DL79** in combination with 3 µM VX445. The black or red dashed lines stand for the QR elicited in the cell preparations incubated with DMSO or VX445, respectively. For each condition, each measurement was repeated at least 5 times.

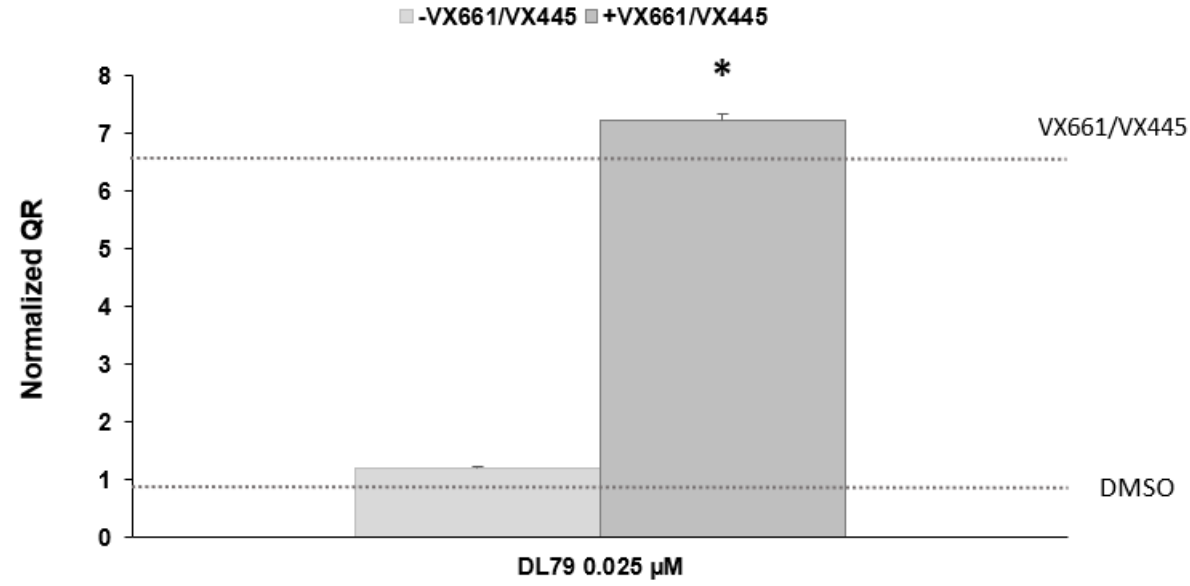

Figure 2.25. *F508del-CFTR channel function assessment after treatment with combinations of VX661/VX445 and* ***DL79***. Bars show the Quenching rate (QR) of the yellow fluorescent protein (YFP) elicited by the iodide influx in CFBE41o- cells permanently co-transfected with the YFP and the F508del-CFTR proteins. Grey bars represent the mean ± SEM of 0.025 µM **DL79** in the absence of

VX661/VX445; black bars represent the mean ± SEM of 0.025 μM **DL79** in combination with the combo VX661/VX445. The black or red dashed lines stand for the QR elicited in the cell preparations incubated with DMSO or VX661/VX445, respectively. For each condition, each measurement was repeated at least 5 times. * $p < 0.05$ with respect to VX661/VX445 in the absence of **DL79**.

3. Discussion

The introduction of a triple combination therapy, comprising two correctors (VX445 and VX661) and one potentiator (VX770), has significantly improved the quality of life for pwCF carrying at least one F508del-CFTR mutation [155, 372]. Compared to earlier approved treatments such as VX809 + VX770 and VX661 + VX770, the triple combination regimen (Kaftrio® or Trikafta®) has shown a remarkable effect on F508del-CFTR, largely due to the additive or synergistic action of the two correctors, which operate via complementary mechanisms. Nevertheless, it has been demonstrated that the triple combination does not fully restore the stability and trafficking of F508del-CFTR [292]. As such, there remains a critical need to continue screening for CFTR correctors with distinct mechanisms of action to further enhance the rescue of F508del-CFTR function. To address the CF research challenge of finding effective therapy for pwCF who do not respond to current modulator treatment, in the present thesis, a multidisciplinary approach was applied, including computational studies and biological assays of the newly synthesised correctors (**1a**, **2a**, and **3a)** and of the FCG, Corr-4a, and 3151 derivatives.

The objective of the study, particularly the paragraphs presented in Part 1 of the Results, was to elucidate the mechanism of action and assess the potential synergistic effects of correctors **1a**, **2a,** and **3a** when combined with FDA-approved modulators. These compounds were designed by integrating the AAT scaffold with the benzodioxole carboxamide moiety, characteristic of the corrector VX809 [278, 282, 283]. Compound **1a**, a VX809-hybrid featuring a benzoyl group at position 5 of the thiazole ring, was the initial derivative selected for investigation. It demonstrated promising CFTR correction activity (EC_{50} = 0.087 μM) [283] and served as the prototype for the development of analogues **2a** and **3a**, which exhibited comparable or greater potency (EC_{50} = 0.10 μM and EC_{50} = 0.070 μM, respectively [373]).

To identify the F508del CFTR regions most likely to be impacted by these three hybrids, structure-based computational analysis was employed. Specifically: (i) cryo-EM structures of full-length F508del-CFTR bound to modulators VX809, VX661, VX445, and VX770 were compiled and compared [291]; (ii) suitable docking protocols were evaluated to best reproduce known experimental data; and (iii) the selected protocol was applied to model the interaction of compounds **1a**, **2a,** and **3a** with the CFTR protein (Figure 2.1-2.4). This analysis confirmed the existence of two surface-accessible binding cavities: pocket B at the MSD1/NBD1 interface, and pocket A on MSD2, used by VX809, VX661, and VX445. It also revealed the likely binding poses of **1a**, **2a,** and **3a**, highlighting pocket B as the primary interaction site, with key π-π stacking and cation-π interactions involving residues Trp361 and Arg74 or Phe78 (Figure 2.4).

Given that low toxicity is essential in drug development, the cytotoxicity of the tested compounds was assessed using the Trypan blue exclusion assay across multiple cell lines. All compounds (i.e., VX661, VX445, **1a**, **2a**, and **3a**) exhibited low toxicity (Table 2.3). As a result, concentrations of 3 μM for VX661 and VX445, and 2 μM for **1a**, **2a**, and **3a**, were selected for subsequent experiments.

Next, the effects of **1a**, **2a**, and **3a** on the expression of both WT and F508del-CFTR proteins, as well as individual CFTR domains transiently transfected in HEK-t cells, were investigated. VX661 and VX445 were included as reference modulators due to their known influence on CFTR domain expression. In lysates from full-length WT CFTR, neither the total (bands B + C) nor the mature (C/(C + B)) protein levels were significantly increased by any compound (Figure 2.5A). In contrast, all tested correctors enhanced both total and mature expression of F508del-CFTR (Figure 2.5B), with VX445 demonstrating the strongest effect and **2a** proving to be the most potent among the hybrids, consistent with previous findings [366].

Interestingly, the selective increase in F508del-CFTR expression, without affecting WT, suggests that these hybrids may target regions of the mutant protein with altered folding. Alternatively, they may act by preventing degradation via ERAD pathways or by modulating the ER quality control machinery to permit the export of misfolded proteins.

Further experiments evaluated the ability of **1a**, **2a,** and **3a** to restore F508del-CFTR-mediated iodide transport in FRT (Figure 2.9A, C) and CFBE41o- (Figure 2.9B, D) cells, both stably expressing YFP and F508del-CFTR. All hybrids improved CFTR function, with activity ranking: VX445 > VX661 > **2a** > **3a** > **1a**. These results mirrored protein expression levels and aligned with previous studies [261, 284, 366].

To map the CFTR domains responsive to these compounds, constructs encoding MSD1 (M1, residues 1–388), NBD1 (N1, residues 348–633), WT and F508del NBD1, R domain (residues 645–834), MSD2 (M2, residues 837–1218), and NBD2 (N2, residues 1210–1480) were expressed. Confirming earlier studies [261, 284, 366], VX661 and VX445 increased MSD1 and MSD2 expression, respectively, while showing negligible effects on other domains. Despite structural similarities with VX809 and VX661, the hybrids **1a**, **2a,** and **3a** did not increase MSD1 expression (Figure 2.6A). Likewise, despite sharing a thiazolyl core with Corr-4a and FCG, which target NBD2, the hybrids did not enhance NBD2 expression (Figure 2.6F), nor did they affect the R domain (Figure 2.6D) or WT NBD1 (Figure 2.6B). Notably, all three compounds significantly increased the expression of the F508del NBD1 domain (Figure 2.6C), possibly due to misfolding-induced exposure of specific binding sites.

To validate this domain-specific action, the effect of the three hybrids on the stability of F508del NBD1 was assessed. Cycloheximide chase experiments in transiently transfected HEK-t cells showed that while VX661 and VX445 had no impact on NBD1 protein half-life (Figure 2.8B, C), all three hybrids prolonged it, indicating a stabilizing effect (Figure 2.8D-F).

Finally, acknowledging that the combined action of modulators targeting distinct structural defects of CFTR protein often results in enhanced functional rescue [256, 287, 374], the VX809-hybrid compounds were tested in combination with VX661 (a class I corrector acting on MSD1) and VX445 (which stabilizes MSD2) [261, 267, 284, 291, 361, 365, 366]. As anticipated, combinations of **2a** or **3a** with either VX661 or VX445 produced additive or synergistic improvements in CFTR function in both FRT and CFBE41o- cells (Figure 2.9A–D), with the combination of **2a** and VX445 yielding effects comparable to the clinically established VX445 + VX661 pairing. These improvements need to be further studied to understand whether they may actually be due to a synergistic or additive effect. However, combinations involving **1a** did not outperform individual treatments. This could be attributed to its lower potency or possible allosteric interference with binding sites on F508del NBD1 by VX661 or VX445.

Based on the promising results obtained with the three VX809-hybrids, additional compounds were designed using the VX809-hybrid **1a** as a starting point, as well as other known correctors, i.e, FCG, Corr-4a, and 3151, previously developed by other research groups (see paragraph 1.3.3). These new candidates incorporated structural modifications aimed at enhancing interactions with the target protein (i.e., F508del-CFTR), guided by dedicated molecular docking studies.

Specifically, as detailed in paragraphs 2.10-2.11 of Part 2 of Results, compounds **1b** and **2b** were developed as close FCG analogues, incorporating bulkier and more hydrophobic substituents (Cl and CF_3) at position 4 of the thiazole ring. The inclusion of a pyridine carboxamide spacer at position 2 of the thiazole led to compound **3b**, which mirrored the amide spacer seen in 3151. For compound **4b**, a folded, non-aromatic cycloaliphatic group was introduced as a terminal substituent to potentially enhance activity.

Starting from scaffolds 3151 and Corr-4a, the design of compound **7b** involved introducing bulkier groups at thiazole positions 4 and 5, along with a carboxamide spacer at position 2, to better mimic the orientation of Corr-4a. Substituting the pyridine moiety of compound **3b** with a cyclohexyl ring resulted in compound **5b**. Similarly, replacing the methyl group on the phenyl ring in 3151 with a fluorine atom led to the development of compound **6b**.

Particular attention was paid to derivatives **4a** and **5a**, which retained the benzodioxole moiety characteristic of VX809 and corrector **1a**. These analogues were specifically designed to explore the impact of methyl (**4a**) or phenyl (**5a**) substituents at position 4 of the thiazole ring as bioisosteres of

the methyl-pyridine ring found in VX809, maintaining structural similarity with hybrid **1a**. Compound **6a**, on the other hand, featured a bulkier group at position 5 of the thiazole ring compared to **4a** and **5a**. Given the significance of substitutions at positions 4 and 5 of the thiazole core, structural cyclization was pursued to increase hydrophobicity, resulting in compounds **1c**–**4c**.

Molecular docking studies (see paragraph 2.10, Part 2 of Results) predicted compounds **4a**, **5a**, **2b**, **3b**, and **7b** as top-performing class I and class II correctors. Notably, folded compounds improved binding to the protein crevice, as expected for class I modulators. These compounds engaged key residues (i.e, Met152, Phe81, Phe191, and Trp361) and aligned with the experimentally observed binding mode of VX809. While modifications at thiazole position 4 were limited to small groups (e.g., methyl), a folded aromatic ring at position 5 appeared to stabilize ligand binding via cation-π–π interactions with Arg74 and π–π stacking with Trp361. Similarly, smaller non-hybrid derivatives such as **2c** preserved essential interactions with Arg74 and Trp361.

For class II modulators, compounds **2b**, **3b**, and **7b** exhibited favourable binding, engaging in hydrophobic interactions with Leu1255, Pro1290, and Gln1291, along with polar contacts with Arg1283. Structural simplification of compounds **1c** and **2c** retained their predicted NBD2-targeting capability, evidenced by Van der Waals contacts with Leu1260.

It is hypothesized that class I corrector activity depends on interactions with Met152, Phe81, Phe191, and Trp361, with additional Arg74 interactions further enhancing potency. Branched or folded molecules, particularly thiazole derivatives with appropriate substituents at positions 2 and 5, were favourable. Cyclization of the thiazole ring into a bicyclic core while maintaining an aromatic pendant group tethered to position 2 was also beneficial. The use of an amide spacer proved crucial for achieving an optimal conformation.

In contrast, class II correctors could benefit from smaller or linear structures featuring an amide moiety at thiazole position 2 (instead of an amine), enabling H-bonding with Gln1291 or Val1288. Engagement of the thiazole ring (or aromatic bioisosteres) in cation-π–π interactions with Arg1283 was essential. Accordingly, compound **1c** emerged as a promising class II candidate. Additionally, the introduction of electron-withdrawing aromatic groups at position 4 (rather than 5) of the thiazole ring appeared advantageous for optimizing thiazole-based correctors, which also showed favourable in silico bioavailability properties. Previously reported pharmacokinetic profiles for prototypes such as FCG [284] and other thiazole analogues [354] revealed high human intestinal absorption (HIA = 100%) and oral bioavailability (%F > 60%), consistent with Lipinski's and Veber's rules [375].

These computational predictions were subsequently validated through functional assays aimed at assessing: (i) the effectiveness of compounds from the a–c series as standalone CFTR

modulators and/or in combination with VX809, and (ii) the rescue potential of new compound combinations based on class I and II derivatives. As for docking results, compounds **1b**, **2b**, and **7b** were evaluated individually or in combination, while compound **1c** was assessed in tandem with **1b**, **2b**, or **7b**. Compound **2c**, predicted to exhibit dual class I/II activity, was evaluated both alone and with VX445.

Remarkably, the **2b** + **5a** and **7b** + **4a** combinations, consistent with docking predictions, exhibited strong functional activity. Compounds **2b** and **7b**, evaluated as class II correctors, targeted the NBD2 domain and formed key interactions with Leu1255, Pro1290, and Gln1291, mirroring reference modulators FCG and Corr-4a. Structural elements from FCG and 3151 were also present in **2b** and **7b**, including the SCH_3-phenyl group (in **2b**, as in FCG) and the furanyl ring (in **7b**, as in 3151). Co-administration with class I correctors **4a** and **5a** yielded synergistic combinations, supported by molecular modelling. Both **4a** and **5a** matched the CFTR binding site observed in VX809-bound structures (PDB 8EIO), facilitated by the benzodioxole group and aromatic/hydrophobic thiazole substituents that interacted with Phe78, Arg74 (cation–π), and Trp361 (π–π stacking).

Further functional validation of these novel, mechanistically distinct correctors demonstrated their ability to address multiple aspects of the F508del-CFTR folding defect and improve channel function. Notably, the presence of the second-site suppressor mutation (p.Arg1070Trp) revealed that effective F508del-CFTR correction involves stabilization of NBD1 and its interface with MSD2 (NBD1-ICL4), addressing the primary folding defect or achieving stabilization of NBD1 [376].

Functional studies in HEK293 cells expressing F508del/R1070W-CFTR revealed that all compounds enhanced F508del-CFTR function (Figure 2.14). However, compounds **1b**, **4b**, and **4a** failed to rescue F508del/R1070W-CFTR, suggesting that **2b**, **3b**, **7b**, **5a**, and **1c**, like VX809, do not act through NBD1-ICL4 interface stabilization, whereas **1b**, **4b**, and **4a** likely function via this pathway (Figure 2.14). This implies that these three compounds may not rescue other CFTR variants beyond F508del, though further validation in models expressing alternative class II CFTR mutations is needed.

As seen with VX809-hybrids, combining newly synthesized compounds, selected based on their domain-specific targeting abilities, significantly enhanced F508del-CFTR functional rescue, with some combinations outperforming VX809 + VX445 in CFBE41o- cells (Figure 2.15). Specifically, the **2b** + **5a** and **7b** + **4a** combinations provided superior rescue and correlated with increased protein processing (Figure 2.15E–F). Although these novel combinations showed enhanced rescue, they may exhibit lower potency compared to Vertex's compounds, considering that higher concentrations (10 μM *vs*. 3 μM, respectively) were used to evaluate their effect (Figure 2.15D).

In contrast, combinations of **2b** + **5a** with **1c** or **7b** + **4a** with **2b** did not exhibit additive or synergistic effects, confirming overlapping mechanisms of action between **1c** and **2b** or between **7b** and **4a**, respectively (Figure 2.15).

Encouragingly, results obtained in CFBE41o- cells were confirmed in primary nasal epithelial cells from four pwCF. Fluorescence-based membrane potential (FMP) assays showed that, despite inter-patient variability, all novel corrector combinations promoted the same level of F508del-CFTR rescue compared to VX809 + VX445 or VX661 + VX445 (reference treatments). Notably, combinations **2b** + **5a** and **7b** + **4a** resulted in even greater rescue than VX809 + VX445, highlighting their therapeutic potential (Figure 2.16).

Finally, the data presented in Part 3 of the Results underscore the therapeutic potential of targeting the Hsp70 chaperone system to enhance the efficacy of pharmacological correctors in rescuing F508del-CFTR trafficking.

Consistent with previous reports highlighting the modulatory role of MKT-077 on Hsp70 function and its synergistic effect with VX809 [262], the herein reported findings confirm and extend this strategy through the development of novel analogues. Among the three newly synthesized compounds (**DL79**, **DL90**, and **AP161**), **DL79** emerged as the most promising Hsp70 inhibitor, exhibiting the highest ATPase inhibitory activity (80%, Table 2.7) and a significant thermal stabilization of the human recombinant protein (Table 2.8). Notably, **DL79** significantly potentiated the corrective effect of VX809 on F508del-CFTR trafficking in CFBE41o- cells (Figure 2.22), with a maximal increase of 39.7% in iodide influx at a remarkably low concentration (0.025 μM). This potentiation surpasses the effects previously reported for both MKT-077 and GR24 [354], suggesting that **DL79** may exhibit superior affinity or more favourable binding dynamics with Hsp70. In contrast, **DL90**, despite its substantial inhibitory activity *in vitro* (Table 2.7), failed to enhance VX809-mediated rescue (Figure 2.22), highlighting that biochemical inhibition of Hsp70 does not necessarily translate into functional correction and may be influenced by additional factors such as cell permeability, target engagement, or off-target effects. Furthermore, the combination of **DL79** with other clinically approved correctors revealed a synergistic interaction with VX661 (+38.1%, Figure 2.23) and a modest but significant enhancement with the VX661/VX445 combination (+12.3%, Figure 2.25), whereas no meaningful effect was observed in combination with VX445 alone (Figure 2.24). These results suggest that **DL79** may specifically complement correctors acting at early folding steps (e.g., VX809, VX661) rather than those targeting later stages of CFTR maturation (e.g., VX445). Collectively, these findings support the continued investigation of **DL79** as a potentiator of corrector-based therapies and highlight the importance of rational chaperone system modulation as a complementary strategy in CF drug development.

4. Conclusions

Overall, this thesis demonstrates that the rational design of mechanistically distinct CFTR correctors, combined with targeted modulation of the cellular quality control machinery, can significantly enhance the rescue of F508del-CFTR. The results presented herein provide new insights into CFTR folding biology, identify promising lead compounds and combinations, and support a precision medicine approach to CF therapy. Among the molecules synthesized, the VX809-hybrid corrector **2a** emerged as a promising candidate for rescuing F508del-CFTR. Moreover, the rational design of additional class I and class II correctors led to the identification of novel, highly effective corrector combinations, particularly **2b** + **5a** and **7b** + **4a**. These combinations surpassed the efficacy of reference treatments such as VX809 + VX445 both in transfected cellular models and in primary airway epithelial cells from pwCF. Further studies are needed to be conducted to investigate the role of these new compounds from a mechanistic point of view, for example, determining whether the combination of newly synthesized correctors with those already approved could lead to a synergistic rather than an additive effect.

In parallel, targeting the cellular proteostasis network emerged as a complementary therapeutic strategy. The Hsp70 inhibitor **DL79** significantly potentiated the corrective effects of early-acting CFTR modulators, supporting the notion that chaperone system modulation can enhance pharmacological correction during early folding stages.

Future efforts should focus on further studies of the most promising compounds and combinations identified in this thesis, with particular attention to evaluate their pharmacokinetic properties, as well as their safety profile and long-term effects by *in vivo* assays. Validation in additional patient-derived models expressing different CFTR mutations, i.e., those carrying the orphan mutations and being poor responders or resistant to ETI treatment, will be essential to assess the broader applicability of these newly synthesized correctors.

In conclusion, the experimental strategy used in this thesis, namely combining structure-guided drug design and functional validation of modulators in specific cell models, (including primary cells from pwCF) has strong potential to further advance the treatment of CF and address the unmet needs of patients who remain underserved by current drug therapies.

5. Materials and methods

5.1. Chemicals

5.1.1. General description of the synthesis of the compounds

All solvents and chemicals used for synthesis and analysis were of reagent grade. If not explicitly indicated in the text, all other chemicals and culture media components were provided by Merck (Milan, Italy), Sigma-Aldrich (St. Louis, MO, USA), and VWR (Radnor Township, PA, USA).

The analytical instrument was an Agilent 1260 high-performance liquid chromatograph (HPLC, Agilent Technologies, Santa Clara, CA, USA). The analytical HPLC column was a Phenomenex C18 Luna (4.6 × 250 mm, 5 μm) (Torrance, CA, USA).

The preparative HPLC was an Agilent 1260 Infinity, and a Phenomenex C18 Luna (21.2 × 250 mm, 15 μm) column was used for preparative chromatography.

Liquid chromatography–electrospray mass spectrometry (HPLC-ESI-MS, Agilent Technologies, Santa Clara, CA, USA) was used to analyse the intermediates and the raw products using an Agilent 1100 series LC/MSD ion trap instrument.

The nuclear magnetic resonance (NMR) analyses were performed using a Jeol 400 MHz spectrometer (Jeol LTD, Akishima, Tokyo, Japan). The proton spectra and the carbon spectra were acquired at room temperature at 400 MHz and at 100 MHz, respectively. Chemical shifts were reported in units (ppm) relative to tetramethylsilane (TMS) as an internal standard. Coupling constants (J), when reported, are expressed in Hertz (Hz).

All raw products were purified with preparative HPLC using the following gradient: from 0 to 5 minutes at 20% eluent B, from 5 minutes to 40 minutes at 100% eluent B, and from 40 to 45 minutes at 100% eluent B. Eluent A was water with 0.1% formic acid (FOA), and eluent B was acetonitrile with 0.1% FOA.

All final products utilized in biological assays had a purity of 95% or higher based on the analytical HPLC/MS analysis. Compound purity was determined by integrating peak areas of the chromatogram obtained in the liquid phase, monitored at 254 nm.

5.1.2. Details of the synthesized compounds

*1-(benzo[d][1,3]dioxol-5-yl)-N-(5-benzoyl-4-phenylthiazol-2-yl) cyclopropanecarboxamide (**1a**)*

2-bromo-1,3-diphenylpropane-1,3-dione (30.3 mg, 0.1 mmol) was conjugated with thiourea (7, 6 mg, 0.1 mmol) in anhydrous ethanol (1 mL) at reflux (24 hours). The intermediate compound obtained, 2-amino-(4-phenylthiazol-5-yl) phenylmethanone, was verified by HPLC and MS and purified with preparative HPLC. To a solution of 1-(benzo[d][1,3]dioxol-5-yl) cyclopropanecarboxylic acid (12.5 mg, 0.06 mmol) in anhydrous DMF (500 µL), HATU (38 mg, 0.1 mmol) and DIPEA (35 µL, 0.2 mmol) were added. Then the thiazole (12,5 mg, 0,06 mmol) was added, and the reaction mixture was stirred at 50 °C. After 20 hours, the reaction was complete. The mixture was concentrated under vacuum and after extraction with ethyl acetate (3 × 3 ml), washed with H_2O (3 × 2 ml). The organic phase was dried over Na_2SO_4, concentrated under reduced pressure, and purified by preparative HPLC. The peak of interest was concentrated to obtain the title compound with a purity of >95% as determined by HPLC-MS (14 mg, 30%) [278].

^{1}H NMR (200 MHz, $CDCl_3$): δ), 8.93 (s, broad, 1H), 7.96–7.39 (m, 10H), 7.08–6.83 (m, 3H), 6.07 (s, 2H), 2.02–1.63 (m, 2H), 1.45–1.19 (m, 2H).

^{13}C NMR (50 MHz, $CDCl_3$): δ 193.6, 172.1, 164.2, 153.8, 148.0, 145.1, 138.2, 136.9, 133.5, 132.4, 129.5, 129.2, 128.6, 128.5, 127.0, 116.5, 112.5, 107.8, 100.3, 29.7, 16.5.

HRMS (ESI) calculated for $C_{27}H_{21}N_2O_4S$: 469.1222 $[M + H]^+$ found 469.1213.

*1-(Benzo[d][1,3]dioxol-6-yl)-N-(5-(4-(methylthio)benzoyl)-4 phenylthiazol-2-yl)cyclo propanecarboxamide (**2a**)*

A mixture of 1-[(4-methoxy)phenyl]methanamine (535 mL, 4 mmol) and 4-(methoxy)benzaldehyde (595 mL, 4.8 mmol) in methanol (2 mL) was heated to reflux for 3 hours, then cooled to T = 0 °C, $NaBH_4$ (228 mg, 6 mmol) was added portion wise to the reaction and the resulting mixture was stirred at room temperature for about 10 hours. Solvent was removed under reduced pressure, and the residue was partitioned between ethyl acetate and H_2O. The combined organic layers were washed with H_2O and then dried over anhydrous Na_2SO_4. After filtration, the solvent was removed under vacuum to afford bis [4-methoxyphenyl]methylamine (962 mg, 94%) as a colourless oil, which was used in the next step without further purification. ESI-MS: m/z 258.0 $[M + H]^+$. To a solution of benzoyl isothiocyanate (140 mL, 1 mmol) in acetone (1 mL) cooled at T = 0 °C, bis [4-methoxyphenyl]methyl amine (257 mg, 1 mmol) in acetone (1 mL) was added at this

temperature and stirred for an additional 1 hour. The mixture was concentrated under reduced pressure to afford N-(bis(4-methoxybenzyl) carbamothioyl)benzamide (398 mg, 95%) as a yellow sticky oil, which was used in the next step without further purification. ESI-MS: m/z 421.0 $[M + H]^+$. A solution of 2-bromo-1-(4-(methylthio)phenyl)ethanone (123 mg, 0.5 mmol) and N-(bis(4-methoxybenzyl)carbamothioyl) benzamide (210 mg, 0.5 mmol) in N, N-dimethylformamide (3 mL) was stirred at T=85 °C for 3 hours. After cooling to room temperature, the mixture was partitioned between ethyl acetate and H_2O. The organic layer was washed with brine and dried over anhydrous Na_2SO_4. After filtration, the solvent was removed under vacuum, and the residue was stirred in trifluoroacetic acid (TFA) (4 mL) at T=80 °C for 24 hours until complete deprotection. Most of TFA was removed under reduced pressure. The residue was then neutralized with $NaHCO_3$ 1N and then extracted with ethyl acetate 3 times. The combined organic layers were washed with brine and dried over anhydrous Na_2SO_4. After filtration, the solution was concentrated and further crystallized in acetonitrile to afford (2-amino-4-phenylthiazol-5-yl) (4-(methylthio)phenyl)methanone (127 mg, 78%) as a brown solid. ESI-MS: m/z 328.1 $[M + H]^+$. Benzo [1,3]dioxol-5-yl-cyclopropanecarboxylic acid (20.6 mg, 0.1 mmol) was resuspended in anhydrous DMF (1 mL); HATU (38 mg, 0.1 mmol) and DIPEA (35 mL, 0.2 mmol) were added.

The reaction was vigorously stirred for 5 minutes and (2-amino-4-phenylthiazol-5-yl) (4-(methylthio)phenyl)methanone (32.7 mg, 0.1 mmol) in anhydrous DMF (500 µL) was added. The reaction was kept at T= 50 °C until completeness (24 hours) and then purified by preparative HPLC. The peak of interest was concentrated to obtain the title compound as a yellow solid with purity of >95% as determined by HPLC-MS (12.7 mg, 25%) [365].

^{1}H NMR (200 MHz, DMSO-d_6): δ 11.89 (s, broad, 1H, NH); 7.71e6.57 (m, 12H, arom); 6.02 (s, 2H OCH_2O); 2.37 (s, 3H, SCH_3); 1.68e1.42 (m, 2H, CH_2, cyclopr); 1.40e1.09 (m, 2H, CH_2, cyclopr).

^{13}C NMR (50 MHz, DMSO-d_6): d 187.3, 165.7, 158.6, 153.9, 146.9, 146.3, 131.8, 130.9, 129.6, 128.9, 128.1, 127.4, 123.1, 114.5, 110.2, 107.8, 100.6, 98.7, 51.8, 30.3, 15.5.

HRMS (ESI) calculated for $C_{28}H_{23}N_2O_4S_2$: $[M + H]^+$ 515.10992; found 515.10971.

*N-(5-([1,1'-biphenyl]-4-carbonyl)-4-phenylthiazol-2-yl)-1-(benzo[d][1,3]dioxol-5-yl)cyclopropane-1-carboxamide (**3a**)*

Compound **3a** (15.3 mg, 28%) was prepared from [1, 1'-biphenyl]-4-yl (2-amino-4-phenylthiazol-5-yl)methanone (35.7 mg, 0.1 mmol) and benzo [1,3] dioxol-5-yl-cyclopropanecarboxylic acid (20.6 mg, 0.1 mmol) in the same manner as described for **2a** as a pale yellow solid [365].

^{1}H NMR (200 MHz, DMSO-d_6): d 12.01 (s, 1H, broad, NH); 7.92e6.76 (m, 17H, arom); 6.05 (s, 2H OCH_2O); 1.78e1.44 (m, 2H, CH_2, cyclopr); 1.42e1.08 (m, 2H, CH_2, cyclopr).
^{13}C NMR (50 MHz, DMSO-d_6): δ 188.2, 172.2, 156.8, 153.2, 146.9, 146.3, 140.7, 137.9, 132.2, 131.3, 129.3, 128.2, 127.4, 123.1, 110.2, 107.8, 100.6, 30.3, 15.4.
HRMS (ESI) calculated for $C_{33}H_{25}N_2O_4S$: $[M + H]^+$ 545.15349; found 545.13351.

*1-(benzo[d][1,3]dioxol-5-yl)-N-(5-(3-fluorophenoxy)-4-methylthiazol-2-yl)cyclopropanecarbox-amide (**4a**)*

To a solution of 4-methylthiazole-2-amine (100 mg, 0.87 mmol) in glacial acetic acid (800 µL) at room temperature N-bromosuccinimide (176 mg, 0.99 mmol) was added. After 2 hours, 5-bromo-4-methylthiazol-2-amine as a dark solid was obtained by precipitation in Diisopropyl ether at T = 0 °C (143 mg, 85%) and washing out with the same solvent at T=0 °C (3 x 1 mL). The crude compound was used in the next step without further purification.
ESI-MS m/z: 192.9 $[M + H]^+$

To a mixture of 5-bromo-4-methylthiazol-2-amine (66 mg, 0.34 mmol) and cesium carbonate (167.8 mg, 0.52 mmol) in acetonitrile (2.5 mL) at T=70 °C was added 3-fluorophenol (50 mg, 0.45 mmol). Then the reaction was stirred at the same temperature for about 1 hour. The reaction was cooled to room temperature and diluted with water (10 mL). The aqueous layer was extracted with ethyl acetate (15 mL x 3). The combined organic layers were dried over Na_2SO_4, filtered, and concentrated in vacuo to give 5-(3-fluorophenoxy)-4-methylthiazol-2-amine as a brown oil, which was used directly in the next step.

To a solution of 1-(benzo[d][1,3]dioxol-5-yl)cyclopropane carboxylic acid (36 mg, 0.17 mmol) in anhydrous DMF (200 µL) at room temperature was added HATU (59 mg, 0.15 mmol) and DIPEA (60 µL, 0.33 mmol). After a few minutes, crude 5-(3-fluorophenoxy)-4-methylthiazol-2-amine (38 mg, 0.17 mmol) in anhydrous DMF (450 µL) was added, and the reaction was kept at T=50 °C for 24 hours. The reaction mixture was extracted with dichloromethane (3 x 3 mL) and washed with water (3 x 3 mL). The organic phase was dried over Na_2SO_4, concentrated under reduced pressure and purified by preparative HPLC. The peak corresponding to the product of interest was concentrated to obtain (12 mg, 17 %) a white solid with purity of >95% as determined by HPLC-MS.
^{1}H NMR (400 MHz, DMSO-d_6): δ 11.05 (s, 1H, NH); 7.41-7.30 (m, 1H, arom); 6.98-6.74 (m, 6H, arom); 5.98 (s, 2H, OCH_2O); 1.99 (s, 3H, CH_3); 1.48-1.38 (m, 2H, CH_2); 1.14-1.03 (m, 2H, CH_2).
^{13}C NMR (100 MHz, DMSO-d_6): δ 164.6, 160.1, 147.8, 147.2, 141.2, 132.9, 131.9, 131.8, 124.2, 111.9, 111.9, 111.2, 110.7, 110.5, 108.7, 104.0, 103.7, 101.5, 31.0, 16.1, 13.2

ESI-MS m/z: 413.4 $[M + H]^+$

*1-(benzo[d][1,3]dioxol-5-yl)-N-(5-phenoxy-4-(p-tolyl)thiazol-2-yl)cyclopropanecarboxamide (**5a**)*

A solution of N-bromosuccinimide (213 mg; 1,2 mmol) in anhydrous tetrahydrofuran (THF) (2 mL) was added to a solution of 4-(p-tolyl)thiazol-2-amine (190 mg, 1 mmol) in THF (5 mL), and the mixture was stirred at T=40 °C for 5 hours. Solvent was removed under reduced pressure, and the residue was partitioned between ethyl acetate and water. The combined organic layers were washed with water and then dried over anhydrous Na_2SO_4. After filtration, the solvent was removed under vacuum to afford 5-bromo-4-(p-tolyl)thiazol-2-amine (200 mg, 75 %) as a colourless oil, which was used in the next step without further purification.
ESI-MS: m/z 268 $[M + H]^+$.

To a mixture of 5-bromo-4-(p-tolyl)thiazol-2-amine (100 mg, 0.37 mmol), phenol (45 mg,0,48 mmol) in acetone (3 mL), caesium carbonate (193 mg, 0.59 mmol) was added.
The reaction mixture was heated to T=55 °C and stirred for 7 hours. Solvent was removed under reduced pressure, and the residue was partitioned between ethyl acetate and water. The combined organic layers were washed with water and then dried over anhydrous Na_2SO_4. After filtration, the solvent was removed under vacuum. The residue was then purified by HPLC chromatography to afford the desired product 5-phenoxy-4-(p-tolyl)thiazol-2-amine (70 mg; 67 %)
ESI-MS m/z 283.1 $[M + H]^+$.

Benzo[1,3]dioxol-5-yl-cyclopropanecarboxylic acid (20 mg, 0.1 mmol) was resuspended in anhydrous DMF (1 mL), HATU (38 mg, 0.1 mmol) and DIPEA (35 µL, 0.2 mmol) were added.
The reaction was vigorously stirred for 5 min, and 5-phenoxy-4-(p-tolyl)thiazol-2-amine (28 mg, 0.1 mmol) in anhydrous DMF (1 mL) was added. The reaction was kept at T = 50 °C for 24 hours and then purified by preparative HPLC. The peak of interest was concentrated to obtain the title compound as a yellow solid with purity of >95% as determined by HPLC-MS (12 mg, 28 %).
^{1}H NMR (400 MHz, DMSO-d_6): δ 11.20 (s, 1H, NH); 7.71-7.62 (m, 2H, arom); 7.39-7.28 (m, 2H, arom); 7.17-7.02 (m, 5H, arom); 6.97 (s, 1H, arom); 6.90-6.81 (m, 2H, arom); 5.99 (s, 2H, OCH_2O); 2.24 (s, 3H, CH_3); 1.51-1.36 (m, 2H, CH_2); 1.16-1.04 (m, 2H, CH_2).
^{13}C NMR (100 MHz, DMSO-d_6): δ 172.5, 158.5, 149.7, 147.8, 147.2, 143.4, 137.5, 134.9, 132.9, 130.6, 130.3, 129.6, 126.9, 124.3, 124.2, 116.4, 111.2, 108.7, 101.5, 31.0, 29.5, 21.3, 16.1.
ESI-MS m/z = 471.1 $[M + H]^+$.

*N-(4-(4-acetamidophenyl)-5-(4-(methylsulfonyl)phenoxy)thiazol-2-yl)-1-(benzo[d][1,3]dioxol-5-yl)cyclopropanecarboxamide (**6a**)*

A solution of N-bromosuccinimide (430 mg, 2.4 mmol) in THF (2mL) was added to a solution of N-(4-(2-aminothiazol-4-yl)phenyl)acetamide (466 mg, 2 mmol) in THF (5 mL) and the mixture was stirred at T=40 °C for 4 hours. Solvent was removed under reduced pressure, and the residue was partitioned between ethyl acetate and water. The combined organic layers were washed with water and then dried over anhydrous Na_2SO_4. After filtration, the solvent was removed under vacuum to afford N-(4-(2-amino-5-bromothiazol-4-yl)phenyl)acetamide (383 mg, 61%) as a colourless oil, which was used in the next step without further purification.

ESI-MS: m/z 311.9 $[M + H]^+$.

To a mixture of N-(4-(2-amino-5-bromothiazol-4-yl)phenyl)acetamide (47 mg; 0.15 mmol), 4-(methylsulfonyl)phenol (25 mg, 0.15 mmol) in acetone (3 mL), caesium carbonate (79 mg, 0.24 mmol) was added. The reaction mixture was heated to T = 55 °C and stirred for 7 hours. Solvent was removed under reduced pressure, and the residue was partitioned between ethyl acetate and water. The combined organic layers were washed with water and then dried over anhydrous Na_2SO_4. After filtration, the solvent was removed under vacuum. The residue was then purified by HPLC to afford the desired product N-(4-(2-amino-5-(4-(methylsulfonyl)phenoxy)thiazol-4-yl)phenyl)acetamide (44,4 mg; 73%).

ESI-MS: m/z 404.1 $[M + H]^+$.

Benzo[1,3]dioxol-5-yl-cyclopropanecarboxylic acid (22.6 mg; 0.11 mmol) was resuspended in anhydrous DMF (1 mL); HATU (38 mg, 0.1 mmol) and DIPEA (38 µL, 0,22 mmol) were added. The reaction was vigorously stirred for 5 minutes, and N-(4-(2-amino-5-(4-(methylsulfonyl)phenoxy)thiazol-4-yl)phenyl)acetamide (44 mg; 0.11 mmol) in anhydrous DMF (1 mL) was added. The reaction was kept at T=50 °C for 24 hours and then purified by preparative HPLC. The peak of interest was concentrated to obtain the title compound as a yellow solid with purity >95% as determined by HPLC-MS (14 mg, 23%).

^{1}H NMR (400 MHz, DMSO-d_6): δ 11.09 (s, 1H, NH); 8.18 (s, 1H, NH); 7.92-7.61 (m, 6H, arom); 7.05-6.73 (m, 5H, arom); 5.97 (s, 2H, OCH_2O); 3.12 (s, 3H, CH_3); 2.28 (s, 3H, CH_3); 1.55-1.39 (m, 2H, CH_2); 1.16-1.04 (m, 2H, CH_2).

^{13}C NMR (100 MHz, DMSO-d_6): δ 166.7, 163.5, 160.2, 156.9, 147.8, 147.2, 145.4, 141.2, 139.5, 138.8, 133.2, 131.5, 127.4, 127.1, 125.8, 124.7, 122.3, 121.4, 121.3, 119.1, 118.5, 110.4, 109.2, 101.5, 41.7, 31.0, 25.7, 16.1, 13.7.

ESI-MS m/z = 592.2 $[M + H]^+$.

*4-(3,4-dichlorophenyl)-N-(3-(methylthio)phenyl)thiazol-2-amine(**1b**)*

Synthesized from 1-(3-(methylthio)phenyl)thiourea and commercially available 2-bromo-3',4' dichloro-acetophenone. To obtain the 1-(3-(methylthio)phenyl)thiourea, a solution of benzoyl isothiocyanate (673 ml, 5 mmol) in anhydrous THF (2 mL) was first dropwise added to a solution of 3-methylthioaniline (616 ml, 5 mmol) in anhydrous THF (2 mL) at room temperature overnight. When the reaction was completed, the mixture was concentrated under vacuum and dissolved in ice-cold water. After 30 minutes of stirring, a white pellet appeared. The reaction was centrifuged at 4000*xg* for 5 minutes, and the pellet was washed with water (3 x 2 mL). Then the pellet was resuspended in a solution of EtOH and 1M NaOH 1:1 (5 mL). The reaction was heated to reflux until the hydrolysis was complete (controlled with HPLC-MS). The mixture was concentrated under vacuum, and a solution of aqueous 1N HCl was added to produce a neutral solution. The reaction mixture was centrifuged at 4000*xg* for 5 minutes, and the pellet was washed with water (3 x 1 mL). The compound was completely dried and lyophilized to obtain the 1-(3-(methylthio)phenyl)thiourea as powder (888 mg, 88%) and used without further purification in the reaction with 2-bromo-3',4'dichloro-acetophenone.

As the last step to synthesize the title compound, the following protocol was used: the haloketone (1 eq) was conjugated with thiourea (1 eq) in anhydrous EtOH (1 mL). The reaction was stirred at reflux for 24 hours until the reaction was judged complete (HPLC-MS). The mixture was then extracted with ethyl acetate (3 x 3 mL). The organic phases were concentrated under vacuum and lyophilized. The product was verified by HPLC and MS and purified with preparative HPLC [283].

Yield: 79%

H NMR (400 MHz, $CDCl_3$): δ 7.96 (d, J=1.5 Hz, 1H), 7.89 (dd, J=7.5, 1.5 Hz, 1H), 7.54 (d, J=7.5 Hz, 1H). 7.43 (t, J = 2.0 Hz, 1H), 7.23 (t, J = 7.7 Hz, 1H), 7.10 (ddd, J = 8.0, 2.2, 0.9 Hz, 1H), 6.94(ddd, J = 7.8, 1.8, 0.9 Hz, 1H), 6.88 (s, 1H), 2.55 (s, 3H).

^{13}C NMR (100 MHz, $CDCl_3$): δ 160.2, 150.6, 143.3, 137.2, 133.4, 132.7, 132.5, 130.7, 128.8, 127.3,126, 119.1, 114.7, 113.4, 105.3, 14.3.

ESI-MS m/z = 367.0 $[M + H]^+$.

*4-(3-chloro-5-(trifluoromethyl)phenyl)-N-(3-(methylthio)phenyl)thiazol-2-amine (**2b**)*

3' chloro 5'(trifluoromethyl)acetophenone (1eq) was brominated with N-bromosuccinimide (2 eq) and trimethylsilyl trifluoromethanesulfonate (TMS-OTf) (1 eq) in acetonitrile. The reaction

was stirred at T = 40 °C until completeness, diluted with diethyl ether (2 mL), washed with H_2O (3 x 2 ml), dried over Na_2SO_4, and concentrated under reduced pressure. This procedure provided a 2-bromoketone intermediate in 75% overall yield, with purity >95% as determined by HPLC-MS. The compound was used without further purification and conjugated with 1-(3(methylthio)phenyl)thiourea (obtained with the method reported in 1b synthesis) as **1b** synthesis [283].

Yield: 60%

^{1}H NMR (400 MHz, $CDCl_3$): δ 8.06 (t, J=1.5 Hz, 1H), 8.01 (t, J = 1.6 Hz, 1H), 7.68 (t, J=1.5 Hz,1H), 7.38 (t, J = 2.0 Hz, 1H), 7.23 (t, J = 7.7 Hz, 1H), 7.11 (ddd, J = 8.0, 2.2, 0.9 Hz, 1H), 6.94 (ddd, J = 7.8, 1.8, 0.9 Hz, 1H), 6.84 (s, 1H), 2.54 (s, 3H).

^{13}C NMR (100 MHz, $CDCl_3$): δ 160.6, 152.2, 142.6, 137.2, 135.1, 134.7, 133, 132.9, 128.3, 124.9, 124.6, 123, 119.6, 114.3, 113.5, 105.4, 14.2.

ESI-MS m/z = 401.0 $[M + H]^+$.

*N-(4-phenylthiazol-2-yl)nicotinamide (**3b**)*

Nicotinic acid (12 mg, 0.1 mmol) was dissolved in anhydrous DMF (500 µL) at room temperature. HATU (38 mg, 0.1 mmol) and DIPEA (35 µl, 0.2 mmol) were added. After a few minutes, 2-Amino-4-phenylthiazole (17 mg, 0.1 mmol) in anhydrous DMF (500 µL) was added, and the reaction was kept at T = 50 °C for 36 hours. The mixture was concentrated under vacuum and after extraction with ethyl acetate (3 x 3 mL), washed with water (3 x 2 mL). The organic phase was dried over Na_2SO_4, concentrated under reduced pressure, and purified by preparative HPLC. The peak of interest was concentrated to obtain the title compound (14 mg, 51%).

^{1}H NMR (400 MHz, DMSO-d_6): δ 9.09 (d, J = 2.4, 1H, arom); 8.44 (dd, J = 4.0, 2.48, 1H, arom); 8.22 (s, 1H, arom), 8.11 (m, 1H arom); 7.83-7.74 (m, 2H, arom); 7.52 (s, 1H, arom), 7.46-7.32 (m, 3H, arom).

^{13}C NMR (100 MHz, DMSO-d_6): 166.9, 161.6, 153.4, 148.1, 147.7, 133.8, 132.1, 130.1,127.1, 124.8, 121.5, 106.9

ESI-MS m/z = 282.1 $[M + H]^+$.

*N-(5-((3-fluorophenyl)(methyl)amino)thiazol-2-yl)cyclohexanecarboxamide (**4b**)*

Cesium carbonate (151 mg, 0.46 mmol) was added to a mixture of 5-bromothiazol-2-amine (100 mg, 0.39 mmol), 3-fluoro-N-methylaniline (72 mg, 0.58 mmol) in acetone (3 mL).

The reaction mixture was heated to T = 55 °C and stirred for 8 hours. Solvent was removed under reduced pressure, and the residue was partitioned between ethyl acetate and water. The combined organic layers were washed with water and then dried over anhydrous Na_2SO_4. After filtration, the solvent was removed under vacuum.

The residue was then purified by HPLC chromatography to afford N-(3-fluorophenyl)-N,2-dimethylthiazol-5-amine as a yellow solid (109 mg, 51 %).

ESI-MS m/z = 224.1 $[M + H]^+$

To a solution of cyclohexane carboxylic acid (12 mg, 0.09 mmol) in anhydrous DMF (200 µL) at room temperature was added HATU (32 mg, 0.08 mmol) and DIPEA (32 µL, 0.19 mmol). After a few minutes, N-(3-fluorophenyl)-N,2-dimethylthiazol-5-amine (21 mg, 0.09 mmol) in anhydrous DMF (400 µL) was added, and the reaction was kept at T = 50 °C for 20 hours. The reaction mixture was diluted with dichloromethane (3 mL) and washed with water (3 x 3 mL). The organic phase was dried over Na_2SO_4, concentrated under reduced pressure, and purified by preparative HPLC. The peak of interest was concentrated to obtain the title compound (14 mg, 46%) as a brown solid with purity >95% as determined by HPLC-MS.

^{1}H NMR (400 MHz, DMSO-d_6): δ 11.95 (s, 1H, NH); 7.25 (s, 1H, arom); 7.22-7.13 (m, 2H, arom); 6.63-6.49 (m, 3H, arom); 3.29 (s, 3H, CH_3); 2.48-2.35 (m, 3H, CH_2 e CH); 1.85-1.52 (m, 4H, CH_2); 1.43-1.04 (m, 4H, CH_2).

^{13}C NMR (100 MHz, DMSO-d_6): δ 174.7, 164.7, 162.3, 154.8, 151.5, 151.4, 140.3, 133.4, 131.0, 130.9, 110.8, 105.7, 105.5, 101.6, 101.4, 43.8, 42.3, 29.2, 25.7, 25.5.

ESI-MS m/z: 334.1 $[M + H]^+$.

*N-(4-phenylthiazol-2-yl)cyclohexanecarboxamide (**5b**)*

To a solution of cyclohexane carboxylic acid (18 mg, 0.14 mmol) in anhydrous DMF (500 µL) at room temperature was added HATU (49 mg, 0.13 mmol) and DIPEA (49 µL, 0.28 mmol). After a few minutes, 4-phenylthiazol-2-amine (25 mg, 0.14 mmol) in anhydrous DMF (400 µL) was added, and the reaction was kept at T = 50 °C for 24 hours.

The reaction mixture was diluted with ethyl acetate (3 mL) and washed with water (3 x 3 mL). The organic phase was dried over Na_2SO_4, concentrated under reduced pressure, and purified by preparative HPLC. The peak of interest was concentrated to obtain the title compound (12 mg, 28%) as a white solid with purity >95% as determined by HPLC-MS.

^{1}H NMR (400 MHz, DMSO-d_6): δ 11.09 (s, 1H, NH); 7.89-7.77 (m, 2H, arom); 7.53-7.32 (m, 3H, arom); 7.25 (s, 1H, arom); 2.49-2.33 (m, 3H, CH_2 e CH); 1.80-1.47 (m, 4H, CH_2); 1.39-1.04 (m, 4H, CH_2).
^{13}C NMR (100 MHz, DMSO-d_6): δ 174.5, 159.3, 150.9, 143.6, 134.3, 127.8, 125.8, 123.1, 122.7, 121.2, 43.7, 29.1, 25.5, 25.2.
ESI-MS m/z: 287.1 $[M + H]^+$

*N-(5-(3-fluorobenzyl)thiazol-2-yl)-2,5-dimethylfuran-3-carboxamide (**6b**)*

To a solution of 2,5-dimethylfuran-3-carboxylic acid (49 mg, 0.35 mmol) in anhydrous DMF (200 μL) at room temperature was added HATU (133 mg, 0.35 mmol) and DIPEA (122 μL, 0.7 mmol). After a few minutes, 5-(3-fluorobenzyl)thiazol-2-amine (73 mg, 0.35 mmol) in anhydrous DMF (100 μL) was added, and the reaction was kept at T = 50 °C for 24 hours.
The reaction mixture was extracted with dichloromethane (3 mL) and washed with water (3 x 3 mL). The organic phase was dried over Na_2SO_4, concentrated under reduced pressure, and purified by preparative HPLC. The peak of interest was concentrated to obtain the title compound (90 mg, 78%) as a brown solid with purity >95% as determined by HPLC-MS.
^{1}H NMR (400 MHz, DMSO-d_6): δ 10.67 (s, 1H, NH); 7.21 (s, 1H, arom); 7.11-6.82 (m, 4H, arom); 6.65 (s, 1H, arom); 4.38 (s, 2H, CH_2); 2.31 (s, 3H, CH_3); 2.23 (s, 3H, CH_3).
^{13}C NMR (100 MHz, DMSO-d_6): δ 165.3, 158.8, 156.7, 154.6, 154.3, 134.5, 131.1, 128.4,126.9, 125.2, 122.7, 121.6, 119.8, 106.3, 39.5, 13.8, 13.2
ESI-MS m/z: 331.1 $[M + H]^+$

*N-(5-(3-fluorophenoxy)-4-methylthiazol-2-yl)-2,5-dimethylfuran-3-carboxamide (7**b**)*

To a solution of 2,5-dimethylfuran-3-carboxylic acid (23.8 mg, 0.17 mmol) in anhydrous DMF (200 μL) at room temperature was added HATU (59 mg, 0.15 mmol) and DIPEA (60 μL, 0.33 mmol). After five minutes, crude 5-(3-fluorophenoxy)-4-methylthiazol-2-amine (obtained through the method reported for compound **4a**) (38 mg, 0.17 mmol), in anhydrous DMF (500 μL) was added, and the reaction was kept at T = 50 °C for 24 hours. The reaction mixture was extracted with dichloromethane (3 x 3 mL) and washed with water (3 x 3 mL).
The organic phase was dried over Na_2SO_4, concentrated under reduced pressure, and purified by preparative HPLC. The peak of interest was concentrated to obtain the title compound (10 mg, 17%) as a white solid with purity of >95% as determined by HPLC-MS.

^{1}H NMR (400 MHz, DMSO-d_6): δ 11.22 (s, 1H, NH); 7.39-7.28 (m, 1H, arom); 6.98-6.55 (m, 4H, arom); 2.28 (s, 3H, CH_3); 2.15 (s, 3H, CH_3); 2.04 (s, 3H, CH_3).
^{13}C NMR (100 MHz, DMSO-d_6): δ 164.8, 160.2, 152.6, 150.1, 147.8, 147.2, 140.8, 130.7, 124.2, 113.3, 112.6, 111.9, 108.7, 104.4,15.6, 13.9, 13.2.
ESI-MS m/z: 347.1 $[M + H]^+$

*N-(4,5,6,7-tetrahydrobenzo[d]thiazol-2-yl)cyclohexanecarboxamide (**1c**)*

To a solution of cyclohexane carboxylic acid (21 mg, 0.16 mmol) in anhydrous DMF (200 μL) at room temperature was added HATU (56 mg, 0.14 mmol) and DIPEA (56.4 μL, 0.33 mmol). After a few minutes, 2-amino-4,5,6,7-tetra-hydrobenzothiazole (25 mg, 0.16 mmol) in anhydrous DMF (400 μL) was added, and the reaction was kept at T = 50 °C for 18 hours. The reaction mixture was diluted with dichloromethane (3 mL) and washed with water (3 x 3 mL). The organic phase was dried over Na_2SO_4, concentrated under reduced pressure, and then purified by preparative HPLC.
The peak of interest was concentrated to obtain the title compound (27 mg, 64%) as a brown solid with purity >95% as determined by HPLC-MS.
^{1}H NMR (400 MHz, DMSO-d_6): δ 11.22 (s, 1H, NH); 2.67-2.29 (m, 7H, CH_2 e CH); 1.91-1.52 (m, 8H, CH_2); 1.39-1.03 (m, 4H, CH_2).
^{13}C NMR (100 MHz, DMSO-d_6): δ 174.6, 152.3, 138.2, 123.1, 43.7, 29.6, 29.2, 26.3, 26.1, 25.5, 25.2.
ESI-MS m/z: 265.1 $[M + H]^+$.

*N-(4,5,6,7-tetrahydrobenzo[d]thiazol-2-yl)-3-((trifluoromethyl)thio)benzamide (**2c**)*

To a solution of 3-((trifluoromethyl)thio)benzoic acid (22 mg, 0.1 mmol) in anhydrous DMF (200 μL) at room temperature was added HATU (38 mg, 0.1 mmol) and DIPEA (37 μL, 0.2 mmol). After a few minutes, 2-amino-4,5,6,7-tetra-hydrobenzothiazole (16 mg, 0.1 mmol) in anhydrous DMF (400 μL) was added, and the reaction was kept at T = 50 °C for 18 hours. The reaction mixture was diluted with dichloromethane (3 mL) and washed with water (3 x 3 mL). The organic phase was dried over Na_2SO_4, concentrated under reduced pressure, and purified by preparative HPLC.
The peak of interest was concentrated to obtain the title compound (23 mg, 65%) as a grey solid with purity >95% as determined by HPLC-MS.
^{1}H NMR (400 MHz, DMSO-d6): δ 8.38 (s, 1H, arom); 8.29-8.21 (m, 1H, arom); 7.95-7.87 (m, 1H, arom); 7.66 (t, J = 7.6, 1H, arom); 2.68-2.59 (m, 2H, CH_2); 2.59-2.51 (m, 2H, CH_2); 1.85-1.66 (m, 4H, CH_2).

^{13}C NMR (100 MHz, DMSO-d_6): 140.1, 136.1, 135.0, 131.6, 131.5, 130.8, 128.5, 124.2, 122.0, 26.0, 23.3, 22.9, 22.7
ESI-MS m/z: 359.1 $[M + H]^+$.

*N-(benzo[d]thiazol-2-yl)cyclohexanecarboxamide (**3c**)*

To a solution of cyclohexane carboxylic acid (21 mg, 0.17 mmol) in anhydrous DMF (200 µL) at room temperature was added HATU (57 mg, 0.15 mmol) and DIPEA (57 µL, 0.33 mmol). After a few minutes, 2-aminobenzo[d]thiazole (25 mg, 0.17 mmol) in anhydrous DMF (100 µL) was added, and the reaction was kept at T = 50 °C for 24 hours.
The reaction mixture was extracted with dichloromethane (3 mL) and washed with water (3 x 3 mL). The organic phase was dried over Na_2SO_4, concentrated under reduced pressure, and purified by preparative HPLC. The peak of interest was concentrated to obtain the title compound (27 mg, 62%) as a brown solid with purity >95% as determined by HPLC-MS.
^{1}H NMR (400 MHz, DMSO-d_6): δ 11.04 (s, 1H, NH); 7.49-7.32 (m, 2H, arom); 7.09-6.97 (m, 2H, arom); 2.44-2.31 (m, 3H, CH_2 e CH); 1.79-1.48 (m, 4H, CH_2); 1.42-1.05 (m, 4H, CH_2).
^{13}C NMR (100 MHz, DMSO-d_6): δ 172.2, 150.9, 145.6, 133.5, 125.8, 123.1, 122.7, 120.2, 44.1, 29.5, 29.2, 25.5, 25.1.
ESI-MS m/z: 261.1 $[M + H]^+$

*N-(benzo[d]thiazol-2-yl)nicotinamide (**4c**)*

To a solution of nicotinic acid (25 mg, 0.17 mmol) in anhydrous DMF (300 µL) at room temperature was added HATU (57 mg, 0.15 mmol) and DIPEA (58 µL, 0.33 mmol). After five minutes, 2-Aminobenzo[d]thiazole (25 mg, 0.17 mmol) in anhydrous DMF (600 µL) was added, and the reaction was kept at T = 50 °C for 24 hours. The reaction mixture was diluted with ethyl acetate (3 mL) and washed with water (3 x 3 mL). The organic phase was dried over Na_2SO_4, concentrated under reduced pressure, and purified by preparative HPLC. The peak of interest was concentrated to obtain the title compound (11.6 mg, 28%) as a brownish solid with purity >95% as determined by HPLC-MS.
^{1}H NMR (400 MHz, DMSO-d_6): δ 11.71 (s, 1H, NH); 8.98 (s, 1H, arom); 8.54-8.39 (m, 2H, arom); 7.58-7.37 (m, 3H, arom); 7.11-7.02 (m, 2H, arom).
^{13}C NMR (100 MHz, DMSO-d_6): δ 174.1, 157.5, 153.8, 151.6, 150.4, 134.7, 131.2, 130.3, 126.8, 123.1, 122.5, 120.6, 120.1.

ESI-MS m/z: 256 $[M + H]^+$

*N-(4-(4-bromophenyl)thiazol-2-yl)-4-(methylthio)benzamide (**AP161**)*

Added HATU (34.2 mg, 0.1mmol) and DIPEA (38 µL, 0.2 mmol) to a solution of 4-(methylthio)benzoic acid (16.8 mg, 0.1 mmol) in anhydrous DMF (400 µL) at room temperature. After five minutes, 4-(4-bromophenyl)thiazol-2-amine (25.5 mg, 0.1 mmol) was added, and the reaction was kept at T = 50 °C for 24 hours. The reaction mixture was diluted with ethyl acetate (3 mL) and washed with water (3 x 3 mL). The organic phase was dried over Na_2SO_4, concentrated under reduced pressure, and purified by preparative HPLC. The peak of interest was concentrated to obtain the title compound (17.8 mg, 44%) as a brownish solid with purity >95% as determined by HPLC-MS.

^{1}H NMR (400 MHz, DMSO-d_6): δ 9.25 (br s, 1H, NH); 7.90 (d, 2H, arom); 7.77 (d, 2H, arom); 7.74 (d, 2H, arom); 7.66 (2, 2H, arom)7.62 (s, 1H, arom); 2,51 (s, 3H, SCH_3).

^{13}C NMR (100 MHz, DMSO-d_6): δ 166.1, 164.3, 152.1, 143.8, 134.3, 133.9, 133.8, 131.7, 129.8, 129.6, 126.9, 126.7, 126.3, 125.9, 122.8, 106, 15.6.

ESI-MS m/z: 406 $[M + H]^+$

*N-(benzo[d]thiazol-2-yl)-2,5-dimethylfuran-3-carboxamide (**DL79**)*

To a solution of 2,5-dimethylfuran-3-carboxylic acid (14.0 mg, 0.1 mmol) in anhydrous DMF (300 µL) at room temperature was added HATU (34.2 mg, 0.1mmol) and DIPEA (38 µL, 0.2 mmol). After five minutes, benzo[*d*]thiazol-2-amine (15 mg, 0.1 mmol) was added, and the reaction was kept at 50 °C for 16 hours. The reaction mixture was diluted with ethyl acetate (3 mL) and washed with water (3 x 3 mL). The organic phase was dried over Na_2SO_4, concentrated under reduced pressure, and purified by preparative HPLC. The peak of interest was concentrated to obtain the title compound (12.2 mg, 45%) as a brownish solid with purity of >95% as determined by HPLC-MS.

^{1}H NMR (400 MHz, DMSO-d_6): δ 10.1 (br s, 1H, NH); 8.21-8.09 (m, 1H, arom); 8.00-7.91 (m, 1H, arom); 7.58-7.46 (m, 2H, arom); 6.5 (s, 1H, arom); 2,51 (s, 3H, SCH_3); 2.41 (s, 3H, CH_3); 2.61 (s, 3H, CH_3).

^{13}C NMR (100 MHz, DMSO-d_6): δ 174.6, 164.7, 156.2, 155.9, 152.2, 140.6, 125.6, 124.9, 123.5, 117.5, 117.1, 102.4, 15.9, 11.6.

ESI-MS m/z: 273 $[M + H]^+$

*N-(benzo[d]thiazol-2-yl)-1H-pyrrole-2-carboxamide (**DL90**)*

Added HATU (34.2 mg, 0.1mmol) and DIPEA (38 µL, 0.2 mmol) to a solution of 1H-pyrrole-2-carboxylic acid (11.0 mg, 0.1 mmol) in anhydrous DMF (400 µL) at room temperature. After five minutes, benzo[*d*]thiazol-2-amine (15 mg, 0.1 mmol) was added, and the reaction was kept at 50 °C for 24 hours. The reaction mixture was diluted with ethyl acetate (3 mL) and washed with water (3 x 3 mL). The organic phase was dried over Na_2SO_4, concentrated under reduced pressure, and purified by preparative HPLC. The peak of interest was concentrated to obtain the title compound (6.1 mg, 26%) as a brownish solid with purity >95% as determined by HPLC-MS.

^{1}H NMR (400 MHz, DMSO-d_6): δ 9.84 (s, 1H, NH); 8.19-8.08 (m, 1H, arom); 8.10-7.99 (m, 1H, arom); 7.89-7.77 (m, 1H, arom); 7.53-7.45 (m, 2H, arom); 7.52-7.45 (m, 1H, arom); 6.47-6.39 (m,1H, arom); 25.16 (s, 1H, NH).

^{13}C NMR (100 MHz, DMSO-d_6): δ 175.9, 161.2, 153.8, 136.4, 127.1, 125.3, 123.6, 122.5, 122.2, 118.6, 111.7, 108.0.

ESI-MS m/z: 244 $[M + H]^+$

5.2. Computational Studies

All the in silico explored compounds were manually built by the Builder tool of the MOE software [377], and then parametrised, referring to the AM1 method (partial charge calculation), and by energy minimisation via the Energy Minimise tool implemented in MOE. The MMFF94x forcefield and RMS (root mean square) gradient equal to 0.0001 were applied. The RMS gradient represents the norm of the gradient times the square root of the number of (unfixed) atoms. This kind of calculation allowed us to obtain a single low-energy conformation for each ligand [377, 378]. All the exploited experimental data of the CFTR protein in the presence of different ligands were downloaded from the Protein Data Bank [378, 379] and managed in silico via QuickPrep module implemented in MOE software, prior to the following computational studies. All the molecular docking calculations have been performed, applying the DOCK tool implemented in MOE based on the template similarity methodology, including all those amino acids placed at 4.5Å distance from the PDB ligand in the experimental conformation. Details of the docking procedure have been previously described [380, 381]. Calculation of the enthalpy-based Affinity dG scoring function (S score) allowed us to rank fifty poses before the final ten ones for each corrector, after pose refinement.

5.3. Cell culture

Human embryonic kidney (HEK) 293 cells were maintained in MEM (Corning, New York, USA) supplied with 10% FBS (Corning, New York, USA), 1% L-glutamine and 1% Penicillin/streptomycin (Corning, New York, USA) at 37 °C with 5% CO_2.

Primary human nasal epithelial (HNE) cells were obtained from people with CF enrolled at Bambino Gesù Hospital (Rome, Italy). This study was approved by the Research Ethics Board of Bambino Gesù Hospital (2961/2022). All study participants or their guardians signed an informed consent. HNE cells were isolated from brushing and subsequently cultured as previously described [368]. Briefly, HNE cells were either seeded on collagen-coated 96-transwell inserts plate (cat. #7369, Corning, New York, USA). Once confluent, the cells were cultured for 18 days at an air-liquid interface (ALI) with basal differentiation media (PneumaCult-ALI, STEMCELL Technologies, Canada).

Human highly transfectable embryonic kidney 293 (HEK293-t) cells were purchased from the Interlab Cell Line Collection (Genoa, Italy) and grown in Dulbecco's modified Eagle's medium (DMEM), supplemented with 2 mM L-glutamine, 1% PenStrep (100 U/mL), and 20% FBS, at 37 °C and 5% CO_2. Fisher rat thyroid (FRT) and human bronchial epithelial, cells stably co-transfected with a halide-sensitive yellow fluorescent protein (YFP-H148Q/I152L [60,61]), and F508del-CFTR (CFBE41o-) were cultured in Coon's modified and MEM media, respectively. In both cases, media were supplemented with 10% FBS, 2 mM L-Glutamine, 1% PenStrep (100 U/mL), 1 mg/mL geneticin (G418), and 0.6 mg/mL zeocin as selection agents. Two μg/mL puromycin (Sigma-Aldrich, Milan, Italy) was used as a selection agent for CFBE41o- cells [368, 382, 383]. Cells were grown under standard CO_2 and temperature conditions. Confluence of cells was avoided to prevent loss of differentiation.

5.4. Cell transfection

Transient transfection of HEK293, with plasmid containing F508del-CFTR or F508del/R1070W-CFTR cDNA, was performed using PolyFect Transfection Reagent (Qiagen, Hilden, Germany) according to the manufacturer's protocol, as previously described [384]. For transfection of HEK293-t, 0.8×10^6 cells were plated onto 60 mm poly-L-lysine-coated culture dishes and grown to 65% confluence in a complete medium. Plasmidic DNA encoding the entire CFTR molecule (residues 1–1480), MSD1 (residues 1–388M), NBD1 (residues 348–633), MSD2 (residues 837–1218), and NBD2 (residues 1210–1480) was digested between Hind III and XhoI, and encoded

the R domain (residues 645–834) between the Hind III and EcoRI restriction sites, and inserted into the expression vector, pCDNA3 (Invitrogen, Paisley, UK) [261, 284, 366].

Site-directed mutagenesis (QuickChange kit, Stratagene, Santa Clara, CA, USA) was used to generate the deletion of the nucleotides encoding the phenylalanine at position 508 of the CFTR molecule. The correctness of the procedure was verified by sequencing (Biofab Research, Rome, Italy). HEK293-t were transiently transfected using Lipofectamine 2000 (Invitrogen, Paisley, UK) with 4 μg of cDNA. The transfection medium was replaced after 6 h with a fresh complete medium (DMEM supplemented with 2 mM L-glutamine and without FBS) containing 2 μM **1a**, 2 μM **2a**, 2 μM **3a**, 3 μM VX661, 3 μM VX445, or vehicle DMSO (control). Cells were harvested after 24 h.

5.5. Toxicity assay

Toxicity of **1a**, **2a**, **3a**, VX661 and VX445 in HEK-t, FRT, and CFBE41o- cells was evaluated by the Trypan blue exclusion staining method [385]. Cells were seeded into 48-well plates at a concentration of 0.3 × 105 cells per well. The day after seeding, cells were exposed to the compounds for 24 hours at the following concentrations: 10, 5, 3, 2, 1, 0.5, 1, 0.5, 0.25, 0.125, and 0 (vehicle, DMSO) μM. After exposition, cells were trypsinised and harvested for toxicity evaluation. To avoid an underestimation of the number of dead cells, the cells that were detached from the plates during exposure to the compounds were collected and considered. For each condition evaluated, at least four technical replicates were evaluated. In each well, at least 100 cells were considered. The concentration resulting in the half maximum toxicity, TD_{50}, was calculated by plotting the percentage of cell survival against the concentration of the analysed compound (C) and fitting the data with a sigmoidal function.

5.6. Cycloheximide Chase Assay

The stability of NBD1-F508del was evaluated according to a previously established procedure [261, 284, 366]. Briefly, HEK-t cells were transfected with the plasmid containing the cDNA encoding this construct and incubated for 24 hours in the presence of 2 μM **1a**, 2 μM **2a**, 2 μM **3a**, 3 μM VX661, 3 μM VX445, or vehicle DMSO (control). Protein synthesis was then inhibited by the addition of 0.5 mg/mL cycloheximide. Cells were harvested at six different time points (after 0, 1, 2, 4, 6, and 8 hours), and samples of whole-cell SDS extracts were subjected to immunoblot analysis.

5.7. YFP Functional Assay

One day after seeding on black-walled, clear-bottomed 96-well microplates at a density of 30,000 cells per well, FRT or CFBE41o- cells stably co-transfected with a halide-sensitive yellow fluorescent protein (YFP-H148Q/I152L [386, 387]) and F508del CFTR were incubated for 18 hours with DMSO (control vehicle), 2 μM **1a**, 2 μM **2a**, 2 μM **3a**, 3 μM VX661, 3 μM VX445, or double or triple combinations of the tested correctors. At the time of the assay, cells were washed twice with phosphate-buffered saline (PBS) containing (in mM) NaCl 136, KNO_3 4.5, $Ca(NO_3)_2$ 1.2, $MgSO_4$ 0.2, glucose 5, HEPES 20 (pH 7.4). Cells were then incubated with 60 μL PBS plus forskolin (20 μM) and VX770 (1 μM) for 25 minutes to maximally stimulate F508del-CFTR. The cells were then transferred to a microplate reader (Tristar2 S, Berthold Technologies, Bad Wildbad, Germany) equipped with 485 nm excitation and 535 nm emission filters. The assay consisted of a fluorescence reading every 0.2 s, 5 s before and 25 s after injection of 100 μL of an extracellular solution containing 136 mM NaI (PBS with Cl^-replaced by I^-; final I^- concentration, 85 mM). Iodide influx was detected as fluorescence quenching as the I^- anion bound to intracellular YFP. After background subtraction and normalisation to the average fluorescence before NaI addition, the initial fluorescence decay rate (QR) was derived by fitting the signal with an exponential function.

5.8. CFTR channel function in HEK293

HEK293 cells were seeded in a 96-well plate (Costar, Corning, New York, USA) and, after 24 hours were transfected with either F508del or F508del/R1070W constructs. 18 hours post-transfection, cells were treated with 0.1% DMSO, 3 μM VX809, 10 μM **1b**, 10 μM **2b**,10 μM **3b**,10 μM **4b**, 10 μM **7b**, 10 μM **4a**, 10 μM **5a**, 10 μM **1c**, for 24 hours at 37 °C. Cells were then loaded with blue membrane potential dye dissolved in chloride-free buffer (136 mM sodium gluconate, 3 mM potassium gluconate, 10 mM glucose, 20 mM HEPES, pH 7,35, 300 mOsm, at a concentration of 0.5 mg/mL, Molecular Devices) for 30 minutes at 37 °C. The plate was read in a fluorescence plate reader (excitation: 530nm, emission: 560 nm; SpectraMax i5; Molecular Devices) at 37 °C. Following 5 minutes of reading the baseline fluorescence, CFTR was stimulated with 10 μM Forskolin (FSK, Sigma, Milan, Italy) and 1 μM VX770 (Selleck Chemicals). CFTR-mediated depolarization of the plasma membrane was detected as an increase in fluorescence. 10 μM CFTR inhibitor (CFTRinh-172, Selleck Chemicals, Houston, USA) was added to inactivated CFTR. The peak changes in fluorescence to CFTR agonist were normalized relative to fluorescence immediately before agonist (FSK + VX770) addition [388, 389].

5.9. Fluorescence-Based Membrane Polarization (FMP) assay

CFBE41o- cells were seeded (20.000/well) in a 96-well plate (Costar, Corning, New York, USA) and cultured at 37 °C. After 5 days post-confluence, cells were treated with 0,1% DMSO, 0.3-20 μM of compounds for 24 hours.

HNE cells were seeded on a 96-transwell plate (4.26 mm diameter, 0.4 μm pore size, Corning, New York, USA) and cultured at 37 °C for 18 days [390]. Cells were treated at the basolateral region with 0.1% DMSO, 3 μM VX809 + 3 μM VX445 (Selleck Chemicals, Houston, USA), and 10 μM of compounds for 24 hours.

The cells were then loaded with blue membrane potential dye dissolved in chloride-free buffer (150 mM NMDG-gluconate, 3 mM potassium gluconate, 10 mM HEPES, pH 7,30, 300 mOsm) and read in a fluorescence plate reader as mentioned above. 10 μM Forskolin (FSK, Sigma, Milan, Italy) and 1 μM VX770 (Selleck Chemicals, Houston, USA) were added to stimulate CFTR. Finally, 10 μM CFTRinh-172 was added to inactive CFTR [391, 392].

5.10. Cytotoxicity MTT assay

CFBE41o- cells (1 × 104 cells/well) were seeded in a 96-well plate (Corning, New York, NY, USA) as previously described [388]. Furthermore, 24 hours before the experiment, the cells were treated for 24 hours at 37 °C with **1b**, **2b**, **4b**, **7b**, **4a**, **5a,** and **1c** at 0.3-20 μM concentrations. Cell viability was then evaluated with the MTT (3-(4,5-dimethylthiazol-2-yl)-2,5 2,5-diphenyl tetrazolium bromide) assay by measurement of the optical density at 595 nm, as previously described [389]. Untreated cells are considered as 100% and cells treated with 1% of Triton-X100 were used as a positive control.

5.11. Western Blot

HEK293-t transiently transfected with CFTR, MSD1, F508del NBD1, R domain, MSD2 and NBD2 were grown to confluence on 60 mm diameter dishes and lysed in RIPA buffer (50 mM Tris-HCl, pH 8.0, 150 mM NaCl, 1% Triton X-100, 1% sodium deoxycholate, 0.1% SDS) containing a complete protease inhibitor cocktail (Sigma-Aldrich, Milan, Italy). Cell lysates were centrifuged at 12,000 rpm for 10 minutes at 4 °C. The protein concentration of the supernatant was calculated by the Bradford method using bovine serum albumin as a standard. Equal amounts of protein (30 μg) were subjected to SDS-PAGE and transferred to a PVDF membrane (Millipore, Billerica, MA, USA).

Blots were incubated with primary antibodies raised against different domains of the CFTR protein. Secondary antibodies were goat anti-mouse or anti-rabbit horseradish peroxidase-conjugated antibodies (1:2,000 dilution; Santa Cruz Biotechnologies, Dallas, TX, USA). Results were visualised by chemiluminescence using Amersham ECL PLUS detection reagents (GE Healthcare Europe GmbH, Milan, Italy), and images were captured using Amersham Hyperfilm ECL. Images were analysed using ImageJ software (National Institutes of Health). The intensity of the bands was analysed as a region of interest (ROI). For quantification, the intensity of the bands in each lane was normalised to the actin loading control. Data are expressed as mean ± SEM of at least four independent experiments.

CFBE41o- cells were lysed in modified radio immunoprecipitation assay (RIPA) buffer (50 mM Tris–HCl, 150 mM NaCl, 1 mM EDTA, pH 7.4, 0.2% SDS, and 0.1% Triton X-100) containing a protease inhibitor cocktail (Roche, Mannheim, Germany) for 10 min. Cell lysates were centrifuged at 12,000 rpm for 10 minutes at 4 °C. The protein concentration of the supernatant was calculated by the Bradford method using bovine serum albumin as a standard. Equal amounts of protein (30 μg) were subjected to SDS-PAGE, transferred to nitrocellulose membranes (Bio-Rad, Feldkirchen, Germany), and incubated with a 1:2,000 dilution of human CFTR-specific murine mAb 596 (Cystic Fibrosis Foundation, USA) and with a 1:10,000 dilution of human Calnexin-specific murine mAb (Sigma, Milan, Italy). The blots were developed with Clarity ECL (Bio-Rad, Feldkirchen, Germany) using the Chemidoc (Bio-Rad, Feldkirchen, Germany) in a linear range of exposure (0.5–2 minutes). Relative levels of CFTR protein were quantified by densitometry of immunoblots using ImageS-tudioLite (LI-COR Biosciences, Lincoln, NE) [368].

5.12. Hsp70 full-length protein expression and purification

The full-length human recombinant Hsp70 protein was produced according to Abbotto et al. [378] in BL21 (DE3) *E. coli* transformed with the pET-6xHis/hHsp70 plasmid containing the coding sequence for full-length human Hsp70 (hHSPA1A gene, NM_005345.6; purchased from Vector Builder, Vector ID VB210930), enabling the production of N-terminal 6xHis tag fusion Hsp70 proteins. Briefly, BL21 cells containing the vector were initially grown in Luria−Bertani medium at 37 °C (Merck, Milan, Italy) with 200 μg/mL ampicillin until the culture reached an OD_{600} of 0.5. The 6xHis/hHSP70 fusion protein was expressed by adding isopropyl-β-d-thiogalactopyranoside (final concentration of 0.2 mM) and incubating the bacterial culture at 37 °C for 3 hours. The cells were harvested by centrifugation and then lysed by sonication in 20 mM Tris-HCl, 250 mM KCl, and 10

mM $MgCl_2$, pH 7.4; after the addition of Triton X-100 to a final concentration of 1% and incubation for 30 minutez at 4 °C, the lysates were centrifuged at 10,000 ×*g* for 15 minutes.

The Hsp70 protein was purified by affinity chromatography using His GraviTrap TALON columns (Euroclone, Milan, Italy). Briefly, after loading the lysate, the resin was washed twice with 20 mM Tris-HCl, 250 mM KCl, and 10 mM $MgCl_2$, pH 7.4, and twice with the same buffer containing 10 mM imidazole. The elution of the recombinant protein was obtained with 150 mM imidazole, pH 7.4. Imidazole was removed from the recombinant protein through overnight dialysis using a dialysis tubing membrane (Merck KGaA, Frankfurter Strasse 250, Darmstadt, Germany), and the protein was concentrated using a Centricon (Merck Millipore, 11 Avenida Norte Bis No. 513, San Salvador, El Salvador). The protein concentrations were determined using the Bradford assay (Bio-Rad Laboratories, Inc., Italy, Segrate), and the protein purity was monitored using SDS-PAGE.

5.13. Malachite green assay

The ATPase catalytic activity of full-length recombinant Hsp70 was measured with a colorimetric assay using the Malachite green reagent according to Abbotto et al. [378]. Briefly, 6 µM of Hsp70 protein was incubated for 30 minutes at 37 °C with 5 mM ATP in 20 mM Tris-HCl, 250 mM KCl, 10 mM $MgCl_2$, and 0.02%TritonX-100, pH 7.4. The released phosphates were quantified by adding the Malachite green reagent to an aliquot of this incubation, and the absorbance was recorded at 620 nm using a Clariostar plate reader. The effects of thiazole-based molecules on the ATPase catalytic activity were measured by adding (or not) the different molecules to the incubation (at 300 µM final concentration). To correct for non-enzymatic hydrolysis of ATP and for a specific absorbance of molecules, the absorbance signal of identically treated samples lacking the Hsp70 protein was subtracted.

5.14. Thermal Shift Analysis

The thermal stability of full-length hrHsp70, alone or in the presence of potential inhibitors, was evaluated using Thermal Shift Analysis (TSA). 5 µL of each form of the Hsp70 protein was added 10 µl 10× Sypro-Orange dye solution diluted from a 5000× stock in the same buffer used for the protein (20 mM Tris-HCl, 250 mM KCl, and 10 mM $MgCl_2$) in TSA 96 wells plate. Hsp70 was tested at 5 µM with or without the synthesized compounds at concentrations up to 1 mM, starting from a 50 µM stock solution in DMSO (6% maximum in the wells); the final volume for each well was 20 µL. As a control, DMSO was used. The Tm temperature was measured using differential

scanning fluorimetry with Sypro-Orange dye (Thermofisher Scientific) on a QuantStudio™ 1 Real-Time PCR System (Thermofisher Scientific). All the Tm measurements were performed in 3 replicates. Fluorescence was monitored during the thermal denaturation occurring to the protein upon increasing the temperature from 15 to 95.3 °C (scanning rate: °C/s). All TSA data were analysed using the Protein Thermal Shift software purchased by Applied Biosystems.

References

[1] K. M. Dickinson and J. M. Collaco, "Cystic Fibrosis", *Pediatr Rev*, vol. 42, no. 2, pp. 55–67, 2021, doi: 10.1542/pir.2019-0212.

[2] P. A. di Sant'agnese *et al.,* "Abnormal electrolyte composition of sweat in Cystic Fibrosis of the pancreas", *Pediatrics*, vol. 12, no. 5, pp. 549–563, 1953, doi: 10.1542/peds.12.5.549.

[3] A. Hamosh *et al*., "Comparison of the clinical manifestations of cystic fibrosis in black and white patients", *J Pediatr*, vol. 132, no. 2, pp. 255–259, 1998, doi: 10.1016/S0022-3476(98)70441-X.

[4] E. M. Rohlfs *et al.*, "Cystic Fibrosis carrier testing in an ethnically diverse US population", *Clin Chem*, vol. 57, no. 6, pp. 841–848, 2011, doi: 10.1373/clinchem.2010.159285.

[5] "Patient Registry Annual Data Report", Bethesda, Maryland, 2018.

[6] A. F. McCague *et al.*, "Correlating cystic fibrosis transmembrane conductance regulator function with clinical features to inform precision treatment of Cystic Fibrosis", *Am J Respir Crit Care Med*, vol. 199, no. 9, pp. 1116–1126, 2019, doi: 10.1164/rccm.201901-0145OC.

[7] Cystic Fibrosis Foundation, "Carrier testing for Cystic Fibrosis", Https://www.cff.org/What-is-CF/Testing/Carrier-Testing-for-Cystic-Fibrosis.

[8] V. Scotet *et al.*, "Evidence for decline in the incidence of cystic fibrosis: a 35-year observational study in Brittany, France", *Orphanet J Rare Dis*, vol. 7, no. 1, p. 14, 2012, doi: 10.1186/1750-1172-7-14.

[9] J. S. Wagener, E. T. Zemanick, and M. K. Sontag, "Newborn screening for cystic fibrosis", *Curr Opin Pediatr*, vol. 24, no. 3, pp. 329–335, 2012, doi: 10.1097/MOP.0b013e328353489a.

[10] S. M. Paranjape and P. J. Mogayzel, "Cystic Fibrosis", *Pediatr Rev*, vol. 35, no. 5, pp. 194–205, 2014, doi: 10.1542/pir.35-5-194.

[11] M. S. Irish *et al.*, "Prenatal diagnosis of the fetus with cystic fibrosis and meconium ileus", *Pediatr Surg Int*, vol. 12, no. 5–6, pp. 434–436, 1997, doi: 10.1007/BF01076961.

[12] R. Rentea and S. St Peter, "Pediatric Rectal Prolapse", *Clin Colon Rectal Surg*, vol. 31, no. 02, pp. 108–116, 2018, doi: 10.1055/s-0037-1609025.

[13] H. Shwachman *et al.*, "Recurrent acute pancreatitis in patients with cystic fibrosis with normal pancreatic enzymes", *Pediatrics*, vol. 55, no. 1, pp. 86–95, 1975.

[14] J. M. Boyd *et al.*, "Fertility and pregnancy outcomes in men and women with cystic fibrosis in the United Kingdom", *Hum Reprod*, vol. 19, no. 10, pp. 2238–2243, 2004, doi: 10.1093/humrep/deh405.

[15] D. Borowitz *et al.*, "Cystic Fibrosis Foundation evidence-based guidelines for management of infants with Cystic Fibrosis", *J Pediatr*, vol. 155, no. 6, pp. S73–S93, 2009, doi: 10.1016/j.jpeds.2009.09.001.

[16] M. J. Rock *et al.*, “Immunoreactive trypsinogen screening for cystic fibrosis: Characterization of infants with a false-positive screening test”, *Pediatr Pulmonol*, vol. 6, no. 1, pp. 42–48, 1989, doi: 10.1002/ppul.1950060111.

[17] L. F. Ross, “Newborn screening for Cystic Fibrosis: a lesson in public health disparities”, *J Pediatr*, vol. 153, no. 3, pp. 308–313, 2008, doi: 10.1016/j.jpeds.2008.04.061.

[18] L. S. Rusakow *et al.*, “Immunoreactive trypsinogen levels in infants with cystic fibrosis complicated by meconium ileus”, *Screening*, vol. 2, no. 1, pp. 13–17, 1993, doi: 10.1016/0925-6164(93)90013-9.

[19] P. M. Farrell *et al.*, “Diagnosis of Cystic Fibrosis: consensus guidelines from the Cystic Fibrosis Foundation”, *J Pediatr*, vol. 181, pp. S4-S15.e1, 2017, doi: 10.1016/j.jpeds.2016.09.064.

[20] P. M. Farrell *et al.*, “Guidelines for diagnosis of Cystic Fibrosis in newborns through older adults: Cystic Fibrosis Foundation consensus report”, *J Pediatr*, vol. 153, no. 2, pp. S4–S14, 2008, doi: 10.1016/j.jpeds.2008.05.005.

[21] L. E. Gibson and R. E. Cooke, “A test for concentration of electrolytes in sweat in Cystic Fibrosis of the pancreas utilizing pilocarpine by iontophoresis”, *Pediatrics*, vol. 23, no. 3, pp. 545–549, 1959.

[22] J. D. Hardy *et al.,* “Sweat tests in the newborn period.”, *Arch Dis Child*, vol. 48, no. 4, pp. 316–318, 1973, doi: 10.1136/adc.48.4.316.

[23] G. E. Palomaki *et al.,* “Clinical sensitivity of prenatal screening for cystic fibrosis via CFTR carrier testing in a United States panethnic population”, *Genet Med*, vol. 6, no. 5, pp. 405–414, 2004, doi: 10.1097/01.GIM.0000139505.06194.39.

[24] F. Liu *et al.,* “Molecular structure of the human CFTR ion channel”, *Cell*, vol. 169, no. 1, pp. 85-95.e8, 2017, doi: 10.1016/j.cell.2017.02.024.

[25] Z. Zhang *et al.,* “Molecular structure of the ATP-bound, phosphorylated human CFTR”, *Proc Natl Acad Sci U.S.A.,* vol. 115, no. 50, pp. 12757–12762, 2018, doi: 10.1073/pnas.1815287115.

[26] M. P. Anderson *et al.*, “Demonstration that CFTR is a chloride channel by alteration of its anion selectivity”, *Science*, vol. 253, no. 5016, pp. 202–205, 1991, doi: 10.1126/science.1712984.

[27] V. Saint-Criq and M. A. Gray, “Role of CFTR in epithelial physiology”, *Cell Mol Life Sci*, vol. 74, no. 1, pp. 93–115, 2017, doi: 10.1007/s00018-016-2391-y.

[28] P. J. Moore and R. Tarran, “The epithelial sodium channel (ENaC) as a therapeutic target for Cystic Fibrosis lung disease”, *Expert Opin Ther Targets*, vol. 22, no. 8, pp. 687–701, 2018, doi: 10.1080/14728222.2018.1501361.

[29] A. Parodi *et al*., “Glycans in glycoprotein quality control. in essentials of glycobiology”, in *Essentials of Glycobiology*, Cold Spring Harbor (NY): Cold Spring Harbor Laboratory Press, 2015, ch. 39.

[30] E. S. Trombetta and A. J. Parodi, “Quality control and protein folding in the secretory pathway”, *Annu Rev Cell Dev Biol*, vol. 19, no. 1, pp. 649–676, 2003, doi: 10.1146/annurev.cellbio.19.110701.153949.

[31] C. D’Alessio *et al*., “UDP-GlC:glycoprotein glucosyltransferase-glucosidase II, the ying-yang of the ER quality control”, *Semin Cell Dev Biol*, vol. 21, no. 5, pp. 491–499, 2010, doi: 10.1016/j.semcdb.2009.12.014.

[32] J. L. Brodsky, “Chaperoning the maturation of the cystic fibrosis transmembrane conductance regulator”, *Am J Physiolo Lung Cell Mol Physiol*, vol. 281, no. 1, pp. L39–L42, 2001, doi: 10.1152/ajplung.2001.281.1.L39.

[33] M. L. McClure *et al*., “Trafficking and function of the cystic fibrosis transmembrane conductance regulator: a complex network of posttranslational modifications”, *Am J Physiolo Lung Cell Mol Physiol*, vol. 311, no. 4, pp. L719–L733, 2016, doi: 10.1152/ajplung.00431.2015.

[34] S. Estabrooks and J. L. Brodsky, “Regulation of CFTR biogenesis by the proteostatic network and pharmacological modulators”, *Int J Mol Sci*, vol. 21, no. 2, p. 452, 2020, doi: 10.3390/ijms21020452.

[35] V. R. Villella *et al.*, “Disease-relevant proteostasis regulation of cystic fibrosis transmembrane conductance regulator”, *Cell Death Differ*, vol. 20, no. 8, pp. 1101–1115, 2013, doi: 10.1038/cdd.2013.46.

[36] S. L. Lindquist and J. W. Kelly, “Chemical and biological approaches for adapting proteostasis to ameliorate protein misfolding and aggregation diseases-progress and prognosis”, *Cold Spring Harb Perspect Biol*, vol. 3, no. 12, pp. a004507–a004507, 2011, doi: 10.1101/cshperspect.a004507.

[37] R. N. Hegde *et al.*, “Unravelling druggable signalling networks that control F508del-CFTR proteostasis”, *eLife*, vol. 4, 2015, doi: 10.7554/eLife.10365.

[38] P. Gomes-Alves *et al*., “Signaling pathways of proteostasis network unraveled by proteomic approaches on the understanding of misfolded protein rescue”, 2011, pp. 217–233. doi: 10.1016/B978-0-12-385928-0.00013-4.

[39] I. Devesa *et al*., “Targeting protein–protein interactions to rescue Δf508-cftr: a novel corrector approach to treat cystic fibrosis”, *EMBO Mol Med*, vol. 5, no. 10, pp. 1462–1464, 2013, doi: 10.1002/emmm.201303301.

[40] W. E. Balch *et al*., “Emergent properties of proteostasis in managing Cystic Fibrosis”, *Cold Spring Harb Perspect Biol*, vol. 3, no. 2, pp. a004499–a004499, 2011, doi: 10.1101/cshperspect.a004499.

[41] M. D. Amaral *et al*., “CFTR processing, trafficking and interactions”, *J Cyst Fibros*, vol. 19, pp. S33–S36, 2020, doi: 10.1016/j.jcf.2019.10.017.

[42] D. M. Roth *et al.*, “Modulation of the maladaptive stress response to manage diseases of protein folding”, *PLoS Biol*, vol. 12, no. 11, p. e1001998, 2014, doi: 10.1371/journal.pbio.1001998.

[43] J. L. Brodsky, “The protective and destructive roles played by molecular chaperones during ERAD (endoplasmic-reticulum-associated degradation)”, *Biochem J*, vol. 404, no. 3, pp. 353–363, 2007, doi: 10.1042/BJ20061890.

[44] T. J. Jensen *et al*., “Multiple proteolytic systems, including the proteasome, contribute to CFTR processing”, *Cell*, vol. 83, no. 1, pp. 129–135, 1995, doi: 10.1016/0092-8674(95)90241-4.

[45] M. Sharma *et al.*, “Misfolding diverts CFTR from recycling to degradation”, *J Cell Biol*, vol. 164, no. 6, pp. 923–933, 2004, doi: 10.1083/jcb.200312018.

[46] M. Gentzsch *et al.*, “Endocytic trafficking routes of wild type and ΔF508 Cystic Fibrosis Transmembrane Conductance Regulator”, *Mol Biol Cell*, vol. 15, no. 6, pp. 2684–2696, 2004, doi: 10.1091/mbc.e04-03-0176.

[47] T. Okiyoneda *et al.*, “Peripheral protein quality control removes unfolded CFTR from the plasma membrane,” *Science*, vol. 329, no. 5993, pp. 805–810, 2010, doi: 10.1126/science.1191542.

[48] B. Kleizen *et al.*, “Co-translational folding of the first transmembrane domain of ABC-transporter CFTR is supported by assembly with the first cytosolic domain”, *J Mol Biol*, vol. 433, no. 13, p. 166955, 2021, doi: 10.1016/j.jmb.2021.166955.

[49] B. Kleizen *et al*., “Folding of CFTR is predominantly co-translational”, *Mol Cell*, vol. 20, no. 2, pp. 277–287, 2005, doi: 10.1016/j.molcel.2005.09.007.

[50] K. Du and G. L. Lukacs, “Cooperative assembly and misfolding of CFTR domains in vivo”, *Mol Biol Cell*, vol. 20, no. 7, pp. 1903–1915, 2009, doi: 10.1091/mbc.e08-09-0950.

[51] S. J. Kim and W. R. Skach, “Mechanisms of CFTR folding at the endoplasmic reticulum”, *Front Pharmacol*, vol. 3, 2012, doi: 10.3389/fphar.2012.00201.

[52] M. A. Loo *et al*., “Perturbation of Hsp90 interaction with nascent CFTR prevents its maturation and accelerates its degradation by the proteasome”, *EMBO J*, vol. 17, no. 23, pp. 6879–6887, 1998, doi: 10.1093/emboj/17.23.6879.

[53] Y. Matsumura *et al*., “Role of Hsc70 binding cycle in CFTR folding and endoplasmic reticulum–associated degradation”, *Mol Biol Cell*, vol. 22, no. 16, pp. 2797–2809, 2011, doi: 10.1091/mbc.e11-02-0137.

[54] G. C. Meacham, “The Hdj-2/Hsc70 chaperone pair facilitates early steps in CFTR biogenesis”, *EMBO J*, vol. 18, no. 6, pp. 1492–1505, 1999, doi: 10.1093/emboj/18.6.1492.

[55] T. S. Scott-Ward and M. D. Amaral, “Deletion of Phe508 in the first nucleotide-binding domain of the cystic fibrosis transmembrane conductance regulator increases its affinity for the heat shock cognate 70 chaperone”, *FEBS J*, vol. 276, no. 23, pp. 7097–7109, 2009, doi: 10.1111/j.1742-4658.2009.07421.x.

[56] M. Bagdany *et al.*, “Chaperones rescue the energetic landscape of mutant CFTR at single molecule and in cell”, *Nat Commun*, vol. 8, no. 1, p. 398, 2017, doi: 10.1038/s41467-017-00444-4.

[57] M. F. N. Rosser *et al*., “Assembly and misassembly of Cystic Fibrosis Transmembrane Conductance Regulator: folding defects caused by deletion of F508 occur before and after the

calnexin-dependent association of membrane spanning domain MSD1 and MSD2", *Mol Biol Cell*, vol. 19, no. 11, pp. 4570–4579, 2008, doi: 10.1091/mbc.e08-04-0357.

[58] K. Harada *et al.*, "Calreticulin negatively regulates the cell surface expression of Cystic Fibrosis Transmembrane Conductance Regulator", *J Biol Chem*, vol. 281, no. 18, pp. 12841–12848, 2006, doi: 10.1074/jbc.M512975200.

[59] S. Pind *et al*., "Participation of the endoplasmic reticulum chaperone calnexin (p88, IP90) in the biogenesis of the cystic fibrosis transmembrane conductance regulator", *J Biol Chem*, vol. 269, no. 17, pp. 12784–12788, 1994.

[60] X. Chang *et al.*, "Role of N-linked oligosaccharides in the biosynthetic processing of the cystic fibrosis membrane conductance regulator", *J Cell Sci*, vol. 121, no. 17, pp. 2814–2823, 2008, doi: 10.1242/jcs.028951.

[61] K. Peter *et al.*, "Ablation of internalization signals in the carboxyl-terminal tail of the Cystic Fibrosis Transmembrane Conductance Regulator enhances cell surface expression", *J Biol Chem*, vol. 277, no. 51, pp. 49952–49957, 2002, doi: 10.1074/jbc.M209275200.

[62] K. M. Weixel and N. A. Bradbury, "The carboxyl terminus of the Cystic Fibrosis Transmembrane Conductance Regulator binds to AP-2 clathrin adaptors", *J Biol Chem*, vol. 275, no. 5, pp. 3655–3660, 2000, doi: 10.1074/jbc.275.5.3655.

[63] L. Fu *et al*., "Dab2 is a key regulator of endocytosis and post-endocytic trafficking of the cystic fibrosis transmembrane conductance regulator", *Biochem J*, vol. 441, no. 2, pp. 633–643, 2012, doi: 10.1042/BJ20111566.

[64] E. Sondo *et al*., "RNF5, DAB2 and friends: novel drug targets for Cystic Fibrosis", *Curr Pharm Des*, vol. 23, no. 1, pp. 176–186, 2017, doi: 10.2174/1381612822666161006161033.

[65] C. M. Farinha and P. Matos, "Rab GTPases regulate the trafficking of channels and transporters – a focus on cystic fibrosis", *Small GTPases*, vol. 9, no. 1–2, pp. 136–144, 2018, doi: 10.1080/21541248.2017.1317700.

[66] T. Okiyoneda *et al.*, "Chaperone-independent peripheral quality control of CFTR by RFFL E3 ligase", *Dev Cell*, vol. 44, no. 6, pp. 694-708.e7, 2018, doi: 10.1016/j.devcel.2018.02.001.

[67] R. Dérand *et al.*, "Activation of VPAC1 receptors by VIP and PACAP-27 in human bronchial epithelial cells induces CFTR-dependent chloride secretion", *Br J Pharmacol*, vol. 141, no. 4, pp. 698–708, 2004, doi: 10.1038/sj.bjp.0705597.

[68] N. A. Ameen *et al*., "CFTR channel insertion to the apical surface in rat duodenal villus epithelial cells is upregulated by VIP in vivo", *J Cell Sci*, vol. 112, no. 6, pp. 887–894, 1999, doi: 10.1242/jcs.112.6.887.

[69] W. Alshafie *et al*., "VIP regulates CFTR membrane expression and function in Calu-3 cells by increasing its interaction with NHERF1 and P-ERM in a VPAC1- and PKCε-dependent manner", *Am J Physiol Cell Physiol*, vol. 307, no. 1, pp. C107–C119, 2014, doi: 10.1152/ajpcell.00296.2013.

[70] N. Alcolado *et al*., "VIP-dependent increase in F508del-CFTR membrane localization is mediated by PKCε", *Am J Physiol Cell Physiol*, vol. 301, no. 1, pp. C53–C65, 2011, doi: 10.1152/ajpcell.00568.2009.

[71] S. M. Snodgrass *et al*., "Tgf-β1 inhibits CFTR biogenesis and prevents functional rescue of ΔF508-CFTR in primary differentiated human bronchial epithelial cells", *PLoS One*, vol. 8, no. 5, p. e63167, 2013, doi: 10.1371/journal.pone.0063167.

[72] V. Prulière-Escabasse *et al.*, "TGF-β1 downregulates CFTR expression and function in nasal polyps of non-CF patients", *Am J Physiol Lung Cell Mol Physiol*, vol. 288, no. 1, pp. L77–L83, 2005, doi: 10.1152/ajplung.00048.2004.

[73] M. J. Lobo *et al*., "EPAC1 activation by cAMP stabilizes CFTR at the membrane by promoting its interaction with NHERF1", *J Cell Sci*, vol. 129, no. 13, pp. 2599–2612, 2016, doi: 10.1242/jcs.185629.

[74] J. D. Santos *et al*., "Cytoskeleton regulators CAPZA2 and INF2 associate with CFTR to control its plasma membrane levels under EPAC1 activation", *Biochem J*, vol. 477, no. 13, pp. 2561–2580, 2020, doi: 10.1042/BCJ20200287.

[75] E. R. Lazarowski and R. C. Boucher, "Purinergic receptors in airway hydration", *Biochem Pharmacol*, vol. 187, p. 114387, 2021, doi: 10.1016/j.bcp.2020.114387.

[76] T. Zhu *et al*., "CFTR Regulation by phosphorylation", in *Methods Mol Med*, pp. 99–110, 2002, doi: 10.1385/1-59259-187-6:99.

[77] R. Alzamora *et al.*, "CFTR Regulation by Phosphorylation", pp. 471–488, 2011, doi: 10.1007/978-1-61779-117-8_29.

[78] S. Luz *et al*., "LMTK2-mediated phosphorylation regulates CFTR endocytosis in human airway epithelial cells", *J Biol Chem*, vol. 289, no. 21, pp. 15080–15093, 2014, doi: 10.1074/jbc.M114.563742.

[79] S. Chin *et al*., "Current insights into the role of PKA phosphorylation in CFTR channel activity and the pharmacological rescue of cystic fibrosis disease-causing mutants", *Cell Mol Life Sci*, vol. 74, no. 1, pp. 57–66, 2017, doi: 10.1007/s00018-016-2388-6.

[80] A. Della Sala *et al*., "Role of protein kinase A-mediated phosphorylation in CFTR channel activity regulation", *Front Physiol*, vol. 12, 2021, doi: 10.3389/fphys.2021.690247.

[81] D. Dahan *et al.*, "Regulation of the CFTR channel by phosphorylation", *Pflugers Arch*, vol. 443, no. 0, pp. S92–S96, 2001, doi: 10.1007/s004240100652.

[82] C. M. Farinha *et al*., "Regulatory crosstalk by protein kinases on CFTR trafficking and activity", *Front Chem*, vol. 4, 2016, doi: 10.3389/fchem.2016.00001.

[83] A. Billet *et al*., "Regulation of the cystic fibrosis transmembrane conductance regulator anion channel by tyrosine phosphorylation", *FASEB J*, vol. 29, no. 9, pp. 3945–3953, 2015, doi: 10.1096/fj.15-273151.

[84] A. Billet *et al.*, "Potential sites of CFTR activation by tyrosine kinases", *Channels*, vol. 10, no. 3, pp. 247–251, 2016, doi: 10.1080/19336950.2015.1126010.

[85] D. F. Cruz *et al*., "TGF-β1 augments the apical membrane abundance of lemur tyrosine kinase 2 to inhibit CFTR-mediated chloride transport in human bronchial epithelia", *Front Cell Dev Biol*, vol. 8, 2020, doi: 10.3389/fcell.2020.00058.

[86] F. S. Seibert *et al*., "Influence of phosphorylation by protein kinase A on CFTR at the cell surface and endoplasmic reticulum", *Biochim Biophys Acta*, vol. 1461, no. 2, pp. 275–283, 1999, doi: 10.1016/S0005-2736(99)00163-7.

[87] V. Chappe *et al*., "Phosphorylation of protein kinase C sites in NBD1 and the R domain control CFTR channel activation by PKA", *J Physiol*, vol. 548, no. 1, pp. 39–52, 2003, doi: 10.1113/jphysiol.2002.035790.

[88] T. Zhu, D. Dahan *et al*., "Association of Cystic Fibrosis Transmembrane Conductance Regulator and protein phosphatase 2C", *J Biol Chem*, vol. 274, no. 41, pp. 29102–29107, 1999, doi: 10.1074/jbc.274.41.29102.

[89] A. Vastiau *et al.*, "Interaction of the protein phosphatase 2A with the regulatory domain of the cystic fibrosis transmembrane conductance regulator channel", *FEBS Lett*, vol. 579, no. 16, pp. 3392–3396, 2005, doi: 10.1016/j.febslet.2005.04.079.

[90] S. M. Travis *et al*., "Protein phosphatase 2C dephosphorylates and inactivates cystic fibrosis transmembrane conductance regulator", *Proc Natl Acad Sci U.S.A.*, vol. 94, no. 20, pp. 11055–11060, 1997, doi: 10.1073/pnas.94.20.11055.

[91] W. R. Thelin *et al.*, "The Cystic Fibrosis Transmembrane Conductance Regulator is regulated by a direct interaction with the protein hosphatase 2A", *J Biol Chem*, vol. 280, no. 50, pp. 41512–41520, 2005, doi: 10.1074/jbc.M507308200.

[92] J. P. Garnett *et al*., "Protein phosphatase 1 coordinates CFTR-dependent airway epithelial HCO3- secretion by reciprocal regulation of apical and basolateral membrane Cl(-)-HCO3- exchangers", *Br J Pharmacol*, vol. 168, no. 8, pp. 1946–1960, 2013, doi: 10.1111/bph.12085.

[93] H. Fischer *et al*., "Regulation of CFTR by protein phosphatase 2B and protein kinase C", *Pflügers Arch*, vol. 436, no. 2, pp. 175–181, 1998, doi: 10.1007/s004240050620.

[94] S. Y. Chang *et al*., "Mechanisms of CFTR regulation by syntaxin 1A and PKA", *J Cell Sci*, vol. 115, no. 4, pp. 783–791, 2002, doi: 10.1242/jcs.115.4.783.

[95] S. H. Cheng *et al*., "Phosphorylation of the R domain by cAMP-dependent protein kinase regulates the CFTR chloride channel", *Cell*, vol. 66, no. 5, pp. 1027–1036, 1991, doi: 10.1016/0092-8674(91)90446-6.

[96] X. B. Chang *et al.*, "Protein kinase A (PKA) still activates CFTR chloride channel after mutagenesis of all 10 PKA consensus phosphorylation sites", *J Biol Chem*, vol. 268, no. 15, pp. 11304–11, 1993.

[97] P. Farrell *et al.*, "Estimating the age of p.(Phe508del) with family studies of geographically distinct European populations and the early spread of cystic fibrosis", *Eur J Hum Genet*, vol. 26, no. 12, pp. 1832–1839, 2018, doi: 10.1038/s41431-018-0234-z.

[98] G. Veit *et al.*, "From CFTR biology toward combinatorial pharmacotherapy: expanded classification of cystic fibrosis mutations", *Mol Biol Cell*, vol. 27, no. 3, pp. 424–433, 2016, doi: 10.1091/mbc.e14-04-0935.

[99] J. E. Ideozu *et al.*, "Diversity of CFTR variants across ancestries characterized using 454,727 UK biobank whole exome sequences", *Genome Med*, vol. 16, no. 1, p. 43, 2024, doi: 10.1186/s13073-024-01316-5.

[100] Cystic Fibrosis Foundation, “CFTR2 website”, https://cftr2.org/mutations_history.

[101] K. De Boeck and M. D. Amaral, “Progress in therapies for Cystic Fibrosis”, *Lancet Respir Med*, vol. 4, no. 8, pp. 662–674, 2016, doi: 10.1016/S2213-2600(16)00023-0.

[102] M. J. Welsh and A. E. Smith, “Molecular mechanisms of CFTR chloride channel dysfunction in cystic fibrosis”, *Cell*, vol. 73, no. 7, pp. 1251–1254, 1993, doi: 10.1016/0092-8674(93)90353-R.

[103] J. Zielenski and L.C. Tsui, “Cystic Fibrosis: Genotypic and phenotypic variations”, *Annu Rev Genet*, vol. 29, no. 1, pp. 777–807, 1995, doi: 10.1146/annurev.ge.29.120195.004021.

[104] M. Haardt *et al*., “C-terminal truncations destabilize the Cystic Fibrosis Transmembrane Conductance Regulator without impairing its biogenesis,” *J Biol Chem*, vol. 274, no. 31, pp. 21873–21877, 1999, doi: 10.1074/jbc.274.31.21873.

[105] F. Stanke and B. Tümmler, “Classification of CFTR mutation classes”, *Lancet Respir Med*, vol. 4, no. 8, p. e36, 2016, doi: 10.1016/S2213-2600(16)30147-3.

[106] L. Linde *et al.*, “Nonsense-mediated mRNA decay affects nonsense transcript levels and governs response of cystic fibrosis patients to gentamicin”, *J Clin Investig*, vol. 117, no. 3, pp. 683–692, 2007, doi: 10.1172/JCI28523.

[107] L. A. Clarke *et al.*, “The effect of premature termination codon mutations on *CFTR* mRNA abundance in human nasal epithelium and intestinal organoids: a basis for read-through therapies in cystic fibrosis”, *Hum Mutat*, vol. 40, no. 3, pp. 326-334, 2019, doi: 10.1002/humu.23692.

[108] M. P. Anderson and M. J. Welsh, “Regulation by ATP and ADP of CFTR chloride channels that contain mutant nucleotide-binding domains”, *Science*, vol. 257, no. 5077, pp. 1701–1704, 1992, doi: 10.1126/science.1382316.

[109] M. D. Amaral and C. M. Farinha, “Rescuing mutant CFTR: a multi-task approach to a better outcome in treating Cystic Fibrosis”, *Curr Pharm Des*, vol. 19, no. 19, pp. 3497–3508, 2013, doi: 10.2174/13816128113199990318.

[110] V. A. LeGrys, “Sweat analysis proficiency testing for cystic fibrosis”, *Pediatr Pulmonol*, vol. 30, no. 6, pp. 476-480, 2000, doi: 10.1002/1099-0496(200012)30:6<476::AID-PPUL7>3.0.CO;2-O.

[111] C. Li *et al.*, “ATPase activity of the Cystic Fibrosis Transmembrane Conductance Regulator”, *J Biol Chem*, vol. 271, no. 45, pp. 28463–28468, 1996, doi: 10.1074/jbc.271.45.28463.

[112] D. N. Sheppard *et al.* “Mutations in CFTR associated with mild-disease-form Cl- channels with altered pore properties”, *Nature*, vol. 362, no. 6416, pp. 160–164, 1993, doi: 10.1038/362160a0.

[113] C.-S. Chu *et al.*, “Genetic basis of variable exon 9 skipping in cystic fibrosis transmembrane conductance regulator mRNA”, *Nat Genet*, vol. 3, no. 2, pp. 151–156, 1993, doi: 10.1038/ng0293-151.

[114] M. R. Silvis *et al.*, “A Mutation in the Cystic Fibrosis Transmembrane Conductance Regulator generates a novel internalization sequence and enhances endocytic rates”, *J Biol Chem*, vol. 278, no. 13, pp. 11554–11560, 2003, doi: 10.1074/jbc.M212843200.

[115] H. Bihler *et al.*, “In vitro modulator responsiveness of 655 CFTR variants found in people with cystic fibrosis”, *J Cyst Fibros*, vol. 23, no. 4, pp. 664–675, 2024, doi: 10.1016/j.jcf.2024.02.006.

[116] G. R. Cutting, “Cystic fibrosis genetics: from molecular understanding to clinical application”, *Nat Rev Genet*, vol. 16, no. 1, pp. 45–56, 2015, doi: 10.1038/nrg3849.

[117] J. P. Clancy *et al.*, “CFTR modulator theratyping: current status, gaps and future directions”, *J Cyst Fibros*, vol. 18, no. 1, pp. 22–34, 2019, doi: 10.1016/j.jcf.2018.05.004.

[118] A. S. Ramalho *et al.*, “Patient-derived cell models for personalized medicine approaches in cystic fibrosis”, *J Cyst Fibros*, vol. 22, pp. S32–S38, 2023, doi: 10.1016/j.jcf.2022.11.007.

[119] P. J. Mogayzel *et al.*, “Cystic Fibrosis Pulmonary Guidelines”, *Am J Respir Crit Care Med*, vol. 187, no. 7, pp. 680–689, 2013, doi: 10.1164/rccm.201207-1160OE.

[120] E. Main *et al.*, “Conventional chest physiotherapy compared to other airway clearance techniques for cystic fibrosis”, *Cochrane Database Syst Rev*, vol. 2013, no. 2, 2005, doi: 10.1002/14651858.CD002011.pub2.

[121] E. Main and S. Rand, “Conventional chest physiotherapy compared to other airway clearance techniques for cystic fibrosis”, *Cochrane Database Syst Rev*, vol. 2023, no. 5, 2023, doi: 10.1002/14651858.CD002011.pub3.

[122] L. M. Wilson *et al.*, “Active cycle of breathing technique for cystic fibrosis”, *Cochrane Database Syst Rev*, vol. 2023, no. 2, 2023, doi: 10.1002/14651858.CD007862.pub5.

[123] C. P. van der Schans *et al.*, “Chest physiotherapy compared to no chest physiotherapy for Cystic Fibrosis”, *Cochrane Database Syst Rev*, 2000. doi: 10.1002/14651858.CD001401.

[124] D. R. Hess, “The evidence for secretion clearance techniques”, *Respir Care*, vol. 46, no. 11, pp. 1276–93, 2001, PMID: 11679147.

[125] P. A. Flume *et al.*, “Cystic fibrosis pulmonary guidelines: airway clearance therapies”, *Respir Care*, vol. 54, no. 4, pp. 522–37, 2009.

[126] C. Yang and M. Montgomery, “Dornase alfa for cystic fibrosis”, *Cochrane Database Syst Rev*, vol. 2021, no. 3, 2021, doi: 10.1002/14651858.CD001127.pub5.

[127] V. Terlizzi *et al.*, “Dornase alfa in Cystic Fibrosis: indications, comparative studies and effects on lung clearance index”, *Ital J Pediatr*, vol. 48, no. 1, p. 141, 2022, doi: 10.1186/s13052-022-01331-5.

[128] K. W. Southern *et al.*, “Standards for the care of people with cystic fibrosis; establishing and maintaining health”, *J Cyst Fibros*, vol. 23, no. 1, pp. 12–28, 2024, doi: 10.1016/j.jcf.2023.12.002.

[129] R. Dentice and M. Elkins, “Timing of dornase alfa inhalation for cystic fibrosis”, *Cochrane Database Syst Rev*, 2021. doi: 10.1002/14651858.CD007923.pub3.

[130] P. Wark *et al.*, “Nebulised hypertonic saline for cystic fibrosis”, *Cochrane Database Syst Rev*, vol. 2023, no. 6, 2023, doi: 10.1002/14651858.CD001506.pub5.

[131] V. Terlizzi *et al.*, “Hypertonic saline in people with cystic fibrosis: review of comparative studies and clinical practice”, *Ital J Pediatr*, vol. 47, no. 1, p. 168, 2021, doi: 10.1186/s13052-021-01117-1.

[132] M. R. Elkins *et al.*, “A controlled trial of long-term inhaled hypertonic saline in patients with Cystic Fibrosis”, *N Engl J Med,* vol. 354, no. 3, pp. 229–240, 2006, doi: 10.1056/NEJMoa043900.

[133] H. A. W. M. Tiddens *et al.*, “The effect of inhaled hypertonic saline on lung structure in children aged 3–6 years with cystic fibrosis (SHIP-CT): a multicentre, randomised, double-blind, controlled trial”, *Lancet Respir Med*, vol. 10, no. 7, pp. 669–678, 2022, doi: 10.1016/S2213-2600(21)00546-4.

[134] M. Stahl *et al.*, “Preventive inhalation of hypertonic saline in infants with Cystic Fibrosis (PRESIS). A randomized, double-blind, controlled study”, *Am J Respir Crit Care Med*, vol. 199, no. 10, pp. 1238–1248, 2019, doi: 10.1164/rccm.201807-1203OC.

[135] S. J. Nevitt *et al.*, “Inhaled mannitol for cystic fibrosis”, *Cochrane Database Syst Rev*, vol. 2020, no. 5, 2020, doi: 10.1002/14651858.CD008649.pub4.

[136] P. A. Flume *et al.*, “Cystic Fibrosis Pulmonary Guidelines”, *Am J Respir Crit Care Med*, vol. 180, no. 9, pp. 802–808, 2009, doi: 10.1164/rccm.200812-1845PP.

[137] M. Cohen-Cymberknoh *et al.*, “Managing Cystic Fibrosis”, *Am J Respir Crit Care Med*, vol. 183, no. 11, pp. 1463–1471, 2011, doi: 10.1164/rccm.201009-1478CI.

[138] P. J. Mogayzel *et al.*, “Cystic Fibrosis Foundation pulmonary guideline. Pharmacologic approaches to prevention and eradication of initial *Pseudomonas aeruginosa* infection”, *Ann Am Thorac Soc*, vol. 11, no. 10, pp. 1640–1650, 2014, doi: 10.1513/AnnalsATS.201404-166OC.

[139] L. Huang *et al.*, “Impact of intrinsic and extrinsic risk factors on early-onset lung disease in Cystic Fibrosis”, *Pediatr Pulmonol*, vol. 58, no. 11, pp. 3071–3082, 2023, doi: 10.1002/ppul.26625.

[140] G. Döring and N. Hoiby, “Early intervention and prevention of lung disease in Cystic Fibrosis: a European consensus”, *J Cyst Fibros*, vol. 3, no. 2, pp. 67–91, n2004, doi: 10.1016/j.jcf.2004.03.008.

[141] S. C. Langton Hewer *et al.*, “Antibiotic strategies for eradicating *Pseudomonas aeruginosa* in people with Cystic Fibrosis”, *Cochrane Database Syst Rev*, vol. 2023, no. 6, 2023, doi: 10.1002/14651858.CD004197.pub6.

[142] T. W. R. Lee *et al.*, “Evaluation of a new definition for chronic *Pseudomonas aeruginosa* infection in Cystic Fibrosis patients”, *J Cyst Fibros*, vol. 2, no. 1, pp. 29–34, 2003, doi: 10.1016/S1569-1993(02)00141-8.

[143] M. Proesmans *et al.*, “Evaluating the ‘Leeds criteria’ for *Pseudomonas aeruginosa* infection in a cystic fibrosis centre”, *Eur Respir J*, vol. 27, no. 5, pp. 937–943, 2006, doi: 10.1183/09031936.06.00100805.

[144] D. A. Stevens *et al.*, “Allergic bronchopulmonary aspergillosis in Cystic Fibrosis-State of the art: Cystic Fibrosis Foundation consensus conference”, *Clin Infect Dis*, vol. 37, no. s3, pp. S225–S264, 2003, doi: 10.1086/376525.

[145] R. Dinwiddie, “Anti-inflammatory therapy in Cystic Fibrosis”, *J Cyst Fibros*, vol. 4, pp. 45–48, 2005, doi: 10.1016/j.jcf.2005.05.010.

[146] L. C. Lands and S. Stanojevic, “Oral non-steroidal anti-inflammatory drug therapy for lung disease in Cystic Fibrosis”, *Cochrane Database Syst Rev*, 2016, doi: 10.1002/14651858.CD001505.pub4.

[147] K. W. Southern *et al.*, “Macrolide antibiotics for Cystic Fibrosis”, in *Cochrane Database Syst Rev*, 2011, doi: 10.1002/14651858.CD002203.pub3.

[148] V. A. Stallings *et al.*, “Evidence-based practice recommendations for nutrition-related management of children and adults with Cystic Fibrosis and pancreatic insufficiency: results of a systematic review”, *J Am Diet Assoc*, vol. 108, no. 5, pp. 832–839, 2008, doi: 10.1016/j.jada.2008.02.020.

[149] S. J. Schwarzenberg *et al.*, “Enteral tube feeding for individuals with cystic fibrosis: Cystic Fibrosis Foundation evidence-informed guidelines”, *J Cyst Fibros*, vol. 15, no. 6, pp. 724–735, 2016, doi: 10.1016/j.jcf.2016.08.004.

[150] T. Lahiri *et al.*, “Clinical practice guidelines from the Cystic Fibrosis Foundation for preschoolers with Cystic Fibrosis”, *Pediatrics*, vol. 137, no. 4,. 2016, doi: 10.1542/peds.2015-1784.

[151] D. S. Borowitz *et al.*, “Use of pancreatic enzyme supplements for patients with Cystic Fibrosis in the context of fibrosing colonopathy”, *J Pediatr*, vol. 127, no. 5, pp. 681–684, 1995, doi: 10.1016/S0022-3476(95)70153-2.

[152] K. W. Reichard *et al.*, “Fibrosing colonopathy in children with Cystic Fibrosis”, *J Pediatr Surg*, vol. 32, no. 2, pp. 237–242, 1997, doi: 10.1016/S0022-3468(97)90186-X.

[153] S. Schibli *et al.*, “Proper usage of pancreatic enzymes”, *Curr Opin Pulm Med*, vol. 8, no. 6, pp. 542–546, 2002, doi: 10.1097/00063198-200211000-00010.

[154] V. Tangpricha *et al.*, “An update on the screening, diagnosis, management, and treatment of vitamin D deficiency in individuals with Cystic Fibrosis: evidence-based recommendations from the Cystic Fibrosis Foundation”, *J Clin Endocrinol Metab*, vol. 97, no. 4, pp. 1082–1093, 2012, doi: 10.1210/jc.2011-3050.

[155] P. G. Middleton *et al.*, “Elexacaftor–Tezacaftor–Ivacaftor for Cystic Fibrosis with a single Phe508del allele”, *N Engl J Med*, vol. 381, no. 19, pp. 1809–1819, 2019, doi: 10.1056/NEJMoa1908639.

[156] D. Hubert *et al.*, “Real-life initiation of Lumacaftor/Ivacaftor combination in adults with Cystic Fibrosis homozygous for the Phe508del CFTR mutation and severe lung disease”, *J Cyst Fibros*, vol. 16, no. 3, pp. 388–391, 2017, doi: 10.1016/j.jcf.2017.03.003.

[157] E. B. Burgener and R. B. Moss, “Cystic Fibrosis Transmembrane Conductance Regulator modulators: precision medicine in Cystic Fibrosis,” *Curr Opin Pediatr*, vol. 30, no. 3, pp. 372–377, 2018, doi: 10.1097/MOP.0000000000000627.

[158] J. R. Riordan *et al.*, “Identification of the Cystic Fibrosis gene: cloning and characterization of complementary DNA”, *Science*, vol. 245, no. 4922, pp. 1066–1073, 1989, doi: 10.1126/science.2475911.

[159] J. A. Wagner *et al.*, “Safety and biological efficacy of an adeno-associated virus vector–Cystic Fibrosis Transmembrane Regulator (AAV-CFTR) in the Cystic Fibrosis maxillary sinus”, *Laryngoscope*, vol. 109, no. 2, pp. 266–274, 1999, doi: 10.1097/00005537-199902000-00017.

[160] E. W. F. W. Alton *et al.*, “Genetic medicines for CF: hype versus reality,” *Pediatr Pulmonol*, vol. 51, no. S44, 2016, doi: 10.1002/ppul.23543.

[161] M. R. Knowles *et al.*, “A controlled study of adenoviral-vector–mediated gene transfer in the nasal epithelium of patients with Cystic Fibrosis”, *N Engl J Med*, vol. 333, no. 13, pp. 823–831, 1995, doi: 10.1056/NEJM199509283331302.

[162] J. B. Zuckerman *et al.*, “A phase I study of adenovirus-mediated transfer of the human Cystic Fibrosis Transmembrane Conductance Regulator gene to a lung segment of individuals with Cystic Fibrosis”, *Hum Gene Ther*, vol. 10, no. 18, pp. 2973–2985, 1999, doi: 10.1089/10430349950016384.

[163] R. A. Pleasants and D. R. Hess, “Aerosol delivery devices for obstructive lung diseases”, *Respir Care*, vol. 63, no. 6, pp. 708–733, 2018, doi: 10.4187/respcare.06290.

[164] M. L. Aitken *et al.*, “A phase I study of aerosolized administration of tgAAVCF to Cystic Fibrosis subjects with mild lung disease”, *Hum Gene Ther*, vol. 12, no. 15, pp. 1907–1916, 2001, doi: 10.1089/104303401753153956.

[165] L. A. Davies *et al.,* “Aerosol delivery of DNA/liposomes to the lung for Cystic Fibrosis gene therapy”, *Hum Gene Ther Clin Dev*, vol. 25, no. 2, pp. 97–107, 2014, doi: 10.1089/humc.2014.019.

[166] A. McCarron *et al.*, “Effective viral-mediated lung gene therapy: is airway surface preparation necessary?”, *Gene Ther*, vol. 30, no. 6, pp. 469–477, 2023, doi: 10.1038/s41434-022-00332-7.

[167] L. Wang *et al.*, “Prednisolone reduces the interferon response to AAV in cynomolgus macaques and may increase liver gene expression”, *Mol Ther Methods Clin Dev*, vol. 24, pp. 292–305, 2022, doi: 10.1016/j.omtm.2022.01.007.

[168] C. A. Muirhead *et al.*, “Evaluation of rescue oral glucocorticoid therapy during inpatient Cystic Fibrosis exacerbations”, *Pediatr Pulmonol*, vol. 56, no. 5, pp. 891–900, 2021, doi: 10.1002/ppul.25204.

[169] S. M. Rowe *et al.*, “Inhaled mRNA therapy for treatment of Cystic Fibrosis: interim results of a randomized, double-blind, placebo-controlled phase 1/2 clinical study”, *J Cyst Fibros*, vol. 22, no. 4, pp. 656–664, 2023, doi: 10.1016/j.jcf.2023.04.008.

[170] L. Regard *et al.*, “Acute and chronic non-pulmonary complications in adults with Cystic Fibrosis”, *Expert Rev Respir Med*, vol. 13, no. 1, pp. 23–38, 2019, doi: 10.1080/17476348.2019.1552832.

[171] B. S. Quon and S. M. Rowe, “New and emerging targeted therapies for Cystic Fibrosis”, *BMJ*, p. i859, 2016, doi: 10.1136/bmj.i859.

[172] K. Harman *et al.*, “Disease-modifying drug therapy in Cystic Fibrosis”, *Paediatr Respir Rev*, vol. 26, pp. 7–9, 2018, doi: 10.1016/j.prrv.2017.03.008.

[173] P. D. W. Eckford, *et al.*, “Cystic Fibrosis Transmembrane Conductance Regulator (CFTR) potentiator VX-770 (Ivacaftor) opens the defective channel gate of mutant CFTR in a phosphorylation-dependent but ATP-independent manner”, *J Biol Chem*, vol. 287, no. 44, pp. 36639–36649, 2012, doi: 10.1074/jbc.M112.393637.

[174] F. J. Accurso *et al.*, “Effect of VX-770 in persons with Cystic Fibrosis and the G551D- *CFTR* utation”, *N Engl J Med*, vol. 363, no. 21, pp. 1991–2003, 2010, doi: 10.1056/NEJMoa0909825.

[175] B. W. Ramsey *et al.*, “A CFTR potentiator in patients with Cystic Fibrosis and the *G551D* mutation”, *N Engl J Med*, vol. 365, no. 18, pp. 1663–1672, 2011, doi: 10.1056/NEJMoa1105185.

[176] S. M. Rowe *et al.*, “Clinical mechanism of the Cystic Fibrosis Transmembrane Conductance Regulator potentiator Ivacaftor in G551D-mediated Cystic Fibrosis”, *Am J Respir Crit Care Med*, vol. 190, no. 2, pp. 175–184, 2014, doi: 10.1164/rccm.201404-0703OC.

[177] J. C. Davies *et al.*, “Efficacy and safety of Ivacaftor in patients aged 6 to 11 years with Cystic Fibrosis with a *G551D* mutation”, *Am J Respir Crit Care Med*, vol. 187, no. 11, pp. 1219–1225, 2013, doi: 10.1164/rccm.201301-0153OC.

[178] K. De Boeck *et al.*, “Efficacy and safety of Ivacaftor in patients with Cystic Fibrosis and a non-G551D gating mutation”, *J Cyst Fibros*, vol. 13, no. 6, pp. 674–680, 2014, doi: 10.1016/j.jcf.2014.09.005.

[179] R. B. Moss *et al.*, “Efficacy and safety of Ivacaftor in patients with Cystic Fibrosis who have an Arg117His-CFTR mutation: a double-blind, randomised controlled trial”, *Lancet Respir Med*, vol. 3, no. 7, pp. 524–533, 2015, doi: 10.1016/S2213-2600(15)00201-5.

[180] P. A. Flume *et al.*, “Ivacaftor in subjects with Cystic Fibrosis who are homozygous for the F508del-CFTR mutation”, *Chest*, vol. 142, no. 3, pp. 718–724, 2012, doi: 10.1378/chest.11-2672.

[181] H. Hebestreit *et al.*, “Effects of Ivacaftor on severely ill patients with Cystic Fibrosis carrying a G551D mutation”, *J Cyst Fibros*, vol. 12, no. 6, pp. 599–603, 2013, doi: 10.1016/j.jcf.2013.05.006.

[182] J. Taylor-Cousar *et al.*, “Effect of Ivacaftor in patients with advanced Cystic Fibrosis and a G551D-CFTR mutation: safety and efficacy in an expanded access program in the United States”, *J Cyst Fibros*, vol. 15, no. 1, pp. 116–122, 2016, doi: 10.1016/j.jcf.2015.01.008.

[183] D. Hubert *et al.*, “Real-world long-term Ivacaftor for Cystic Fibrosis in France: clinical effectiveness and healthcare resource utilization”, *Pulm Ther*, vol. 7, no. 2, pp. 455–468, 2021, doi: 10.1007/s41030-021-00158-5.

[184] D. Hubert *et al.*, “Retrospective observational study of French patients with Cystic Fibrosis and a Gly551Asp-CFTR mutation after 1 and 2 years of treatment with Ivacaftor in a real-world setting”, *J Cyst Fibros*, vol. 17, no. 1, pp. 89–95, 2018, doi: 10.1016/j.jcf.2017.07.001.

[185] N. Volkova *et al.*, “Disease progression in patients with Cystic Fibrosis treated with Ivacaftor: data from national US and UK registries”, *J Cyst Fibros*, vol. 19, no. 1, pp. 68–79, 2020, doi: 10.1016/j.jcf.2019.05.015.

[186] L. Kirwan *et al.*, “Longitudinal trends in real-world outcomes after initiation of Ivacaftor. a cohort study from the Cystic Fibrosis registry of Ireland”, *Ann Am Thorac Soc*, vol. 16, no. 2, pp. 209–216, 2019, doi: 10.1513/AnnalsATS.201802-149OC.

[187] C. E. Wainwright *et al.*, “Lumacaftor-Ivacaftor in patients with Cystic Fibrosis homozygous for Phe508del CFTR”, *N Engl J Med*, vol. 373, no. 18, pp. 1783–1784, 2015, doi: 10.1056/NEJMc1510466.

[188] J. L. Taylor-Cousar *et al.*, “Tezacaftor–Ivacaftor in patients with Cystic Fibrosis homozygous for Phe508del”, *N Engl J Med*, vol. 377, no. 21, pp. 2013–2023, 2017, doi: 10.1056/NEJMoa1709846.

[189] S. M. Rowe *et al.*, “Tezacaftor–Ivacaftor in residual-function heterozygotes with Cystic Fibrosis”, *N Engl J Med*, vol. 377, no. 21, pp. 2024–2035, 2017, doi: 10.1056/NEJMoa1709847.

[190] H. G. M. Heijerman *et al.*, “Efficacy and safety of the Elexacaftor plus Tezacaftor plus Ivacaftor combination regimen in people with Cystic Fibrosis homozygous for the F508del mutation: a double-blind, randomised, phase 3 trial”, *Lancet*, vol. 394, no. 10212, pp. 1940–1948, 2019, doi: 10.1016/S0140-6736(19)32597-8.

[191] P. G. Middleton *et al.*, “Elexacaftor–Tezacaftor–Ivacaftor for Cystic Fibrosis with a single phe508del Allele”, *N Engl J Med,* vol. 381, no. 19, pp. 1809–1819, 2019, doi: 10.1056/NEJMoa1908639.

[192] D. Keating *et al.*, “VX-445–Tezacaftor–Ivacaftor in patients with Cystic Fibrosis and one or two phe508del alleles”, *N Engl J Med*, vol. 379, no. 17, pp. 1612–1620, 2018, doi: 10.1056/NEJMoa1807120.

[193] P. Barry *et al.*, “Triple therapy for Cystic Fibrosis Phe508del-gating and residual function genotypes”, *N Engl J Med*, vol. 385, no. 23, pp. 2207–2208, 2021, doi: 10.1056/NEJMc2115966.

[194] M. P. Boyle *et al.*, “A CFTR corrector (Lumacaftor) and a CFTR potentiator (Ivacaftor) for treatment of patients with Cystic Fibrosis who have a phe508del CFTR mutation: a phase 2 randomised controlled trial”, *Lancet Respir Med*, vol. 2, no. 7, pp. 527–538, 2014, doi: 10.1016/S2213-2600(14)70132-8.

[195] A. Munck *et al.*, “Tezacaftor/Ivacaftor in people with Cystic Fibrosis heterozygous for minimal function CFTR mutations”, *J Cyst Fibros*, vol. 19, no. 6, pp. 962–968, 2020, doi: 10.1016/j.jcf.2020.04.015.

[196] P.-R. Burgel *et al.*, “Real-life safety and effectiveness of Lumacaftor–Ivacaftor in patients with Cystic Fibrosis”, *Am J Respir Crit Care Med*, vol. 201, no. 2, pp. 188–197, 2020, doi: 10.1164/rccm.201906-1227OC.

[197] J. L. Taylor-Cousar *et al.*, “Lumacaftor/Ivacaftor in patients with Cystic Fibrosis and advanced lung disease homozygous for F508del-CFTR”, *J Cyst Fibros*, vol. 17, no. 2, pp. 228–235, 2018, doi: 10.1016/j.jcf.2017.09.012.

[198] C. Schwarz *et al.*, "Tezacaftor/Ivacaftor in people with Cystic Fibrosis who stopped Lumacaftor/Ivacaftor due to respiratory adverse events", *J Cyst Fibros*, vol. 20, no. 2, pp. 228–233, 2021, doi: 10.1016/j.jcf.2020.06.001.

[199] P.-R. Burgel *et al.*, "Clinical response to Lumacaftor-Ivacaftor in patients with Cystic Fibrosis according to baseline lung function", *J Cyst Fibros*, vol. 20, no. 2, pp. 220–227, 2021, doi: 10.1016/j.jcf.2020.06.012.

[200] J. L. Taylor-Cousar *et al.*, "Clinical development of triple-combination CFTR modulators for Cystic Fibrosis patients with one or two *F508del* alleles", *ERJ Open Res*, vol. 5, no. 2, pp. 00082–02019, 2019, doi: 10.1183/23120541.00082-2019.

[201] M. Griese *et al.*, "Safety and efficacy of Elexacaftor/Tezacaftor/Ivacaftor for 24 weeks or longer in people with Cystic Fibrosis and one or more *F508del* alleles: interim results of an open-label phase 3 clinical trial", *Am J Respir Crit Care Med*, vol. 203, no. 3, pp. 381–385, 2021, doi: 10.1164/rccm.202008-3176LE.

[202] S. Sutharsan *et al.*, "Efficacy and safety of Elexacaftor plus Tezacaftor plus Ivacaftor versus Tezacaftor plus Ivacaftor in people with Cystic Fibrosis homozygous for F508del-CFTR: a 24-week, multicentre, randomised, double-blind, active-controlled, phase 3b trial", *Lancet Respir Med*, vol. 10, no. 3, pp. 267–277, 2022, doi: 10.1016/S2213-2600(21)00454-9.

[203] P.-R. Burgel *et al.*, "Rapid improvement after starting Elexacaftor–Tezacaftor–Ivacaftor in patients with Cystic Fibrosis and advanced pulmonary disease", *Am J Respir Crit Care Med*, vol. 204, no. 1, pp. 64–73, 2021, doi: 10.1164/rccm.202011-4153OC.

[204] C. Martin *et al.*, "Sustained effectiveness of Elexacaftor-Tezacaftor-Ivacaftor in lung transplant candidates with Cystic Fibrosis", *J Cyst Fibros*, vol. 21, no. 3, pp. 489–496, 2022, doi: 10.1016/j.jcf.2022.01.012.

[205] D. P. Nichols *et al.*, "Clinical effectiveness of Elexacaftor/Tezacaftor/Ivacaftor in people with Cystic Fibrosis: a clinical trial", *Am J Respir Crit Care Med*, vol. 205, no. 5, pp. 529–539, 2022, doi: 10.1164/rccm.202108-1986OC.

[206] J. C. Davies *et al.*, "Ivacaftor in infants aged 4 to <12 Months with Cystic Fibrosis and a gating mutation. results of a two-part phase 3 clinical trial", *Am J Respir Crit Care Med*, vol. 203, no. 5, pp. 585–593, 2021, doi: 10.1164/rccm.202008-3177OC.

[207] M. Rosenfeld *et al.*, "Ivacaftor treatment of Cystic Fibrosis in children aged 12 to <24 months and with a CFTR gating mutation (ARRIVAL): a phase 3 single-arm study", *Lancet Respir Med*, vol. 6, no. 7, pp. 545–553, 2018, doi: 10.1016/S2213-2600(18)30202-9.

[208] S. Walker *et al.*, "A phase 3 study of Tezacaftor in combination with ivacaftor in children aged 6 through 11 years with Cystic Fibrosis", *J Cyst Fibros*, vol. 18, no. 5, pp. 708–713, 2019, doi: 10.1016/j.jcf.2019.06.009.

[209] M. Rosenfeld *et al.*, "An open-label extension study of ivacaftor in children with CF and a CFTR gating mutation initiating treatment at age 2–5 years (KLIMB)", *J Cyst Fibros*, vol. 18, no. 6, pp. 838–843, 2019, doi: 10.1016/j.jcf.2019.03.009.

[210] E. T. Zemanick *et al.*, "A Phase 3 open-label study of Elexacaftor/Tezacaftor/Ivacaftor in children 6 through 11 years of age with Cystic Fibrosis and at least one F508del allele", *Am J*

Respir Crit Care Med, vol. 203, no. 12, pp. 1522–1532, 2021, doi: 10.1164/rccm.202102-0509OC.

[211] M. A. Mall *et al.*, "Efficacy and safety of Elexacaftor/Tezacaftor/Ivacaftor in children 6 through 11 years of age with Cystic Fibrosis heterozygous for F508del and a minimal Function mutation: a phase 3b, randomized, placebo-controlled study", *Am J Respir Crit Care Med*, vol. 206, no. 11, pp. 1361–1369, 2022, doi: 10.1164/rccm.202202-0392OC.

[212] G. Sette *et al.*, "Theratyping Cystic Fibrosis in vitro in ALI culture and organoid models generated from patient-derived nasal epithelial conditionally reprogrammed stem cells", *Eur Respir J*, vol. 58, no. 6, p. 2100908, 2021, doi: 10.1183/13993003.00908-2021.

[213] V. K. Singh and S. J. Schwarzenberg, "Pancreatic insufficiency in Cystic Fibrosis", *J Cyst Fibros*, vol. 16, pp. S70–S78, 2017, doi: 10.1016/j.jcf.2017.06.011.

[214] R. Megalaa *et al.*, "Time for a gut check: pancreatic sufficiency resulting from CFTR modulator use", *Pediatr Pulmonol*, vol. 54, no. 8, 2019, doi: 10.1002/ppul.24353.

[215] D. Munce *et al.*, "Persistent recovery of pancreatic function in patients with Cystic Fibrosis after Ivacaftor", *Pediatr Pulmonol*, vol. 55, no. 12, pp. 3381–3383, 2020, doi: 10.1002/ppul.25065.

[216] J. Crowley *et al.*, "Restoration of exocrine pancreatic function in child with Lumacaftor/Ivacaftor therapy in Cystic Fibrosis", *J Cyst Fibros*, vol. 21, no. 2, p. 264, 2022, doi: 10.1016/j.jcf.2021.08.032.

[217] A. Carrion *et al.*, "Reduction of recurrence risk of pancreatitis in Cystic Fibrosis with Ivacaftor", *J Pediatr Gastroenterol Nutr*, vol. 66, no. 3, pp. 451–454, 2018, doi: 10.1097/MPG.0000000000001788.

[218] M. L. Ramsey *et al.*, "Cystic Fibrosis Transmembrane Conductance Regulator modulator use is associated with reduced pancreatitis hospitalizations in patients with Cystic Fibrosis", *Am J Gastroenterol*, vol. 116, no. 12, pp. 2446–2454, 2021, doi: 10.14309/ajg.0000000000001527.

[219] M. D. Bellin *et al.*, "Insulin secretion improves in Cystic Fibrosis following Ivacaftor correction of CFTR: a small pilot study", *Pediatr Diabetes*, vol. 14, no. 6, pp. 417–421, 2013, doi: 10.1111/pedi.12026.

[220] D. Hayes *et al.*, "Resolution of Cystic Fibrosis–related diabetes with Ivacaftor therapy", *Am J Respir Crit Care Med*, vol. 190, no. 5, pp. 590–591, 2014, doi: 10.1164/rccm.201405-0882LE.

[221] B. Misgault *et al.*, "Effect of one-year Lumacaftor–Ivacaftor treatment on glucose tolerance abnormalities in Cystic Fibrosis patients", *J Cyst Fibros*, vol. 19, no. 5, pp. 712–716, 2020, doi: 10.1016/j.jcf.2020.03.002.

[222] H. Gaines *et al.*, "Effect of CFTR modulator therapy on Cystic Fibrosis-related diabetes", *J Diabetes Complications*, vol. 35, no. 6, p. 107845, 2021, doi: 10.1016/j.jdiacomp.2020.107845.

[223] K. J. Scully *et al.*, "The effect of Elexacaftor/Tezacaftor/Ivacaftor (ETI) on glycemia in adults with Cystic Fibrosis", *J Cyst Fibros*, vol. 21, no. 2, pp. 258–263, 2022, doi: 10.1016/j.jcf.2021.09.001.

[224] I. Korten *et al.*, “Short-term effects of Elexacaftor/Tezacaftor/Ivacaftor combination on glucose tolerance in young people with Cystic Fibrosis-an observational pilot study”, *Front Pediatr*, vol. 10, 2022, doi: 10.3389/fped.2022.852551.

[225] S. I. Sheikh *et al.*, “Ivacaftor improves appearance of sinus disease on computerised tomography in Cystic Fibrosis patients with G551D mutation”, *Clin Otolaryngol*, vol. 40, no. 1, pp. 16–21, 2015, doi: 10.1111/coa.12310.

[226] J. E. Douglas *et al.*, “Impact of novel CFTR modulator on sinonasal quality of life in adult patients with Cystic Fibrosis”, *Int Forum Allergy Rhinol*, vol. 11, no. 2, pp. 201–203, 2021, doi: 10.1002/alr.22716.

[227] E. DiMango *et al.*, “Effect of highly effective modulator treatment on sinonasal symptoms in Cystic Fibrosis”, *J Cyst Fibros*, vol. 20, no. 3, pp. 460–463, 2021, doi: 10.1016/j.jcf.2020.07.002.

[228] D. M. Beswick *et al.*, “Machine learning evaluates improvement in sinus computed tomography opacification with CFTR modulator therapy”, *Int Forum Allergy Rhinol*, vol. 11, no. 5, pp. 953–954, 2021, doi: 10.1002/alr.22722.

[229] A. L. Stapleton *et al.*, “Elexacaftor-Tezacaftor- Ivacaftor improves sinonasal outcomes in Cystic Fibrosis”, *J Cyst Fibros*, vol. 21, no. 5, pp. 792–799, 2022, doi: 10.1016/j.jcf.2022.03.002.

[230] J. Bailey *et al.*, “Effect of CFTR modulators on anthropometric parameters in individuals with Cystic Fibrosis: an evidence analysis center systematic review”, *J Acad Nutr Diet*, vol. 121, no. 7, pp. 1364-1378, 2021, doi: 10.1016/j.jand.2020.03.014.

[231] S. J. King *et al.*, “Body composition and weight changes after Ivacaftor treatment in adults with Cystic Fibrosis carrying the G551 D Cystic Fibrosis Transmembrane Conductance Regulator mutation: a double-blind, placebo-controlled, randomized, crossover study with open-label extension”, *Nutrition*, vol. 85, p. 111124, 2021, doi: 10.1016/j.nut.2020.111124.

[232] A. Gramegna *et al.*, “Overweight and obesity in adults with Cystic Fibrosis: an Italian multicenter cohort study”, *J Cyst Fibros*, vol. 21, no. 1, pp. 111–114, 2022, doi: 10.1016/j.jcf.2021.05.002.

[233] M. Litvin and J. C. Yoon, “Nutritional excess in Cystic Fibrosis: the skinny on obesity”, *J Cyst Fibros*, vol. 19, no. 1, pp. 3–5, 2020, doi: 10.1016/j.jcf.2019.12.002.

[234] R. Bass *et al.*, “The impact of highly effective CFTR modulators on growth and nutrition status”, *Nutrients*, vol. 13, no. 9, p. 2907, 2021, doi: 10.3390/nu13092907.

[235] L. Bessonova *et al.*, “Data from the US and UK Cystic Fibrosis registries support disease modification by CFTR modulation with Ivacaftor”, *Thorax*, vol. 73, no. 8, pp. 731–740, 2018, doi: 10.1136/thoraxjnl-2017-210394.

[236] D. Drummond *et al.*, “Lumacaftor-Ivacaftor effects on Cystic Fibrosis-related liver involvement in adolescents with homozygous F508 del-CFTR”, *J Cyst Fibros*, vol. 21, no. 2, pp. 212–219, 2022, doi: 10.1016/j.jcf.2021.07.018.

[237] K. Kutney *et al.*, “Lumacaftor/Ivacaftor therapy is associated with reduced hepatic steatosis in Cystic Fibrosis patients”, *World J Hepatol*, vol. 11, no. 12, pp. 761–772, 2019, doi: 10.4254/wjh.v11.i12.761.

[238] K. A. Despotes and S. H. Donaldson, “Current state of CFTR modulators for treatment of Cystic Fibrosis”, *Curr Opin Pharmacol*, vol. 65, p. 102239, 2022, doi: 10.1016/j.coph.2022.102239.

[239] E. F. Nash *et al.*, “Outcomes of pregnancy in women with Cystic Fibrosis (CF) taking CFTR modulators – an international survey”, *J Cyst Fibros*, vol. 19, no. 4, pp. 521–526, 2020, doi: 10.1016/j.jcf.2020.02.018.

[240] J. L. Taylor-Cousar and R. Jain, “Maternal and fetal outcomes following Elexacaftor-Tezacaftor-Ivacaftor use during pregnancy and lactation”, *J Cyst Fibros*, vol. 20, no. 3, pp. 402–406, 2021, doi: 10.1016/j.jcf.2021.03.006.

[241] C. N. Fortner *et al.*, “Normal pancreatic function and false-negative CF newborn screen in a child born to a mother taking CFTR modulator therapy during pregnancy”, J *Cyst Fibros*, vol. 20, no. 5, pp. 835–836, 2021, doi: 10.1016/j.jcf.2021.03.018.

[242] G. Alicandro *et al.*, “Heterogeneity in response to Elexacaftor/Tezacaftor/Ivacaftor in people with Cystic Fibrosis”, *J Cyst Fibros*, vol. 23, no. 6, pp. 1072–1079, 2024, doi: 10.1016/j.jcf.2024.04.013.

[243] A. P. Kass *et al.*, “Eating disorders in adolescents and young adults with Cystic Fibrosis”, *Pediatr Pulmonol*, vol. 57, no. 11, pp. 2791–2797, 2022, doi: 10.1002/ppul.26102.

[244] “Kaftrio European Medicines Agency”, https://www.ema.europa.eu/en/medicines/human

[245] E. Hong *et al.*, “Drug-drug interactions involving CFTR modulators: a review of the evidence and clinical implications”, *Expert Opin Drug Metab Toxicol*, vol. 19, no. 4, pp. 203–216, 2023, doi: 10.1080/17425255.2023.2220960.

[246] V. Terlizzi *et al.*, “Reported adverse events in a multicenter cohort of patients ages 6-18 years with Cystic Fibrosis and at least one F508del allele receiving Elexacaftor/Tezacaftor/Ivacaftor”, *J Pediatr*, vol. 274, p. 114176, 2024, doi: 10.1016/j.jpeds.2024.114176.

[247] D. H. Tewkesbury *et al.*, “Longitudinal effects of Elexacaftor/Tezacaftor/Ivacaftor on liver tests at a large single adult Cystic Fibrosis centre”, *J Cyst Fibros*, vol. 22, no. 2, pp. 256–262, 2023, doi: 10.1016/j.jcf.2023.01.007.

[248] A. Castaldo *et al.*, “Liver biochemical indexes and cholesterol metabolism in Cystic Fibrosis patients with F508del/CFTR variant genotype after Elexacaftor/Tezacaftor/Ivacaftor treatment”, *Sci Rep*, vol. 14, no. 1, p. 17422, 2024, doi: 10.1038/s41598-024-68511-7.

[249] A. Castaldo *et al.*, “One year of treatment with Elexacaftor/Tezacaftor/Ivacaftor in patients with Cystic Fibrosis homozygous for the F508del mutation causes a significant increase in liver biochemical indexes”, *Front Mol Biosci*, vol. 10, 2024, doi: 10.3389/fmolb.2023.1327958.

[250] Cystic Fibrosis Foundation, “Cystic Fibrosis Foundation Patient Registry Highlights 2023”, https://filotimofoundation.org/resource-library/2023-cystic-fibrosis-foundation-patient-registry-highlights-handout/.

[251] K. W. Southern *et al.*, “Raised intracranial pressure in three children with Cystic Fibrosis receiving Elexacaftor-Tezacaftor-Ivacaftor modulator therapy”, *Am J Respir Crit Care Med*, vol. 208, no. 1, pp. 103–105, 2023, doi: 10.1164/rccm.202303-0380LE.

[252] M. B. VanElzakker *et al.*, “Neuropsychiatric adverse effects from CFTR modulators deserve a serious research effort”, *Curr Opin Pulm Med*, vol. 29, no. 6, pp. 603–609, 2023, doi: 10.1097/MCP.0000000000001014.

[253] I. Sermet-Gaudelus *et al.*, “Behavioural and sleep issues after initiation of Elexacaftor–Tezacaftor–Ivacaftor in preschool-age children with Cystic Fibrosis”, *Lancet*, vol. 404, no. 10448, pp. 117–120, 2024, doi: 10.1016/S0140-6736(24)01134-6.

[254] T. Manciulli *et al.*, “Prevalence of adverse events in Cystic Fibrosis patients treated with Elexacaftor/Tezacaftor/Ivacaftor: Experience of the regional referral center in Tuscany, Italy”, *Pediatr Pulmonol*, vol. 58, no. 12, pp. 3626–3629, 2023, doi: 10.1002/ppul.26673.

[255] L. Cao, Y. Wu, Y. Gong, and Q. Zhou, “Small molecule modulators of Cystic Fibrosis Transmembrane Conductance Regulator (CFTR): Structure, classification, and mechanisms”, *Eur J Med Chem*, vol. 265, p. 116120, 2024, doi: 10.1016/j.ejmech.2023.116120.

[256] T. Okiyoneda *et al.*, “Mechanism-based corrector combination restores ΔF508-CFTR folding and function”, *Nat Chem Biol*, vol. 9, no. 7, pp. 444–454, 2013, doi: 10.1038/nchembio.1253.

[257] F. Van Goor *et al.*, “Rescue of ΔF508-CFTR trafficking and gating in human Cystic Fibrosis airway primary cultures by small molecules”, *Am J Physiol Lung Cell Mol Physiol*, vol. 290, no. 6, pp. L1117–L1130, 2006, doi: 10.1152/ajplung.00169.2005.

[258] T. W. Loo *et al.*, “Correctors enhance maturation of ΔF508 CFTR by promoting interactions between the two halves of the molecule”, *Biochemistry*, vol. 48, no. 41, pp. 9882–9890, 2009, doi: 10.1021/bi9004842.

[259] W. Yu *et al.*, “Probing conformational rescue induced by a chemical corrector of F508del-Cystic Fibrosis Transmembrane Conductance Regulator (CFTR) mutant”, *J Biol Chem*, vol. 286, no. 28, pp. 24714–24725, 2011, doi: 10.1074/jbc.M111.239699.

[260] Y. Wang *et al.*, “Correctors promote maturation of Cystic Fibrosis Transmembrane Conductance Regulator (CFTR)-processing mutants by binding to the protein”, *J Biol Chem*, vol. 282, no. 46, pp. 33247–33251, 2007, doi: 10.1074/jbc.C700175200.

[261] G. Amico *et al.*, “Unravelling the Regions of Mutant F508del-CFTR more susceptible to the action of four Cystic Fibrosis correctors”, *Int J Mol Sci*, vol. 20, no. 21, p. 5463, 2019, doi: 10.3390/ijms20215463.

[262] P. K. Chiaw *et al.*, “A chemical corrector modifies the channel function of F508del-CFTR”, *Mol Pharmacol*, vol. 78, no. 3, pp. 411–418, 2010, doi: 10.1124/mol.110.065862.

[263] F. Van Goor *et al.*, “Correction of the F508del-CFTR protein processing defect in vitro by the investigational drug VX-809”, *Proc Natl Acad Sci U.S.A.*, vol. 108, no. 46, pp. 18843–18848, 2011, doi: 10.1073/pnas.1105787108.

[264] C. M. Farinha *et al.*, “Revertants, low temperature, and correctors reveal the mechanism of F508del-CFTR rescue by VX-809 and suggest multiple agents for full correction”, *Chem Biol*, vol. 20, no. 7, pp. 943–955, 2013, doi: 10.1016/j.chembiol.2013.06.004.

[265] K. Fiedorczuk and J. Chen, “Mechanism of CFTR correction by type I folding correctors”, *Cell*, vol. 185, no. 1, pp. 158-168, 2022, doi: 10.1016/j.cell.2021.12.009.

[266] B. Kleizen *et al.*, “Co-translational folding of the first transmembrane domain of ABC-transporter CFTR is supported by assembly with the first cytosolic domain”, *J Mol Biol*, vol. 433, no. 13, p. 166955, 2021, doi: 10.1016/j.jmb.2021.166955.

[267] H. Y. Ren *et al.*, “VX-809 corrects folding defects in Cystic Fibrosis Transmembrane Conductance Regulator protein through action on membrane-spanning domain 1”, *Mol Biol Cell*, vol. 24, no. 19, pp. 3016–3024, 2013, doi: 10.1091/mbc.e13-05-0240.

[268] M. Ensinck *et al.*, “Phenotyping of rare CFTR mutations reveals distinct trafficking and functional defects”, *Cells*, vol. 9, no. 3, p. 754, 2020, doi: 10.3390/cells9030754.

[269] E. D. Deeks, “Lumacaftor/Ivacaftor: A review in Cystic Fibrosis”, *Drugs*, vol. 76, no. 12, pp. 1191–1201, 2016, doi: 10.1007/s40265-016-0611-2.

[270] J. Hukkanen, “Induction of cytochrome P450 enzymes: a view on human *in vivo* findings”, *Expert Rev Clin Pharmacol*, vol. 5, no. 5, pp. 569–585, 2012, doi: 10.1586/ecp.12.39.

[271] S. H. Donaldson *et al.*, “Tezacaftor/Ivacaftor in Subjects with Cystic Fibrosis and *F508del* / *F508del-CFTR* or *F508del*/*G551D-CFTR*”, *Am J Respir Crit Care Med*, vol. 197, no. 2, pp. 214–224, 2018, doi: 10.1164/rccm.201704-0717OC.

[272] E. F. McKone *et al.*, “A phase 3, randomized, double-blind, parallel-group study to evaluate Tezacaftor/Ivacaftor in people with Cystic Fibrosis heterozygous for F508del-CFTR and a gating mutation”, *J Cyst Fibros*, vol. 20, no. 2, pp. 234–242, 2021, doi: 10.1016/j.jcf.2020.11.003.

[273] H. G. M. Heijerman *et al.*, “Efficacy and safety of the Elexacaftor plus Tezacaftor plus Ivacaftor combination regimen in people with Cystic Fibrosis homozygous for the F508del mutation: a double-blind, randomised, phase 3 trial”, *Lancet*, vol. 394, no. 10212, pp. 1940–1948, 2019, doi: 10.1016/S0140-6736(19)32597-8.

[274] N. Kapouni *et al.*, “Efficacy and safety of Elexacaftor-Tezacaftor-Ivacaftor in the treatment of Cystic Fibrosis: a systematic review”, *Children*, vol. 10, no. 3, p. 554, 2023, doi: 10.3390/children10030554.

[275] X. Wang *et al.*, “Discovery of 4-[(2R,4R)-4-({[1-(2,2-Difluoro-1,3-benzodioxol-5-yl)cyclopropyl]carbonyl}amino)-7-(difluoromethoxy)-3,4-dihydro-2H-chromen-2-yl]benzoic Acid (ABBV/GLPG-2222), a potent Cystic Fibrosis Transmembrane Conductance Regulator (CFTR) corrector for the treatment of Cystic Fibrosis”, *J Med Chem*, vol. 61, no. 4, pp. 1436–1449, 2018, doi: 10.1021/acs.jmedchem.7b01339.

[276] S. C. Bell *et al.*, “CFTR activity is enhanced by the novel corrector GLPG2222, given with and without Ivacaftor in two randomized trials”, *J Cyst Fibros*, vol. 18, no. 5, pp. 700–707, 2019, doi: 10.1016/j.jcf.2019.04.014.

[277] N. Pedemonte *et al.*, “Discovery of a picomolar potency pharmacological corrector of the mutant CFTR chloride channel”, *Sci Adv*, vol. 6, no. 8, 2020, doi: 10.1126/sciadv.aay9669.

[278] N. Liessi *et al.*, “Synthesis and biological evaluation of novel thiazole-VX-809 hybrid derivatives as F508del correctors by QSAR-based filtering tools”, *Eur J Med Chem*, vol. 144, pp. 179–200, 2018, doi: 10.1016/j.ejmech.2017.12.030.

[279] N. Pedemonte, “Small-molecule correctors of defective F508-CFTR cellular processing identified by high-throughput screening”, *J Clin Invest*, vol. 115, no. 9, pp. 2564–2571, 2005, doi: 10.1172/JCI24898.

[280] D. E. Grove *et al.*, “Mechanisms for rescue of correctable folding defects in CFTRΔF508”, *Mol Biol Cell*, vol. 20, no. 18, pp. 4059–4069, 2009, doi: 10.1091/mbc.e08-09-0929.

[281] T. W. Loo *et al.*, “Bithiazole correctors rescue CFTR mutants by two different mechanisms”, *Biochemistry*, vol. 52, no. 31, pp. 5161–5163, 2013, doi: 10.1021/bi4008758.

[282] N. Pedemonte *et al.*, “Dual Activity of aminoarylthiazoles on the trafficking and gating defects of the Cystic Fibrosis Transmembrane Conductance Regulator chloride channel caused by Cystic Fibrosis mutations”, *J Biol Chem*, vol. 286, no. 17, pp. 15215–15226, 2011, doi: 10.1074/jbc.M110.184267.

[283] E. Pesce *et al.*, “Synthesis and structure–activity relationship of aminoarylthiazole derivatives as correctors of the chloride transport defect in Cystic Fibrosis”, *Eur J Med Chem*, vol. 99, pp. 14–35, 2015, doi: 10.1016/j.ejmech.2015.05.030.

[284] C. Brandas *et al.*, “NBD2 Is Required for the Rescue of Mutant F508del CFTR by a thiazole-based molecule: a class II corrector for the multi-drug therapy of Cystic Fibrosis,” *Biomolecules*, vol. 11, no. 10, p. 1417, 2021, doi: 10.3390/biom11101417.

[285] P.-W. Phuan *et al.*, “Synergy-based small-molecule screen using a human lung epithelial cell line yields ΔF508-CFTR correctors that augment VX-809 maximal efficacy”, *Mol Pharmacol*, vol. 86, no. 1, pp. 42–51, 2014, doi: 10.1124/mol.114.092478.

[286] L. He *et al.*, “Restoration of NBD1 thermal stability is necessary and sufficient to correct ΔF508 CFTR folding and assembly”, *J Mol Biol*, vol. 427, no. 1, pp. 106–120, 2015, doi: 10.1016/j.jmb.2014.07.026.

[287] G. Veit *et al.*, “Structure-guided combination therapy to potently improve the function of mutant CFTRs”, *Nat Med*, vol. 24, no. 11, pp. 1732–1742, 2018, doi: 10.1038/s41591-018-0200-x.

[288] O. Laselva *et al.*, “Rescue of multiple class II CFTR mutations by Elexacaftor+Tezacaftor+Ivacaftor mediated in part by the dual activities of Elexacaftor as both corrector and potentiator”, *Eur Respir J*, vol. 57, no. 6, p. 2002774, 2021, doi: 10.1183/13993003.02774-2020.

[289] G. Veit *et al.*, “Elexacaftor co-potentiates the activity of F508del and gating mutants of CFTR”, *J Cyst Fibros*, vol. 20, no. 5, pp. 895–898, 2021, doi: 10.1016/j.jcf.2021.03.011.

[290] G. Veit *et al.*, “Allosteric folding correction of F508del and rare CFTR mutants by Elexacaftor-Tezacaftor-Ivacaftor (Trikafta) combination”, *JCI Insight*, vol. 5, no. 18, 2020, doi: 10.1172/jci.insight.139983.

[291] K. Fiedorczuk and J. Chen, “Molecular structures reveal synergistic rescue of Δ508 CFTR by Trikafta modulators”, *Science*, vol. 378, no. 6617, pp. 284–290, 2022, doi: 10.1126/science.ade2216.

[292] V. Capurro *et al.*, “Partial rescue of F508del-CFTR stability and trafficking defects by double corrector treatment”, *Int J Mol Sci*, vol. 22, no. 10, p. 5262, 2021, doi: 10.3390/ijms22105262.

[293] J. C. Davies *et al.*, “VX-659–Tezacaftor–Ivacaftor in patients with Cystic Fibrosis and one or two Phe508del alleles”, *N Engl J Med*, vol. 379, no. 17, pp. 1599–1611, 2018, doi: 10.1056/NEJMoa1807119.

[294] L. Guerra *et al.*, “The preclinical discovery and development of the combination of Ivacaftor + Tezacaftor used to treat Cystic Fibrosis”, *Expet Opin Drug Discov*, vol. 15, no. 8, pp. 873–891, 2020, doi: 10.1080/17460441.2020.1750592.

[295] O. Laselva *et al.*, “Phenotyping rare CFTR mutations reveal functional expression defects restored by TRIKAFTATM”, *J Pers Med*, vol. 11, no. 4, p. 301, 2021, doi: 10.3390/jpm11040301.

[296] M. Renda *et al.*, “Novel tricyclic pyrrolo-quinolines as pharmacological correctors of the mutant CFTR chloride channel”, *Sci Rep*, vol. 13, no. 1, p. 7604, 2023, doi: 10.1038/s41598-023-34440-0.

[297] C. Jolly, “Role of the heat shock response and molecular chaperones in oncogenesis and cell death”, *J Natl Cancer Inst*, vol. 92, no. 19, pp. 1564–1572, 2000, doi: 10.1093/jnci/92.19.1564.

[298] A. J. L. Macario, “Molecular chaperones: multiple functions, pathologies, and potential applications”, *Front Biosci*, vol. 12, no. 1, p. 2588, 2007, doi: 10.2741/2257.

[299] T. K. Chaudhuri and S. Paul, “Protein-misfolding diseases and chaperone-based therapeutic approaches”, *FEBS J*, vol. 273, no. 7, pp. 1331–1349, 2006, doi: 10.1111/j.1742-4658.2006.05181.x.

[300] Y. E. Kim *et al.*, “Molecular chaperone functions in protein folding and proteostasis”, *Annu Rev Biochem*, vol. 82, no. 1, pp. 323–355, 2013, doi: 10.1146/annurev-biochem-060208-092442.

[301] V. Dahiya and J. Buchner, “Functional principles and regulation of molecular chaperones”, *Adv Protein Chem Struct Biol*, pp. 1–60, 2019, doi: 10.1016/bs.apcsb.2018.10.001.

[302] A. J. L. Macario *et al.*, *The Chaperonopathies*. Dordrecht: Springer Netherlands, 2013. doi: 10.1007/978-94-007-4667-1.

[303] R. M. L. Colunga Biancatelli *et al.*, “HSP90 inhibition and modulation of the proteome: therapeutical implications for idiopathic pulmonary fibrosis (IPF)”, *Int J Mol Sci*, vol. 21, no. 15, p. 5286, 2020, doi: 10.3390/ijms21155286.

[304] L. Noori *et al.*, “Putative roles and therapeutic potential of the chaperone system in amyotrophic lateral sclerosis and multiple sclerosis”, *Cells*, vol. 13, no. 3, p. 217, 2024, doi: 10.3390/cells13030217.

[305] F. Scalia *et al.*, “Myelin pathology: involvement of molecular chaperones and the promise of chaperonotherapy”, *Brain Sci*, vol. 9, no. 11, p. 297, 2019, doi: 10.3390/brainsci9110297.

[306] J. R. Riordan, “CFTR function and prospects for therapy”, *Annu Rev Biochem*, vol. 77, no. 1, pp. 701–726, 2008, doi: 10.1146/annurev.biochem.75.103004.142532.

[307] C. M. Farinha *et al.*, “The human DnaJ homologue (Hdj)-1/heat-shock protein (Hsp) 40 co-chaperone is required for the in vivo stabilization of the Cystic Fibrosis Transmembrane Conductance Regulator by Hsp70”, *Biochem J*, vol. 366, no. 3, pp. 797–806, 2002, doi: 10.1042/bj20011717.

[308] J. M. Younger *et al.*, “A foldable CFTRΔF508 biogenic intermediate accumulates upon inhibition of the Hsc70–CHIP E3 ubiquitin ligase”, *J Cell Biol*, vol. 167, no. 6, pp. 1075–1085, 2004, doi: 10.1083/jcb.200410065.

[309] Y. Matsumura *et al.*, “Role of Hsc70 binding cycle in CFTR folding and endoplasmic reticulum–associated degradation”, *Mol Biol Cell*, vol. 22, no. 16, pp. 2797–2809, 2011, doi: 10.1091/mbc.e11-02-0137.

[310] B. Z. Schmidt *et al.*, “Cysteine string protein promotes proteasomal degradation of the Cystic Fibrosis Transmembrane Conductance Regulator (CFTR) by increasing its interaction with the C terminus of Hsp70-interacting protein and promoting CFTR ubiquitylation”, *J Biol Chem*, vol. 284, no. 7, pp. 4168–4178, 2009, doi: 10.1074/jbc.M806485200.

[311] Y. Yamamoto *et al.*, “A novel ER J-protein DNAJB12 accelerates ER-associated degradation of membrane proteins including CFTR”, *Cell Struct Funct*, vol. 35, no. 2, pp. 107–116, 2010, doi: 10.1247/csf.10023.

[312] X. Wang *et al.*, “Hsp90 cochaperone Aha1 downregulation rescues misfolding of CFTR in Cystic Fibrosis”, *Cell*, vol. 127, no. 4, pp. 803–815, 2006, doi: 10.1016/j.cell.2006.09.043.

[313] O. V. Singh *et al.*, “Chemical rescue of deltaF508-CFTR mimics genetic repair in Cystic Fibrosis bronchial epithelial cells”, *Mol Cell Proteomics*, vol. 7, no. 6, pp. 1099–1110, 2008, doi: 10.1074/mcp.M700303-MCP200.

[314] M. Lopes-Pacheco, “CFTR modulators: the changing face of Cystic Fibrosis in the era of precision medicine”, *Front Pharmacol*, vol. 10, 2020, doi: 10.3389/fphar.2019.01662.

[315] V. Spanò *et al.*, “Evaluation of Fused pyrrolothiazole systems as correctors of mutant CFTR protein”, *Molecules*, vol. 26, no. 5, p. 1275, 2021, doi: 10.3390/molecules26051275.

[316] M. J. C. Scanio *et al.*, “Discovery and SAR of 4-aminopyrrolidine-2-carboxylic acid correctors of CFTR for the treatment of Cystic Fibrosis”, *Bioorg Med Chem Lett*, vol. 72, p. 128843, 2022, doi: 10.1016/j.bmcl.2022.128843.

[317] M. Barreca *et al.*, “Identification of 6,9-dihydro-5H-pyrrolo[3,2-h]quinazolines as a new class of F508del-CFTR correctors for the treatment of Cystic Fibrosis”, *Eur J Med Chem*, vol. 276, p. 116691, 2024, doi: 10.1016/j.ejmech.2024.116691.

[318] V. Spanò *et al.*, “An overview on chemical structures as ΔF508-CFTR correctors”, *Eur J Med Chem*, vol. 180, pp. 430–448, 2019, doi: 10.1016/j.ejmech.2019.07.037.

[319] V. Spanò *et al.*, “Current development of CFTR potentiators in the last decade”, *Eur J Med Chem*, vol. 204, p. 112631, 2020, doi: 10.1016/j.ejmech.2020.112631.

[320] E. Bardin *et al.*, “Modulators of CFTR. Updates on clinical development and future directions”, *Eur J Med Chem*, vol. 213, p. 113195, 2021, doi: 10.1016/j.ejmech.2021.113195.

[321] X. Fu *et al.*, “The role of Heat Shock Protein 70 subfamily in the hyperplastic prostate: from molecular mechanisms to therapeutic opportunities”, *Cells*, vol. 11, no. 13, p. 2052, 2022, doi: 10.3390/cells11132052.

[322] A. J. Massey, “ATPases as drug targets: insights from Heat Shock Proteins 70 and 90”, *J Med Chem*, vol. 53, no. 20, pp. 7280–7286, 2010, doi: 10.1021/jm100342z.

[323] D. Guin and M. Gruebele, “Chaperones Hsc70 and Hsp70 bind to the protein PGK differently inside living cells”, *J Phys Chem B*, vol. 124, no. 18, pp. 3629–3635, 2020, doi: 10.1021/acs.jpcb.0c00519.

[324] R. Rosenzweig, N. B. Nillegoda, M. P. Mayer, and B. Bukau, “The Hsp70 chaperone network”, *Nat Rev Mol Cell Biol*, vol. 20, no. 11, pp. 665–680, 2019, doi: 10.1038/s41580-019-0133-3.

[325] A. J. Ambrose and E. Chapman, “Function, therapeutic potential, and inhibition of Hsp70 chaperones”, *J Med Chem*, vol. 64, no. 11, pp. 7060–7082, 2021, doi: 10.1021/acs.jmedchem.0c02091.

[326] J. A. Coppinger *et al.*, “A Chaperone trap contributes to the onset of Cystic Fibrosis”, *PLoS One*, vol. 7, no. 5, p. e37682, 2012, doi: 10.1371/journal.pone.0037682.

[327] J. C. Young, “The role of the cytosolic HSP70 chaperone system in diseases caused by misfolding and aberrant trafficking of ion channels”, *Dis Model Mech*, vol. 7, no. 3, pp. 319–329, 2014, doi: 10.1242/dmm.014001.

[328] E. Nieddu *et al.*, “F508del-CFTR rescue: a matter of cell stress response”, *Curr Pharm Des*, vol. 19, no. 19, pp. 3476–3496, 2013, doi: 10.2174/13816128113199990317.

[329] A. Saxena *et al.*, “Human Heat Shock Protein 105/110 kDa (Hsp105/110) regulates biogenesis and quality control of misfolded Cystic Fibrosis Transmembrane Conductance Regulator at multiple levels”, *J Biol Chem* vol. 287, no. 23, pp. 19158–19170, 2012, doi: 10.1074/jbc.M111.297580.

[330] D. M. Hutt *et al.*, “Silencing of the Hsp70-specific nucleotide-exchange factor BAG3 corrects the F508del-CFTR variant by restoring autophagy”, *J Biol Chem*, vol. 293, no. 35, pp. 13682–13695, 2018, doi: 10.1074/jbc.RA118.002607.

[331] P. Kim Chiaw *et al.*, “Hsp70 and DNAJA2 limit CFTR levels through degradation”, *PLoS One*, vol. 14, no. 8, p. e0220984, 2019, doi: 10.1371/journal.pone.0220984.

[332] R. A. Chanoux and R. C. Rubenstein, “Molecular chaperones as targets to circumvent the CFTR defect in Cystic Fibrosis”, *Front Pharmacol*, vol. 3, 2012, doi: 10.3389/fphar.2012.00137.

[333] I. Brusa *et al.*, “Proteostasis regulators in Cystic Fibrosis: current development and future perspectives”, *J Med Chem*, vol. 65, no. 7, pp. 5212–5243, 2022, doi: 10.1021/acs.jmedchem.1c01897.

[334] E. Strickland *et al.*, “The molecular chaperone Hsc70 Assists the in vitro folding of the N-terminal Nucleotide-binding Domain of the Cystic Fibrosis Transmembrane Conductance Regulator”, *J Biol Chem*, vol. 272, no. 41, pp. 25421–25424, 1997, doi: 10.1074/jbc.272.41.25421.

[335] C. M. Farinha and M. D. Amaral, “Most F508del-CFTR is targeted to degradation at an early folding checkpoint and independently of calnexin”, *Mol Cell Biol*, vol. 25, no. 12, pp. 5242–5252, 2005, doi: 10.1128/MCB.25.12.5242-5252.2005.

[336] Y. Zhang *et al.*, “Hsp70 molecular chaperone facilitates Endoplasmic Reticulum-associated protein degradation of Cystic Fibrosis Transmembrane Conductance Regulator in yeast”, *Mol Biol Cell*, vol. 12, no. 5, pp. 1303–1314, 2001, doi: 10.1091/mbc.12.5.1303.

[337] L. R. Choo-Kang and P. L. Zeitlin, “Induction of HSP70 promotes ΔF508 CFTR trafficking”, *Am J Physiol Lung Cell Mol Physiol*, vol. 281, no. 1, pp. L58–L68, 2001, doi: 10.1152/ajplung.2001.281.1.L58.

[338] L. García-Bermejo *et al.,* “Modulation of HSP70 and HSP27 gene expression by the differentiation inducer sodium butyrate in U-937 human promonocytic leukemia cells”, *Leuk Res*, vol. 19, no. 10, pp. 713–718, 1995, doi: 10.1016/0145-2126(95)00045-P.

[339] L. Garcia-Bermejo *et al.*, “Modulation of Heat-Shock Protein 70 (HSP70) gene expression by sodium butyrate in U-937 promonocytic cells: relationships with differentiation and apoptosis”, *Exp Cell Res*, vol. 236, no. 1, pp. 268–274, 1997, doi: 10.1006/excr.1997.3725.

[340] R. C. Rubenstein *et al.*, “In vitro pharmacologic restoration of CFTR-mediated chloride transport with sodium 4-phenylbutyrate in Cystic Fibrosis epithelial cells containing delta F508-CFTR.”, *J Clin Invest*, vol. 100, no. 10, pp. 2457–2465, 1997, doi: 10.1172/JCI119788.

[341] A. Basile *et al.*, “Matrine modulates HSC70 levels and rescues ΔF508-CFTR”, *J Cell Physiol*, vol. 227, no. 9, pp. 3317–3323, 2012, doi: 10.1002/jcp.24028.

[342] R. C. Rubenstein and P. L. Zeitlin, “Sodium 4-phenylbutyrate downregulates Hsc70: implications for intracellular trafficking of ΔF508-CFTR,” *Am J Physiol Cell Physiol*, vol. 278, no. 2, pp. C259–C267, 2000, doi: 10.1152/ajpcell.2000.278.2.C259.

[343] R. C. Rubenstein and B. M. Lyons, “Sodium 4-phenylbutyrate downregulates HSC70 expression by facilitating mRNA degradation”, *Am J Physiol Lung Cell Mol Physiol*, vol. 281, no. 1, pp. L43–L51, 2001, doi: 10.1152/ajplung.2001.281.1.L43.

[344] L. Suaud *et al.*, “4-Phenylbutyrate stimulates Hsp70 expression through the Elp2 component of elongator and STAT-3 in Cystic Fibrosis epithelial cells”, *J Biol Chem*, vol. 286, no. 52, pp. 45083–45092, 2011, doi: 10.1074/jbc.M111.293282.

[345] B. Marengo *et al.*, “Matrine in association with FD-2 stimulates F508del-Cystic Fibrosis Transmembrane Conductance Regulator activity in the presence of corrector VX809”, *Mol Med Rep*, vol. 16, no. 6, pp. 8849–8853, 2017, doi: 10.3892/mmr.2017.7736.

[346] C. M. Haws *et al.*, “Delta F508-CFTR channels: kinetics, activation by forskolin, and potentiation by xanthines”, *Am J Physiol Cell Physiol*, vol. 270, no. 5, pp. C1544–C1555, 1996, doi: 10.1152/ajpcell.1996.270.5.C1544.

[347] D. R. Williams *et al.*, “An apoptosis-inducing small molecule that binds to Heat Shock Protein 70”, *Angew Chem Int Ed*, vol. 47, no. 39, pp. 7466–7469, 2008, doi: 10.1002/anie.200802801.

[348] H. J. Cho *et al.*, “A small molecule that binds to an ATPase domain of Hsc70 promotes membrane trafficking of mutant Cystic Fibrosis Transmembrane Conductance Regulator”, *J Am Chem Soc*, vol. 133, no. 50, pp. 20267–20276, 2011, doi: 10.1021/ja206762p.

[349] D. S. Williamson *et al.*, “Novel adenosine-derived inhibitors of 70 kDa Heat Shock Protein, discovered through structure-based design”, *J Med Chem*, vol. 52, no. 6, pp. 1510–1513, 2009, doi: 10.1021/jm801627a.

[350] H.-J. Park *et al.*, “A soluble sulfogalactosyl ceramide mimic promotes ΔF508 CFTR escape from Endoplasmic Reticulum associated degradation”, *Chem Biol*, vol. 16, no. 4, pp. 461–470, 2009, doi: 10.1016/j.chembiol.2009.02.014.

[351] D. J. Propper *et al.*, “Phase I trial of the selective mitochondrial toxin MKT 077 in chemo-resistant solid tumours”, *Ann Oncol*, vol. 10, no. 8, pp. 923–927, 1999, doi: 10.1023/A:1008336904585.

[352] X. Li *et al.*, “Analogues of the allosteric Heat Shock Protein 70 (Hsp70) inhibitor, MKT-077, as anti-cancer agents”, *ACS Med Chem Lett*, vol. 4, no. 11, pp. 1042–1047, 2013, doi: 10.1021/ml400204n.

[353] H. Shao *et al.*, “Exploration of benzothiazole rhodacyanines as allosteric inhibitors of protein–protein interactions with Heat Shock Protein 70 (Hsp70)”, *J Med Chem*, vol. 61, no. 14, pp. 6163–6177, 2018, doi: 10.1021/acs.jmedchem.8b00583.

[354] R. Sabbadini *et al.*, “Probing allosteric Hsp70 inhibitors by molecular modelling studies to expedite the development of novel combined F508del CFTR modulators”, *Pharmaceuticals*, vol. 14, no. 12, p. 1296, 2021, doi: 10.3390/ph14121296.

[355] F. Van Goor *et al.*, “Rescue of CF airway epithelial cell function in vitro by a CFTR potentiator, VX-770”, *Proc Natl Acad Sci*, vol. 106, no. 44, pp. 18825–18830, 2009, doi: 10.1073/pnas.0904709106.

[356] K.-Y. Jih and T.-C. Hwang, “VX-770 potentiates CFTR function by promoting decoupling between the gating cycle and ATP hydrolysis cycle”, *Proc Natl Acad Sci*, vol. 110, no. 11, pp. 4404–4409, 2013, doi: 10.1073/pnas.1215982110.

[357] F. C. Ferreira *et al.*, “PTI-801 (Posenacaftor) shares a common mechanism with VX-445 (Elexacaftor) to rescue p.Phe508del-CFTR”, *Eur J Pharmacol*, vol. 967, p. 176390, 2024, doi: 10.1016/j.ejphar.2024.176390.

[358] M. A. Mall *et al.*, “Cystic Fibrosis: emergence of highly effective targeted therapeutics and potential clinical implications”, *Am J Respir Crit Care Med*, vol. 201, no. 10, pp. 1193–1208, 2020, doi: 10.1164/rccm.201910-1943SO.

[359] P. A. Flume *et al.*, “Recovery of lung function following a pulmonary exacerbation in patients with Cystic Fibrosis and the G551D-CFTR mutation treated with Ivacaftor”, *J Cyst Fibros*, vol. 17, no. 1, pp. 83–88, 2018, doi: 10.1016/j.jcf.2017.06.002.

[360] G. S. Sawicki *et al.*, “Sustained benefit from Ivacaftor demonstrated by combining clinical trial and Cystic Fibrosis patient registry data”, *Am J Respir Crit Care Med*, vol. 192, no. 7, pp. 836–842, 2015, doi: 10.1164/rccm.201503-0578OC.

[361] D. Baroni *et al.*, “In silico and in vitro evaluation of the mechanism of action of three VX809-based hybrid derivatives as correctors of the F508del CFTR protein”, *Pharmaceuticals*, vol. 16, no. 12, p. 1702, 2023, doi: 10.3390/ph16121702.

[362] A. Lester *et al.*, “Computational exploration of potential CFTR binding sites for type I corrector drugs”, *Biochemistry*, vol. 62, no. 16, pp. 2503–2515, 2023, doi: 10.1021/acs.biochem.3c00165.

[363] D. Ramírez and J. Caballero, “Is it reliable to take the molecular docking top scoring position as the best solution without considering available structural data?”, *Molecules*, vol. 23, no. 5, p. 1038, 2018, doi: 10.3390/molecules23051038.

[364] E. Cichero *et al.*, “Probing in silico the benzimidazole privileged scaffold for the development of drug-like anti-RSV agents”, *Pharmaceuticals*, vol. 14, no. 12, p. 1307, 2021, doi: 10.3390/ph14121307.

[365] A. Parodi *et al.*, “Discovery of novel VX-809 hybrid derivatives as F508del-CFTR correctors by molecular modeling, chemical synthesis and biological assays”, *Eur J Med Chem*, vol. 208, p. 112833, 2020, doi: 10.1016/j.ejmech.2020.112833.

[366] T. W. Loo *et al.*, “Corrector VX-809 stabilizes the first transmembrane domain of CFTR”, *Biochem Pharmacol*, vol. 86, no. 5, pp. 612–619, 2013, doi: 10.1016/j.bcp.2013.06.028.

[367] R. Bongiorno *et al.*, “Elexacaftor mediates the rescue of F508del CFTR functional expression interacting with MSD2”, *Int J Mol Sci*, vol. 24, no. 16, p. 12838, 2023, doi: 10.3390/ijms241612838.

[368] D. Lunaccio *et al.*, “Structure-guided combination of novel CFTR correctors to improve the function of F508del-CFTR in airway epithelial cells”, *Biochem Pharmacol*, vol. 240, p. 117127, 2025, doi: 10.1016/j.bcp.2025.117127.

[369] O. Laselva *et al.*, “Correctors of the major Cystic Fibrosis mutant interact through membrane-spanning domains”, *Mol Pharmacol*, vol. 93, no. 6, pp. 612–618, 2018, doi: 10.1124/mol.118.111799.

[370] C. Allegretta *et al.*, “Olive leaf extract (OLE) as a novel antioxidant that ameliorates the inflammatory response in Cystic Fibrosis”, *Cells*, vol. 12, no. 13, p. 1764, 2023, doi: 10.3390/cells12131764.

[371] J. X. Jiang *et al.*, “A new platform for high-throughput therapy testing on iPSC-derived lung progenitor cells from Cystic Fibrosis patients”, *Stem Cell Rep*, vol. 16, no. 11, pp. 2825–2837, 2021, doi: 10.1016/j.stemcr.2021.09.020.

[372] D. Keating *et al.*, “VX-445–Tezacaftor–Ivacaftor in patients with Cystic Fibrosis and one or two Phe508del alleles”, *N Engl J Med*, vol. 379, no. 17, pp. 1612–1620, 2018, doi: 10.1056/NEJMoa1807120.

[373] A. Parodi *et al.*, “Journey on VX-809-based hybrid derivatives towards drug-like F508del-CFTR Correctors: from molecular modeling to chemical synthesis and biological assays”, *Pharmaceuticals*, vol. 15, no. 3, p. 274, 2022, doi: 10.3390/ph15030274.

[374] K. De Boeck *et al.*, “The relative frequency of CFTR mutation classes in European patients with Cystic Fibrosis”, *J Cyst Fibros*, vol. 13, no. 4, pp. 403–409, 2014, doi: 10.1016/j.jcf.2013.12.003.

[375] D. F. Veber *et al.*, “Molecular properties that influence the oral bioavailability of drug candidates”, *J Med Chem*, vol. 45, no. 12, pp. 2615–2623, 2002, doi: 10.1021/jm020017n.

[376] L. He *et al.*, “Restoration of NBD1 Thermal Stability Is Necessary and Sufficient to Correct ΔF508 CFTR folding and assembly”, *J Mol Biol*, vol. 427, no. 1, pp. 106–120, 2015, doi: 10.1016/j.jmb.2014.07.026.

[377] “Chemical Computing Group ULC Molecular Operating Environment (MOE2019.01),” http://www.chemcomp.com/.

[378] H. M. Berman *et al.*, “The Protein data bank”, *Acta Crystallogr D Biol Crystallogr*, vol. 58, no. 6, pp. 899–907, 2002, doi: 10.1107/S0907444902003451.

[379] H. M. Berman, “The protein data bank”, *Nucleic Acids Res*, vol. 28, no. 1, pp. 235–242, 2000, doi: 10.1093/nar/28.1.235.

[380] E. Abbotto *et al.*, “Novel thiazole-based SIRT2 inhibitors discovered via molecular modelling studies and enzymatic assays”, *Pharmaceuticals*, vol. 16, no. 9, p. 1316, 2023, doi: 10.3390/ph16091316.

[381] N. Scarano *et al.*, “Virtual screening combined with enzymatic assays to guide the discovery of novel SIRT2 inhibitors”, *Int J Mol Sci*, vol. 24, no. 11, p. 9363, 2023, doi: 10.3390/ijms24119363.

[382] S. Chin *et al.*, “Cholesterol interaction directly enhances intrinsic activity of the Cystic Fibrosis Transmembrane Conductance Regulator (CFTR)”, *Cells*, vol. 8, no. 8, p. 804, 2019, doi: 10.3390/cells8080804.

[383] O. Laselva *et al.*, “Insulin-like growth factor binding protein (IGFBP-6) as a novel regulator of inflammatory response in Cystic Fibrosis Airway cells”, *Front Mol Biosci*, vol. 9, 2022, doi: 10.3389/fmolb.2022.905468.

[384] O. Laselva *et al.*, “Preclinical studies of a rare CF-causing mutation in the second nucleotide binding domain show robust functional rescue in primary nasal cultures by novel CFTR modulators”, *J Pers Med*, vol. 10, no. 4, p. 209, 2020, doi: 10.3390/jpm10040209.

[385] K. S. Louis and A. C. Siegel, “Cell viability analysis using trypan blue: manual and automated methods”, pp. 7–12, 2011, doi: 10.1007/978-1-61779-108-6_2.

[386] L. J. V. Galietta *et al.*, “Green fluorescent protein-based halide indicators with improved chloride and iodide affinities”, *FEBS Lett*, vol. 499, no. 3, pp. 220–224, 2001, doi: 10.1016/S0014-5793(01)02561-3.

[387] L. V. J. Galietta, S. Jayaraman, and A. S. Verkman, “Cell-based assay for high-throughput quantitative screening of CFTR chloride transport agonists,” *American Journal of Physiology-Cell Physiology*, vol. 281, no. 5, pp. C1734–C1742, Nov. 2001, doi: 10.1152/ajpcell.2001.281.5.C1734.

[388] O. Laselva, M. C. Ardelean, and C. E. Bear, “Phenotyping rare CFTR mutations reveal functional expression defects restored by TRIKAFTATM”, *J Pers Med*, vol. 11, no. 4, p. 301, 2021, doi: 10.3390/jpm11040301.

[389] O. Laselva *et al.*, “Activity of Lumacaftor is not conserved in zebrafish CFTR bearing the major Cystic Fibrosis-causing mutation”, *FASEB Bioadv*, vol. 1, no. 10, pp. 661–670, 2019, doi: 10.1096/fba.2019-00039.

[390] C. Allegretta *et al.*, “Deleterious effect of *Pseudomonas aeruginosa* on F508del-CFTR rescued by Elexacaftor/Tezacaftor/Ivacaftor is clinical strain-dependent in patient-derived nasal cells”, *ERJ Open Res*, vol. 11, no. 3, pp. 00970–02024, 2025, doi: 10.1183/23120541.00970-2024.

[391] O. Laselva *et al.*, “Anti-inflammatory and anti-oxidant effect of dimethyl fumarate in Cystic Fibrosis bronchial epithelial cells”, *Cells*, vol. 10, no. 8, p. 2132, 2021, doi: 10.3390/cells10082132.

[392] Y. S. Oren et al., “Antisense oligonucleotide splicing modulation as a novel Cystic Fibrosis therapeutic approach for the W1282X nonsense mutation,” J Cyst Fibros, vol. 21, no. 4, pp. 630–636, 2022, doi: 10.1016/j.jcf.2021.12.012.